



Master of Science in  
Cultural Heritage Materials & Technologies



UNIVERSITY OF THE PELOPONNESE  
DEPARTMENT OF HISTORY, ARCHAEOLOGY  
AND CULTURAL RESOURCES MANAGEMENT



NATIONAL CENTER  
FOR SCIENTIFIC RESEARCH  
“DEMOKRITOS”



NATIONAL  
OBSERVATORY  
OF ATHENS

**Master of Science in  
«Cultural Heritage Materials and Technologies»**

**Andrea Christova**

R. N. 1012201502018

**A Comparison of Selected Photogrammetric Techniques  
for Creating 3D Models of Cultural Objects with Specular Surface**

**SUPERVISING COMMITTEE:**

Prof. Nikos Zacharias  
Assist. Prof. Angeliki Antoniou

**EXAMINATION COMMITTEE:**

Prof. Nikos Zacharias  
Assist. Prof. Angeliki Antoniou  
Dr. Aphrodite Kamara

**EXTERNAL ADVISOR:**

Dr. Branislav Meres

Kalamata, October 2020

---

## Table of Contents

<b>ABSTRACT</b>	<b>3</b>
<b>ACKNOWLEDGEMENTS</b>	<b>4</b>
<b>1 INTRODUCTION</b>	<b>5</b>
1.1 Digitization and Photogrammetry	5
1.2 Utilization of Photogrammetry in Cultural Heritage	6
1.3 Cultural Heritage – Terminology	6
1.4 Cultural Heritage Within the Context of Slovakia	7
1.5 Related Works & Literature	9
1.6 Study Objectives	10
<b>2 MATERIALS AND METHODS</b>	<b>12</b>
2.1 Studied Objects	12
2.1.1 Object 1 - Ciborium	12
2.1.2 Object 2 - Crucifix	13
2.2 Experimental Setup - Equipment	13
2.2.1 Capture Device	14
2.2.2 Computer Hardware Specification	15
2.2.3 Software	15
2.2.4 Other technical equipment	17
2.3 General workflow	20
2.3.1 Description of the methodology	21
2.3.2 Proposed workflow	22
2.4 Object and Studio Preparation	24
2.4.1 Defining the Parameters of the Photo Session	25
2.5 Image Capturing	28
2.5.1 Camera Settings	29
2.5.2 Data Acquisition Variants	33
2.6 Photo Processing	38
2.7 Data Processing Workflow using Reality Capture	39
2.7.1 Aligning	40
2.7.2 Mesh Reconstruction	49
2.7.3 Simplification	57
2.7.4 Texturing	58
2.7.5 Exporting	62
<b>3 RESULTS AND DISCUSSION</b>	<b>68</b>
3.1 Comparison of Applied Methods	68
3.1.1 Comparison with CT scan	68
3.1.2 Comparison of Volume and Surface Deviations in CloudCompare	72
3.1.3 Quantitative Evaluation	100
3.1.4 Qualitative Evaluation	103
3.2 Evaluation of the Results	108
3.3 Conclusions	115
<b>4 BIBLIOGRAPHY</b>	<b>116</b>
<b>5 APPENDICES</b>	<b>119</b>
5.1 List of Abbreviations	119
5.2 List of Figures	120
5.3 List of Tables	123

## Abstract

As specular surfaces present a known challenge for most scanning and surface capturing technologies in terms of 3D model creation, the purpose of this study is to present, explore and compare three selected approaches for creating digital 3-dimensional representations of existing historical liturgical objects which have a specular (i.e. reflective, mirror-like) surface.

Based on the interest of the Hospitaller Order of St. John of God in Bratislava, Slovakia to have their object inventory digitized for their internal documentation purposes, two studied objects - a silver-plated brass ciborium and a stainless-steel crucifix - were as a trial subjected to image capturing by a digital camera under three different conditions in an effort to minimize the effect of the reflected light. The first approach was using diffused light only, then cross-polarization was applied, while for the third approach a scanning spray was used. The acquired data was used for the creation of the respective 3D models of these objects. In the first two cases the data was used for both the model and the texture, whereas for the third option the data was used for creating the model only, while data from CPL (cross-polarization) was utilized for the texture due to the real surface being covered in white layer created by the spray.

The selected techniques are discussed with their main features, while presenting the respective outcomes in the form of digital 3D object models, which are compared against each other in terms of output quality. The most accurate 3D models were produced by cross-polarization.

Keywords: Digitization, photogrammetry, Structure from Motion, 3D models, specular – shiny – glossy – reflective surfaces, cultural heritage

## Acknowledgements

The help and support of many people has been essential for the successful completion and submission of this thesis. I would like to thank the Hospitaller Order of St. John of God in Bratislava - administratively represented by my mother - for granting access to the studied artefacts, my loving and supportive partner Brano for providing all necessary equipment and assisting with it, as well as for his active help, consultations and guidance of the progress, further to Mr. Milos Lukac for exchanging his photogrammetric experience through numerous insights and remarks concerning the primarily used software and of course to Prof. Nikos Zacharias for his endless support, understanding and patience, which he has always offered to me. I would also like to express my gratitude to the staff of the Laboratory of Archaeometry of the University of the Peloponnese for assisting me with various (far more than just) administrative matters throughout my studies (being the only foreign student of my class).

I would sincerely like to thank my family, especially to my parents and maternal grand-parents, who supported and believed in me ever since having been accepted to this study programme and throughout my whole studies and I would like to dedicate this thesis to the memory of my paternal grand-mother and my uncle.

# 1 Introduction

The framework of this study was established by the intention of the Hospitaller Order of St. John of God in Bratislava, Slovakia to have their object inventory digitized for their internal documentation purposes. As many of these objects are made of metals (mostly ecclesiastical artefacts), they have a shiny surface and therefore present a known challenge for most scanning or surface capturing technologies in terms of 3D model creation (this issue is discussed further in greater detail). Thus a kind of a feasibility study was to be executed, in order to establish if and how the digitization of these artefacts can be performed, by selecting two specular objects out of the inventory of the Order and subjecting them to the trial, so as to explore the applicability of available digitizing approaches (using a digital camera) for the creation of 3D model of the objects.

## 1.1 Digitization and Photogrammetry

The topic of digitization, a widely discussed subject in recent years, has been associated with the question of long-term preservation and access to data and information which is nowadays considered a focus of considerable interest. Consequently, the demand for obtaining and sharing 3-dimensional data is also growing, having thus progressed from digitization of documents, image and sound to the digitization of 3D objects. Together with the advancement of internet and 3D technologies new possibilities and applications are available for the digitization of 3D objects and also for the creation and utilization of 3D models.

The subject of this study is dealing with the application of a digitization method in the field of cultural heritage, namely photogrammetry, which is increasingly becoming the gold standard for 3D digitizing as recent technological advances in digital cameras, computer processors, and computational techniques make it a portable and powerful technique.

Photogrammetry as a method has been defined as the art, science, and technology of obtaining reliable information about physical objects and the environment through processes of recording, measuring, and interpreting photographic images and patterns of recorded radiant electromagnetic energy and other phenomena (Wolf and Dewitt 2000; McGlone 2004). According to Schenk *“Photogrammetry is distinguished by the measurement on photographs, allowing to obtain from any object its real dimensions, position, shape, and textures”* (Schenk 2005).

Derived from the Greek words for light, writing or record and measurement, photogrammetry can be translated as measurement of the record created by light. Thus, photogrammetry as such deals with measurement procedures based on a photograph, from which it analyses the shape, size and position of the objects shown in the image. Its task is then to convert information from the central projection of the image to orthogonal projection. Simply put, it is a non-contact method of optical measurement of objects (Dedik 2016).

Photogrammetry uses optical, photographic and geometric-mathematical methods. In the past, mainly analogue methods were used, such as optical and geodetic measurements. Since digital photography is mainly used today and the coordinates are processed digitally and online, we can consider these methods as digitizing (Bartoš and Gregor 1995).

The goal of photogrammetry is to create a 3D digital surface that replicates the actual subject as closely as possible, in shape and colour. It produces extremely dense and accurate 3D surface data with an adequately limited number of photos, taken with standard digital photography equipment, in a relatively short period of time. The variety and strength of photogrammetry and related procedures have increased significantly in recent years (culturalheritageimaging.org).

Photogrammetry can be categorized based on various criteria (Luhman et. al. 2006), such as according to the sensing position, from where the image is captured, or according to the number of processed images. According to camera position and object distance, we distinguish two main types of photogrammetry, aerial (topographic mapping, archaeology, landscaping, etc.) and terrestrial or close-range (used for architecture, medicine, construction, etc.) (Novaković et al. 2017). Based on the number of captured images, there can be single-image, where objects are evaluated only in two dimensions (e.g. ground plan or wall), and two- or multi-image photogrammetry (Pavelka 2009).

It can be utilized in a wide range of areas and domains, such as engineering, machine, car and aerospace industry, medicine, forensic analysis, information systems, natural sciences, various interdisciplinary scientific applications, however also in architecture, archaeology and cultural heritage, the latter representing the main field this study is focusing on.

### 1.2 Utilization of Photogrammetry in Cultural Heritage

The term cultural heritage (CH) refers mainly to objects related to libraries, museums, archives, galleries, monuments and audiovisuals. At present there is an effort to digitize it, as documentation in digital form has many advantages over the hitherto used documentation procedure. The goal of digitization within the framework of informatization in the knowledge society is thus not only the preservation, but also the accessibility and especially the use of digital content in various areas - economics, science, innovation, education and culture, not excluding (Katušćák 2008).

Within the framework of cultural heritage photogrammetry is applied in archaeology, conservation science, museum studies, art, history, epigraphy and ancient document studies, for the documentation, visualization and preservation of cultural heritage objects and sites, conservation planning and restoration recording (enabling conservators to understand key features and issues in 2D and 3D), as well as for the analysis of archaeological materials and representation of archaeological data (The Digital Ark 2016).

The main advantages of utilizing photogrammetry comprise enabling the access to various CH collections while enhancing detail, facilitating spatial understanding for easier collaboration, crowdsourcing and educational opportunities, providing measurements for exhibit planning, allowing monetizing of objects through 3D printing, obtaining and producing data for virtual reality, which has the potential to engage a wide spectrum of viewers delivering an immediate „wow“ effect by inducing immersion.

### 1.3 Cultural Heritage – Terminology

Cultural heritage is unique and irreplaceable wealth of human society, documenting the history and development of society. It comprises a huge number of elements from material results of human activity, through languages, religions and traditions to life values and knowledge. It can be defined as a set of tangible

and intangible values that is inherited from past generations, rather as a product of selection by society (heritageconsulting.sk), (Logan 2007).

Within the European context, the meaning and use of the term heritage is defined in the thesaurus terminology of the Council of Europe encompassing the following terms (coe.int):

- archaeological heritage
- anthropological heritage
- built heritage
- civil engineering heritage
- cultural heritage
- documentary heritage
- film heritage
- geological heritage
- historic heritage
- industrial heritage
- intangible heritage
- intellectual heritage
- landscape heritage
- maritime heritage
- military heritage
- monumental heritage
- movable heritage
- natural heritage
- parietal heritage
- photographic heritage
- protected heritage
- religious heritage
- rural heritage
- scientific heritage
- technical heritage
- urban heritage
- waterways heritage

#### 1.4 Cultural Heritage Within the Context of Slovakia

On the national level, in the case of Slovakia, we distinguish between intangible and tangible cultural heritage.

Intangible heritage comprises non-material culture such as customs, folklore (dance, music, song, literature, etc.), traditions, language and knowledge. The identification of the immaterial aspect of intangible heritage is in most cases possible only through representative material objects and monuments that are associated e.g. with historical events or personalities (birth houses, monuments, memorials ...) (Measures for CH SR 2006).

The most problematic area of intangible heritage is the protection of the talent and skills of creators of cultural values in professions and activities, the result of which is not a material product, but usually a musical, verbal or visual work. With the current development of science and technology however, it is possible to document intangible heritage also digitally, through media, Internet, on sound carriers, etc. Today, any video or audio data disseminated by various forms on traditional and contemporary media has irreplaceable value for the future. This applies not only to folklore and other forms of folk art, however also to documenting of technological processes and various traditional techniques (Measures for CH SR 2006).

Tangible cultural heritage includes monuments that have a material nature, thus being a creation of human activity or an object that recalls the past (buildings, jewellery, coins, objects of everyday use).

We can divide it into the following categories (Measures for CH SR 2006):

- Archival documents
- Historical library collections and documents

- Collections of museums and galleries
- Monuments fund
- Works of music, dramatic art, dance and scenography
- Film and audio-visual field
- Works of fine arts, applied arts, design and architecture
- Works of folk art and folk art production

The most important element of cultural heritage is the Monuments fund. It consists of national cultural monuments, among which we include e.g. castles, chateaux, manors, burgher houses, monument areas. A separate category is represented by monuments, or territories that belong to the UNESCO World Heritage List, as well as monuments of European heritage. Cultural heritage also includes archaeological heritage and archaeological finds, which form a specific component of cultural heritage. Movable parts of cultural heritage are preserved and presented in the collections of museums, galleries, libraries and archives. The most important of them can be declared movable national cultural monuments ([heritageconsulting.sk](http://heritageconsulting.sk)).

The protection of the Monuments fund is served by Act No. 49/2002 Coll., implemented by Decree No. 253/2010 Coll. as amended. "This Act regulates the conditions for the protection of cultural monuments, monument areas, archaeological finds and archaeological sites in accordance with scientific knowledge and on the basis of international agreements in the field of European and world cultural heritage by which the Slovak Republic is bound. The protection of the monuments fund is a set of activities and measures aimed at the identification, research, registration, preservation, renovation, restoration, regeneration, use and presentation of cultural monuments and monument areas (Act no. 49/2002).

The protection of cultural heritage is in public interest and the individual types of cultural heritage are subject to care and protection also in accordance with international agreements and special regulations, by which the Slovak republic is bound.

In order to comply with the requirements for documentation with the EU, the Operational Program Informatization of Society (OPIS) was established in Slovakia in 2007. OPIS ([opis.gov.sk](http://opis.gov.sk) 2010) is a reference document based on which financial support is provided from the structural funds of the European Union for projects of informatization of society, digitization of fund institutions and support of broadband internet. The document was approved by the Government of the Slovak Republic and subsequently by the European Commission (Protection of Monuments SR 2006). In Slovakia, there are 13 212 immovable and 30 410 movable objects, which need to be documented within the OPIS project (Katuščák 2008).

In 2012, the Monuments Office of the Slovak Republic created the Digital Monuments Fund project. This project is focused on documenting selected national cultural monuments using various geodetic methods. (Information technology and libraries 2020).



## 1.5 Related Works & Literature

For many years, the acquisition of artefacts based on the application of the photogrammetric method has been established. Initially designed for larger areas, aerial photogrammetry has progressed to close range photogrammetry for smaller objects and enclosed locations (Luhmann et al. 2007).

Nowadays, the techniques allow versatile acquisition in a broad spectrum of conditions, however, due to being a passive acquisition technique, an external light source is required for photogrammetry. Changing lighting conditions can cause difficulties in model adjustment, during the feature detection process as well as during automatic image comparison. Reflection points cause errors in reconstruction and create artefacts in final models (Hallot and Gil 2019).

Therefore, in photogrammetry (and also in laser or structured light scanning), it is very problematic to scan some types of materials, objects or their surfaces. Koutsoudis et al. stated the following object materials to be unsuitable for photogrammetric image acquisition: water, glass, plants and vegetation, varnish, monochromatic glossy surfaces (featureless surfaces), wood, steel, plastic (featureless), glossy - gold, iron, copper, bronze (Koutsoudis et al. 2015). According to Lachambre it can be difficult or impossible to get good enough result with the following types of objects (Lachambre et. al. 2017):

- Clear objects
- Glossy objects
- Featureless textures
- Repetitive features on the objects
- Very thin objects

Photogrammetry works based on exact positions of reference points on a given surface. Current software assumes that all surfaces are non-reflective and opaque and cannot distinguish between white pixels on the object and the reflection of light (Mallison and Wings 2014). Light reflections on the surface of the objects are interpreted by the software as an empty, non-existent surface as these reflections have no texture or details which software can pick up on. Therefore, during reconstruction, irregular holes are formed in the body of the model at the point of reflection, the geometry is distorted or a part of the surface of the model is completely missing. If the position of the light source relative to the object changes (eg. rotating turntable), these defects appear all over the surface of the model reflecting the incident light.

Most of the scanned objects are generally made of opaque materials. The incident light can therefore only be divided into the absorbed and reflected part. The reflection occurs from a surface that has properties listed between two extremes:

- The Lambert (also an ideally matt, ideally diffuse) surface is defined as a surface that reflects light in all directions equally, or diffusely.
- The ideal mirror surface reflects incident radiation at a mirror-symmetrical angle to the angle of incidence.

The glossy (or specular) surface is a combination of a Lambert and ideal mirror surface. Most of the radiation is reflected by specular reflection based on the law of reflection. A smaller part is reflected by diffuse reflection.

In the Fig. 1 is a comparison of a light distributions for Lambert diffuse (a), glossy (b) and ideal mirror (c) surfaces (Konrad 2016):

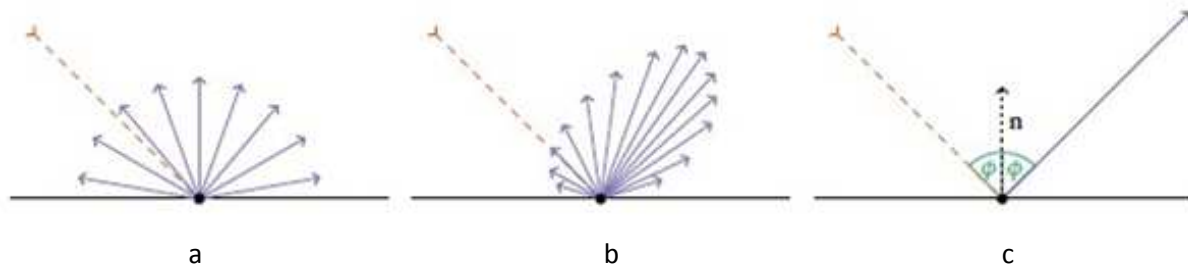


**Fig. 1: Distribution of light for diffused, glossy and mirror surface**

The variable lighting conditions directly influence and limit the final texture applied to the 3D models in photogrammetry, therefore the necessary basis for a successful reconstruction is a good shot with appropriate lighting conditions. Capturing images of good quality for reflective objects applies not only to photogrammetric use or heritage documentation, however also e.g. in medical applications (Edwards 2011) or palaeontology (Crabb 2001), where cross-polarized lighting technique is utilized in order to avoid reflections on specular objects.

Most real-world objects often consist of materials which have a mixture of glossy and diffuse reflective properties. On the contrary, these elements tend to reflect incident light in all directions, creating radiance on the acquired image. By using a polarized filter which permits the light wave to move in one direction, the polarization of light is achieved (Edwards 2011).

This principle is applied during the acquisition process with two filters – placing one at the light source and the other in front of the acquisition device, i.e. the lens of a digital camera. Using cross-polarized images in photogrammetry improves photogrammetric reconstruction and measurement on reflective surfaces (Wells et al. 2005). Conen et al. prove that also image matching improves significantly when applying polarized light conditions (Conen et al. 2018).

### 1.6 Study Objectives

In this study, we are dealing with glossy objects made out of metal creating light reflections when subjected to image acquisition. The objectives comprise a theoretical and practical exploration of the selected methods on how to approach the phenomenon of specular surfaces (shiny metal, mirror-like), as a known issue and based on the comparison of their outcomes to draw conclusion which of these approaches produces the most accurate results when comparing the final 3D models of the given objects.

Furthermore, the goal was to establish if and how the digitization of these artefacts can be performed using a digital camera and available equipment producing 3D object models with sufficient quality for internal digital documentation purposes.

The selected methods were chosen according to the following considerations: the accessibility of equipment, the restrictions on the treatment and manipulation of the borrowed objects and the purpose to mitigate the reflective effects of the specular surfaces. Therefore in an effort to meet the objectives the conditions for the three methods were set while the only light source used was diffused light (photo shooting was taking place in a completely dark studio), with employing the use of polarization filters and scanning spray. All three methods (diffused light only, cross polarization, and scanning spray) are described in detail in the chapter Materials and Methods.

## 2 Materials and Methods

### 2.1 Studied Objects

For this study two historical liturgical objects borrowed out by the Hospitaller Order of St. John of God in Bratislava are being studied. They were chosen for this purpose as they are difficult to be captured being made of materials with reflective surfaces generating highlights generally unsuitable for photogrammetry such as glossy metal, marble, etc. Both objects became the property of the Order as donations or through inheritance, therefore no information is available regarding their provenance, origin or history.

#### 2.1.1 Object 1 - Ciborium

A Ciborium used for liturgical purposes (with missing lid). Its top and bottom is made of pressed brass sheet, connected together with a brass column. The surface is (probably) silvered and polished with marks of oxidations, while the inside surface of the bowl is gilded. The chalice has shiny surface with lots of details. The top diameter is 100 mm, while its height is 163 mm (Fig. 2).



Fig. 2: Object 1 - Ciborium

### 2.1.2 Object 2 - Crucifix

A liturgical crucifix (Fig. 3) made of stainless steel with brass statue and small embossment of Virgin Mary on the base. The bottom of the base is made out of a polished marble block. The surface of the cross is polished with signs of oxidation. Based on the style, the item is estimated to date to 20s-30s of the 20<sup>th</sup> century. The dimensions are 618 x 254 x 99 mm (height x width x depth).



Fig. 3: Object 2 - Crucifix

## 2.2 Experimental Setup - Equipment

For realization of this study various technical equipment was required, both hardware and software. The respective equipment was either borrowed or provided by own resources. In Tab.1 all used hardware equipment is specified.

Tab.1: List of technical equipment

Equipment	Supplier	Approximate cost Eur	Comment
Nikon D500 + Sigma 18-50 lens	Nikon, Sigma	-	borrowed
Workstation	DIY	-	borrowed
Turntable	DIY	-	borrowed
Scale bar	Past Horizons	2,50	
LED lights	Yongnuo	260,00	
Backdrop	Local haberdashery	15,00	
Circular polarizing filter for lens	Hoya	-	borrowed
Linear polarizing filter for lights	Polarization.com	45,00	
Tripod	Quickset	-	borrowed
Scanning spray	Aesub	35,00	

### 2.2.1 Capture Device

General requirements for capturing device:

- Any camera will work, but the higher the resolution of the sensor and the lower amount of image noise, the better the results will be.
- Camera should allow manual settings of the exposure.
- Camera body should support interchangeable lenses, so quality lenses could be used.

#### Camera body

For the workflow, the Nikon D500 camera body was used (Fig. 4). It is a 20,9-megapixel (5599 x 3728 px) DSLR (digital single-lens reflex) camera using an APS-C sensor (DX format, 23,5 mm x 15,7 mm CMOS; 4,2  $\mu$ m pixel size), with ISO 100–51200.



Fig. 4: D500 Camera body

#### Lens

Prime lenses usually produce higher quality images. For this purpose, the Sigma 18-50mm f/2.8 EX DC lens was used (Fig. 5). This wide to normal angle zoom lens is designed for digital crop DSLR with an APS-C sized sensor. The lens offers good results for sharpness even if setting the aperture of f/16 or f/22. With Nikon

D500 camera body, the lens provides a field of view equivalent to a 27–75mm lens mounted on a 35mm frame body.



Fig. 5: Sigma 18-50 lens

Used zoom lens helped to cover the maximum part of the sensor with the photographed item without the necessity of moving the tripod.

### 2.2.2 Computer Hardware Specification

General requirements for computer hardware:

- Higher CPU core count – as in Reality Capture, the main used software, more than half of the computing processes use the CPU.
- RAM – the higher the RAM, the better, with 32 GB being the absolute minimum, 64 GB recommended and 128 GB or more allowing optimal performance.
- Storage – using SSD for fast read and write speeds. It is recommended to set the Cache location on a separate SSD, having at least 256 GB. Project files can be stored on a slower non-SSD drive.

The workstation of the following parameters was used for computing:

Processor:	Intel(R) Xeon(R) CPU E5-2670 0 @ 2.60GHz
Operating system:	Microsoft Windows 8.1 Pro 64-bit
Motherboard:	Asus Z9PE-D16
GPU:	Asus GeForce GTX 1080 Ti
RAM:	128 GB DDR3
Storage device:	SSD 256 GB (system disk) SSD 512 GB (dedicated to Cache for RC) 1 TB HDD (data storage)

### 2.2.3 Software

In last years there has been a boom in computer vision programs with Structure from Motion approach which makes the possibilities of creating 3D models and measurements from photos accessible to a wider audience. Simply put, the software matches features in the images, figures out the position and orientation of the camera for each photo and generates a very high density geometric model.

There is currently a large number of software on the market that are able to create a point cloud from the photos. These can be divided into the following types:

- **Free downloadable** – usually simple software for creating the models, doesn't contain lot of settings for the processing.
- **Commercial software** - calculates models directly on the user's computer. The advantage is the ability of the user to set-up each step of creating the model and influence the process according to specific needs and preferences. The disadvantage is the high demands on the hardware.
- **Cloud computing software** - the main disadvantage is the inability to influence the process. The problem also lies in the copyrights to the generated 3D models, which according to the License Agreement are acquired by companies operating the Cloud computing services.
- **Editing software** - used only for editing of the created models, both commercial and freely downloadable are available

**Tab.2: Overview of the most commonly used software:**

Software	Web	License	Price	Solution
RealityCapture	<a href="https://www.capturingreality.com">https://www.capturingreality.com</a>	commercial	19,99 EUR PPI license, 249 EUR/month PGM license and more	desktop
Agisoft Metashape Professional	<a href="http://www.agisoft.com/">http://www.agisoft.com/</a>	commercial	3499 USD	desktop
Photomodeler Premium	<a href="https://www.photomodeler.com/">https://www.photomodeler.com/</a>	commercial	2995 USD permanent version	desktop
3D Zephyr	<a href="https://www.3dflow.net/">https://www.3dflow.net/</a>	commercial	149 Eur Lite version, 2400 Eur Pro version	desktop
Autodesk Recap	<a href="https://www.autodesk.com/products/recap/overview">https://www.autodesk.com/products/recap/overview</a>	commercial	325 USD/year	online
ARC3D	<a href="https://www.arc3d.be/">https://www.arc3d.be/</a>	open-source	-	online
Pix4Dmapper Bentley ContextCapture	<a href="https://www.pix4d.com/">https://www.pix4d.com/</a> <a href="https://www.bentley.com/en/products/brands/contextcapture">https://www.bentley.com/en/products/brands/contextcapture</a>	commercial	216 Eur/month ? (only price quote)	desktop
VisualSFM	<a href="http://ccwu.me/vsfm/">http://ccwu.me/vsfm/</a>	open-source	-	desktop
Regard3D	<a href="http://www.regard3d.org/">http://www.regard3d.org/</a>	open-source	-	desktop
Meshlab	<a href="http://www.meshlab.net/">http://www.meshlab.net/</a>	open-source	-	desktop
CloudCompare	<a href="http://www.cloudcompare.org/">http://www.cloudcompare.org/</a>	open-source	-	desktop



For this assignment, in Tab. 3 is the list of used software:

**Tab.3: Used software**

Software	Supplier	Usage
RealityCapture	Capturing Reality	Creating photogrammetry meshes
DXO Photolab	DxO Labs	Processing and preparing RAW photos
CloudCompare	CloudCompare	Processing and comparison between points clouds or triangular meshes
MS Office	Microsoft	Writing this thesis

RealityCapture (also known as RC) is a photogrammetry software which creates 3D models out of unordered photographs (terrestrial and/or aerial) or laser scans without seams. Its features include image registration (alignment), automatic calibration, calculating a polygon mesh, colouring, texturing, parallel projections, georeferencing, coordinate system conversion, simplification, scaling, filtration, smoothing, measurement, inspection, and various exports and imports ([capturingreality.com](http://capturingreality.com)). Currently it is several times faster than any other software for photogrammetry.

#### 2.2.4 Other technical equipment

##### Turntable

For the photo acquisition, a DIY turntable was used (Fig. 6). It is a small programmable device, allowing to set the number of steps between shots and the number of shots. The turntable was connected directly to the camera so after each rotating step, a photo was taken. The advantage is that no manual intervention to turn the object after each exposure is required and photos are evenly distributed in the full rotation. The turntable is equipped with two diameters of platforms for different sizes of the photographed items, the small one is 120 mm, the large one with 350 mm diameter is painted in matt black colour.



**Fig. 6: Turntable**

##### Scale bars

The scale bar is placed next to the item during the photo session. It has to be present in at least three photos with the item, in order for the 3D model to be created in real proportion by the photogrammetry software.

For the purpose of this work, a small ID card-sized scale from Past Horizons (pasthorizonstools.com), (Fig. 7) was used with 80 mm black and white scale, 20 mm micro scale and rectification target with 50 mm x 20 mm reticules. It's printed on matte white, non-reflective rigid plastic.



Fig. 7: Scale bar

### Lights

Two Yongnuo YN600 Air 5500k Pro LED lights (Fig. 8) were used for illumination of the items. This light is made up of 192 SMD LEDs of ultra-high CRI (colour rendering index). The colour temperature is 5500 K, the luminous flux is 4000 lm and the luminance angle is 110° which ensures good diffused lighting of the items.



Fig. 8: LED light

### Backdrop

Heavy matt black fabric was used as a backdrop behind the photographed item. The backdrop creates a uniform background while hiding all extraneous elements, such as workspace, tabletops, etc.

### Polarizing filters

For one out of the three studied techniques/approaches, polarizing filters were used. Polarizing filters were mounted on both lights and the camera lens. The filters remove specular reflection and improve the image quality, increase the contrast and colour saturation while leaving the overall colour balance unaffected.

On the camera lens, the Hoya Pro1 circular PL filter was used.

On the lights, the PF006 linear polarizing filter film from Polarization.com was installed. This Polyvinyl Alcohol-Iodine filter is 0.15 mm thick, has no colour distortion (neutral) and very good polarization efficiency (99.9 %). It comes with a width of 43 cm and the size was cut to match the size of the LED light.

### Tripod

A heavy-duty Quickset 473010-7 tripod with 47211-6 head was used (Fig. 9). The tripod allows to take blur-free photos which can otherwise cause bad alignment and thus bad surface reconstruction.



Fig. 9: Quickset tripod

### Scanning spray

The sublimating scanning spray Aesub blue from Aesub (aesub.com) was used for one part of the photo acquisition (Fig. 10). It should create a thin and homogenous coating on the surface. The scanning spray should reduce specularity and improve the quality of models of shiny or translucent materials by creating more details on the surface. It is a vanishing or self-disappearing spray so the coating should disappear after a certain time, thus no cleaning should be required. The sublimation time depends on temperature, air flow, material and layer thickness, thicker coat of spray or multiple layers will stay longer. Different materials will have different evaporation times. After about 1 h certain parts start disappearing, after that it will take some more hours until the coat has completely disappeared, as stated by the manufacturer.

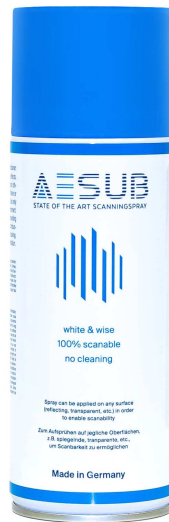
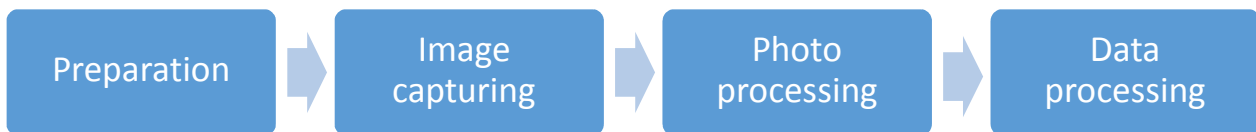


Fig. 10: Aesub scanning spray

### 2.3 General workflow

The general photogrammetrical workflow for scanning the items described in chapter 2.1 can be divided into the following subsections:



**Preparation** covers all the factors necessary for good reconstruction process that involve the decision about the methodology based on the project requirements, such as purpose of the final 3D model or required geometry resolution. Also the process is influenced by the scanning environment (studio or in situ), technical equipment and also the budget.

**Image capturing** is the main process of data acquisition based on the methodology from the Preparation step.

**Photo processing** covers all the process of converting of RAW files from the camera to JPEG format with recovering the information in highlights and shadows which is important for good alignment and mesh calculations as well as setting the proper white balance for recovering the true colour for texturing.

**Data processing** covers modelling of the digitized item through the aligning, mesh reconstruction, simplification, texturing and exporting of the final 3D model.

### 2.3.1 Description of the methodology

#### Definition of a 3D model

(Novaković et al. 2017) writes: “A digital three-dimensional (3D) model is a digital representation of the 3D geometry of an object. The three geometrical dimensions are usually represented in a Cartesian coordinate system with three perpendicular axes: X, Y and Z. Virtual environment enables viewing of a 3D model from all possible directions, rotating the 3D model, zooming, creating cross-sections, measuring and other operations.”

(Tobler et al. 2006) describes the 3D surface geometry: “The 3d surface geometry can be represented in several ways, mostly by polygonal meshes. The 3D polygon mesh model consists of linked polygon facets (also known as faces) that represent 3D surface of a specific form. The line segments that link the faces are called edges, and the point where the edges meet is called vertex”.

3D models are mostly created of triangular (tris) or quadrilateral (quads) polygons, a triangle consists of a triangular face, three edges and three vertices. 3D model is further represented by the texture. The texture is created by projecting a 2D image to the 3D model.

#### Structure from Motion

The Structure from Motion (SfM) is a photogrammetric range imaging technique for estimating and recovering the 3D structure of objects from 2D transformations of their projected images when no 3D information is conveyed by the individual projections. In biological vision, SfM refers to the phenomenon by which humans (and other living creatures) can recover 3D structure from the projected 2D (retinal) motion field of a moving object or scene (Ullman 1979).

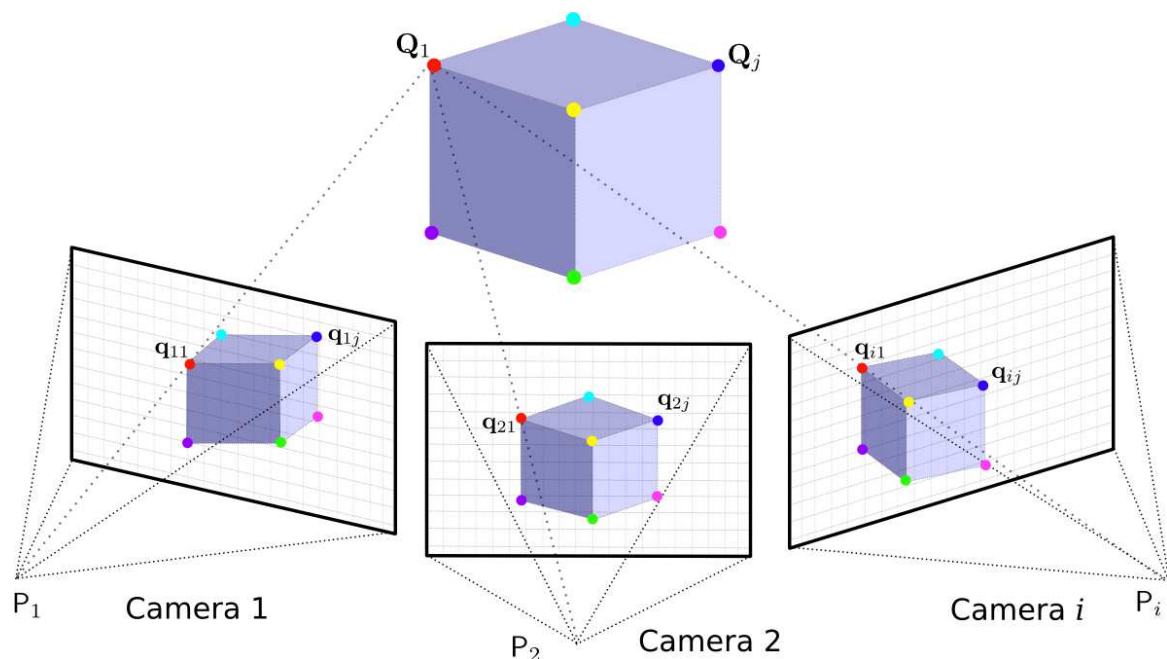


Fig. 11: SfM principle

SfM method is used by modern software for photogrammetry. The software uses various multi-viewpoint stereo algorithms to analyse the set of photos, calculates the relative position and orientation of the camera

in each photo with regard to the position of the scanned object and generates the point cloud of key points representing the same feature in more than two overlapping photos. The spatial coordinates and the position of the camera are determined by the trajectory of these points, how light travels from the object through the optical system of the camera. (Fig. 11), (Michot 2010). Processing time depends mainly on the performance of the computer (especially the processor and RAM).

### 2.3.2 Proposed workflow

The two objects described in Chapter 2.1 were selected for their characteristics, which are very common in the cultural heritage field and also known to be problematic for non-contact optical measuring systems.

The figure below (Fig. 12) shows a flowchart of the work process used for each object. Basically the workflow is the same for all three used methods, just the workflow of scanning spray model and CPL model were connected, as after taking the sprayed photos, the sprayed surface of the items was left to evaporate and the series of CPL photos was taken directly after, without any movement of the object on the turntable. This way, the CPL photos were used as the basis for creating the texture of the scanning spray model, as this model was white during photo shooting, i.e. not suitable for image acquisition for the texture.

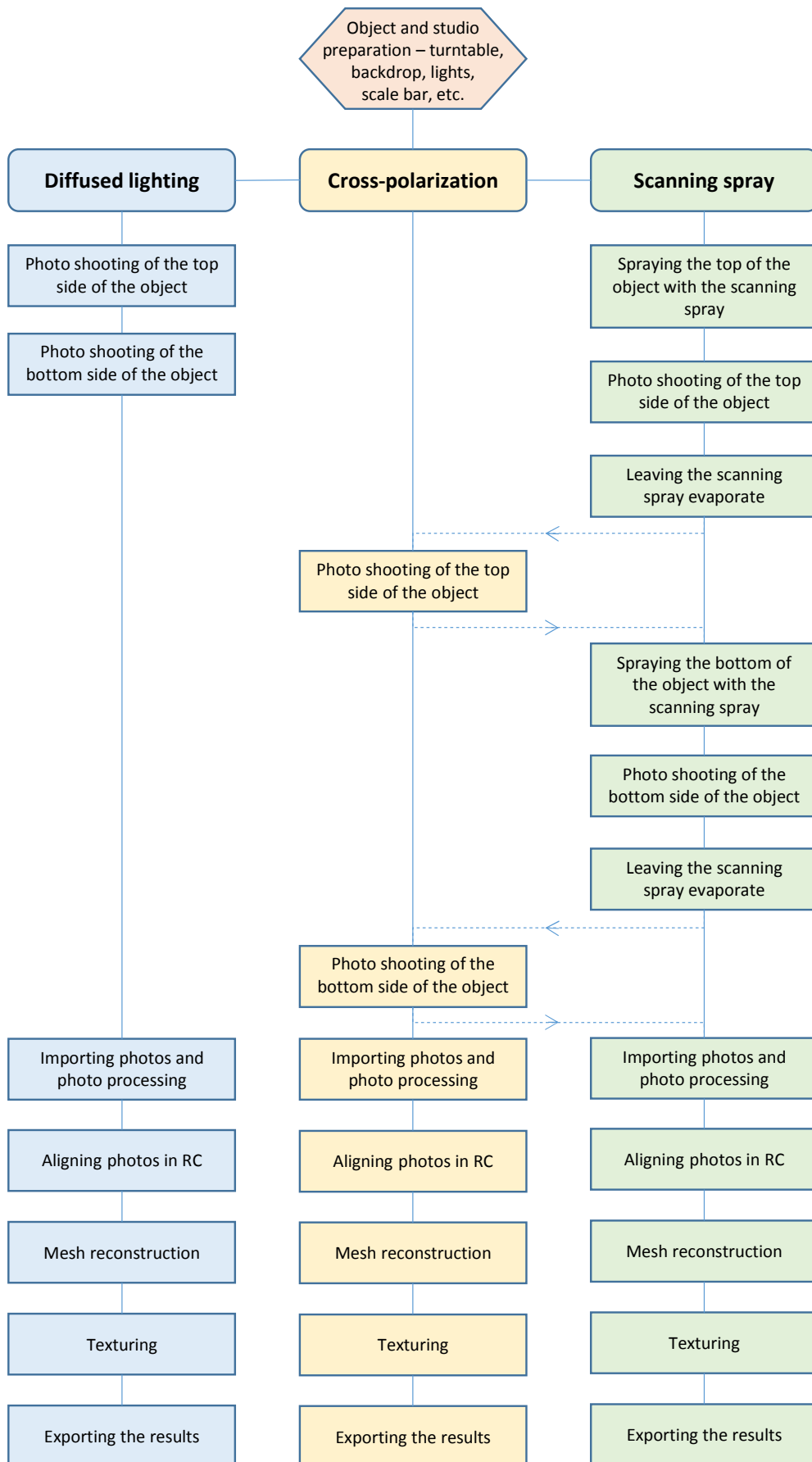


Fig. 12: Workflow flowchart

## 2.4 Object and Studio Preparation

Depending on the size of the scanned items, these can be either transported to the location where the scanning takes place or the scanning equipment can be taken to the place of location of large or valuable items, such as statues, tombs, buildings, items in museums, etc. It is also important to determine under which conditions the scanning will take place and whether there are some scanning restrictions while establishing what kind of lighting of the objects would be most suitable.

There are two basic methods of scanning objects:

- **The walk-around method.** As the name describes, the camera moves around the scanned object. The photos are taken in a several 360 degrees rings from different heights with at least 30 photos per one ring. This method is used for large objects outdoors, but also for small objects indoors which cannot be moved into the studio, eg. in museum.
- **The turntable method.** In this method, the object is placed on a base that rotates while the camera is mounted on a tripod. There are several 360 degree shooting rings from different heights (above and below the object) with at least 30 photos per ring. The position of the object can be changed to take the photos of all sides of the object (eg. top and bottom). Monochrome background is necessary to facilitate easier aligning of the photos. This method is suitable for portable objects located in the studio.

The process of taking photos of the items is based on the turntable method. In this method, the camera is on the tripod, the item is positioned on a turntable or rotating platform and is rotated with a small angle between the shots. This method is suitable for portable and not too heavy items (according to the turntable limit) which can be positioned on the turntable. The camera is always aimed at the vertical axis of the turntable the series of photos forms a circle around the item. The item is lit by two lights, the platform of the turntable is matt black and a black backdrop ensures featureless background.

In the Fig. 13 is a scheme of the studio with the turntable and equipment. Polarizing filters were used only for one part of the assignment.



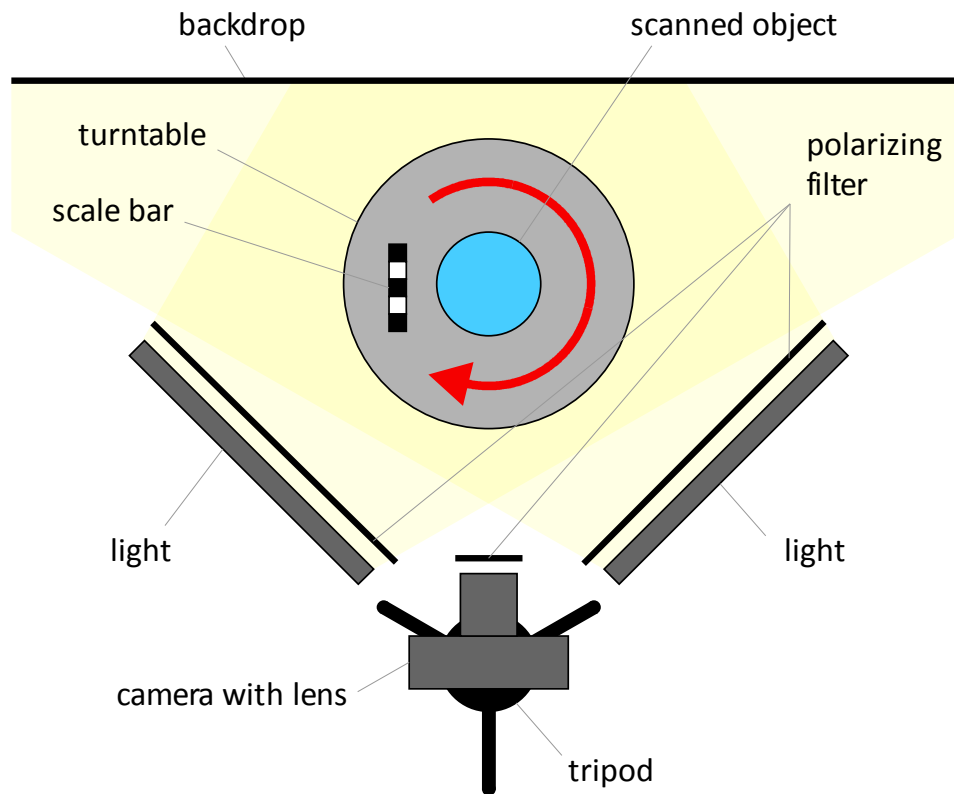


Fig. 13: Scheme of the studio

#### 2.4.1 Defining the Parameters of the Photo Session

The resolution of the 3D models is essential for documentation and research. Current DSLR cameras allow creating models with a resolution measured in tens to hundreds of micrometers (Falkingham 2012). According to (Ray 2002), for an image viewed at near distance of distinct vision ( $\approx 250$  mm), any subject detail resolved and recorded optically within an image circle of 0,2-0,3 mm diameter may not be perceived. It means, that the details of maximum this size should be visible on the final 3D model.

It is important to define the resolution that we can achieve with used photo gear and define the shooting distance from the item and between the photos. The resolution is different if the 3D model is used for virtual presentation, when low resolution is required or for archiving purposes (digital copy). For the purpose of archiving the 3D models of cultural objects (Kulíková 2009) is recommended the resolution of 0,1 mm or higher.

The final resolution of the model depends on the resolution of the camera's sensor and the distance between the sensor and the photographed item. The closer the camera is, the higher the resolution can be. However if the camera is too close, so that only a part of the item is visible in the photos, then a higher number of photos is required to cover the whole item, requiring longer processing time while alignment errors could also appear during the processing.

If we know the size of the pixel of the sensor  $p$  of used camera, focal length  $f$  of the used lens and required size of detail on the surface of the item (also known as the ground sampling distance - GSD), we can calculate the maximum working distance  $d$  (Fig. 14).

GSD represents the distance between two consecutive pixel centres measured on the ground (in our case on the surface of the item). The lower the value of the GSD, the bigger the spatial resolution of the image and the more visible details. For example, a GSD of 1 mm means that one pixel in the photo represents linearly 1 mm on the ground/surface.

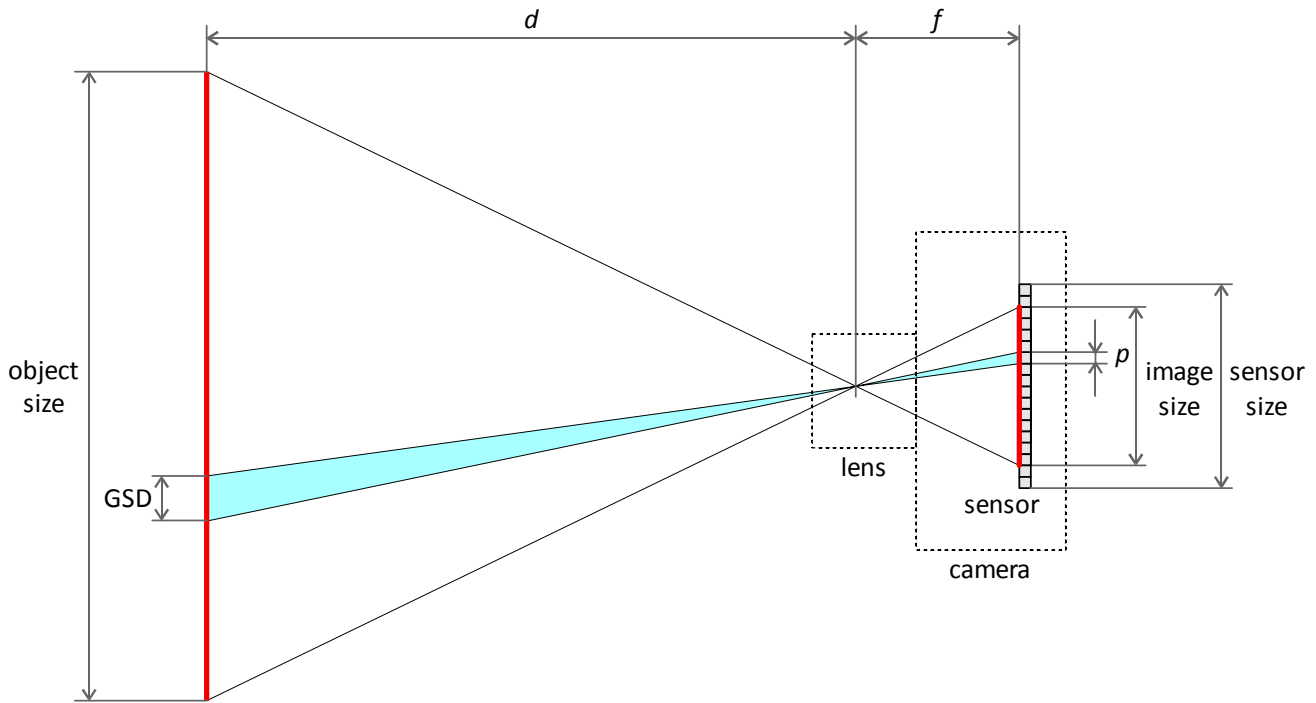


Fig. 14: Scale of the object and the image

The ratio between the size of the object and the image is the same as the ratio between the object distance  $d$  and focal length  $f$ . The same ratio is between the size of the pixel  $p$  on the image sensor and the size of the pixel (detail) GSD on the surface of the item:

$$GSD = \frac{d}{f} \cdot p \quad (m)$$

So the object distance can be expressed as:

$$d = \frac{GSD}{p} \cdot f \quad (m)$$

For this work, Nikon D500 camera was used. The image sensor size of this camera is 23,5 mm x 15,7 mm with maximum resolution of 5599 x 3728 pixels, so the horizontal pixel size  $p$  is  $23,5/5599 = 0,0042$  mm (4,2  $\mu$ m or 0,0000042 m). Pixels are squared, so the same result is also for the vertical pixel size.

The focal length  $f$  was set to 35 mm in order to fill the picture optimally with the whole object. The average distance  $d$  from the object 1 is 0,4 m.

If the target GSD is 0,1 mm (0,0001 m), the object distance  $d$  according to the above formula should be less than:

$$d = \frac{0,0001}{0,0000042} \cdot 0,035 = 0,83 \quad (\text{m})$$

The real object distance will be shorter in order to fill the photo as much as possible with the object on given focal length. For this purpose, the real object distance  $d$  will be 0,4 m for the object 1. For this object distance, the GSD will be:

$$GSD = \frac{0,4}{0,035} \cdot 0,0000042 = 0,000048 \quad (\text{m})$$

It means that the GSD on the final 3D model of Object 1 taken with described camera and lens with given shooting distance should be 0,048 mm. For Object 2, which is larger than Object 1, the real object distance  $d$  will be 0,6 m. Using the same formula above, the GSD on the final 3D model of Object 2 should be 0,072 mm.

### Photo-shooting Scenario

As mentioned before, 36 photos were taken in one rotation of the turntable. Also, it is necessary to take the photos from different angles in elevation. These photo sets were taken in 20 degrees elevation intervals, as seen in the scheme in Fig. 15.

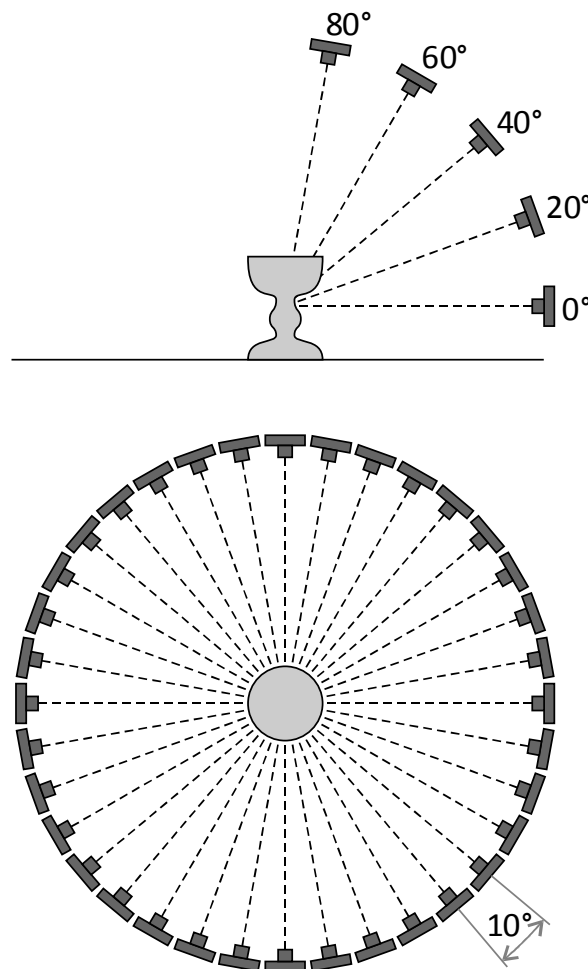


Fig. 15: Definition of the steps and angles between the photo shoots

For Object 1 (Ciborium) the elevations from 0° to 80° were used to capture also the interior part of the cup. For Object 2 (Crucifix), elevations from 0° to 60° were used, as it was not necessary to capture the images at 80° as the top parts of the object were already visible at 60° elevation. For Object 2, also a series of detailed images of the statue and embossment on the base were taken.

After the photo session was finished, the orientation of the object was changed upside down to capture the images also from the bottom side. Thus the upper and bottom parts of the object were merged to create a single object.

## 2.5 Image Capturing

The most important element of the photogrammetry process is acquiring good quality data, i.e. images. If the input is not decent, neither the result can be satisfactory. It's similar to the general principle in the information sciences: "GIGO" - Garbage In, Garbage Out. So the quality of the photos directly impacts the quality of the final model. There are several rules, which are helpful to follow in order to align photos in later reconstruction well.

General rules:

- Photogrammetry software require sharp, clean and evenly lit photos.
- It is always better to take more photos than less. Too few photos result in bad alignment and gaps in the model.
- Any detail which has not been captured on the photo, will not show on the final model, therefore it is necessary to capture systematically the whole surface of an object.
- Photos should be taken with at least 60 % overlap.
- Each point on the item surface should be visible on at least three angles as aligning of the photos requires parallax (i.e. different positions and angles) between the photos.
- It is beneficial to start with taking pictures of the whole object first and then move gradually to details.
- The view point shouldn't be changed more than 30° between two consecutive shots
- The photos around the item should create a complete loop in a circular way with the item in the centre.
- The picture frame should be filled with the object
- During the photo session, no moving of the objects is allowed between the shots, such as changing the position of the scale bar, adding anything in the background etc.
- For capturing the top and bottom part of the item, multiple acquisitions are required.

For scaling the 3D model, a reference scale bar is placed next to the item on the turntable during the photo session and cannot be moved relative to the item. The scale bar must be at least on three photos, keeping it for the whole session is better for aligning. When taking another set of photos, e.g. of the bottom side, the scale bar has to be removed. Otherwise the aligning of the photos would be not possible.

Fig. 16 shows capturing of the Object 1 positioned on the turntable with the scale bar, lit by the diffused light and with black backdrop in the background.



Fig. 16: Capturing the object 1

### 2.5.1 Camera Settings

For the best capturing of the initial data, proper setup of the camera is essential. Generally, the following practices should be followed:

- Manual camera settings
- ISO values should be as low as possible in order to minimize the amount of noise in each photo
- To keep a bigger depth of field, higher  $f$  numbers should be set
- Always shooting in RAW image format

The exposure can generally be adjusted using the three basic parameters – exposure time, aperture and ISO. The same exposure can be achieved by a combination of all three parameters, but the photo will be different, depending on what result or goal has to be achieved.

#### Exposure Time

The exposure time (or shutter speed) determines how long the shutter is open and the sensor is exposed to the light coming from the photographed scene. The exposure time is adjustable to the values of the rounded square of 2 (1/1000, 1/500, 1/250, 1/125, 1/60, 1/30, 1/15, 1/8, 1/4, 1/2, 1, 2, 4, 8, 15, etc.), where increasing the time by one value leads to doubling of the exposure.

The shutter speed needs to be short in order to avoid motion blur. Using the tripod allows to use longer shutter speeds which is necessary under low light conditions.

## Aperture

The aperture can be defined as the diameter of the hole through which the light passes through the lens, so it is a physical limitation on the amount of light coming into the sensor. The aperture is expressed in f-numbers (e.g. 1, 1,4, 2, 2,8, 4, 5,6, 8, 11, 16, 22). When changed by one value higher, the exposure is halved. Generally,  $f$  numbers between  $f/5,6$  –  $f/8$  are optimal with regards to sharpness or depth of field for most of the lens.

## ISO

In both analogue or digital photography, ISO defines the light sensitivity of either the film or imaging sensor. In digital photography, ISO represents the amplification of the signal from the sensor, directly affecting the amount of noise in the sensor. If ISO is increased twice (e.g. from ISO 100 to ISO 200), only half of the light-induced energy is sufficient for the same exposure, so the shutter speed can be halved, e.g. 1/500 instead of 1/250 (if the aperture is not changed). ISO affects the photo quality, with a higher ISO resulting in noisy or “grainy” photos, while a lower ISO value gives low noise in the photos.

As mentioned before, ISO values should be set as low as possible to minimize the amount of noise in photos, as during aligning the photos in the photogrammetry software this noise can be interpreted as a feature and then cause errors, decrease the accuracy or noise in the 3D model surface.

In Tab. 4 is an overview of used settings of ISO, exposure time and aperture for each photo acquisition of both objects:

**Tab.4: Used camera settings during the workflow**

Object 1	ISO	Exposure time	Aperture
Diffused light	100	1/8	f/13
Cross-polarization	400	1/2	f/13
Scanning spray	200	1/8	f/13

Object2	ISO	Exposure time	Aperture
Diffused light	200	1/4	f/13
Cross-polarization	800	1/2	f/13
Scanning spray	200	1/4	f/13

## Focal Length

The focal length also has the effect of reducing the amount of light incident on the sensor. When the focal length is doubled, the amount of incident light drops four times.

## Focus and Sharpness

Focus is very important, as the out-of-focus photos would process poor reconstruction with errors and noise. Also, for the reconstruction, sharp images are very important but the sharpness has to be a result of quality lens and not photo post-processing.

## RAW Format

It's necessary to shoot the photos in RAW format than straight in JPEG. RAW files can be converted in post-processing software, eg. Adobe Photoshop or DXO Photolab and much better quality can be obtained than shooting directly in JPEG format.

## Depth of Field

Depth of field (DOF) is the distance between the nearest and the farthest objects that are in acceptably sharp focus in the photo. The factors which influences the depth of field is the focal length, distance to the object and aperture. Large apertures (small  $f$  numbers) produce a very shallow depth of field and small apertures (large  $f$  numbers) produce photos with a bigger depth of field.

Recommended tool for calculating the depth of field according to selected focal length, aperture and distance is the Depth of Field Calculator for Windows or Android (DoF), Fig. 17.

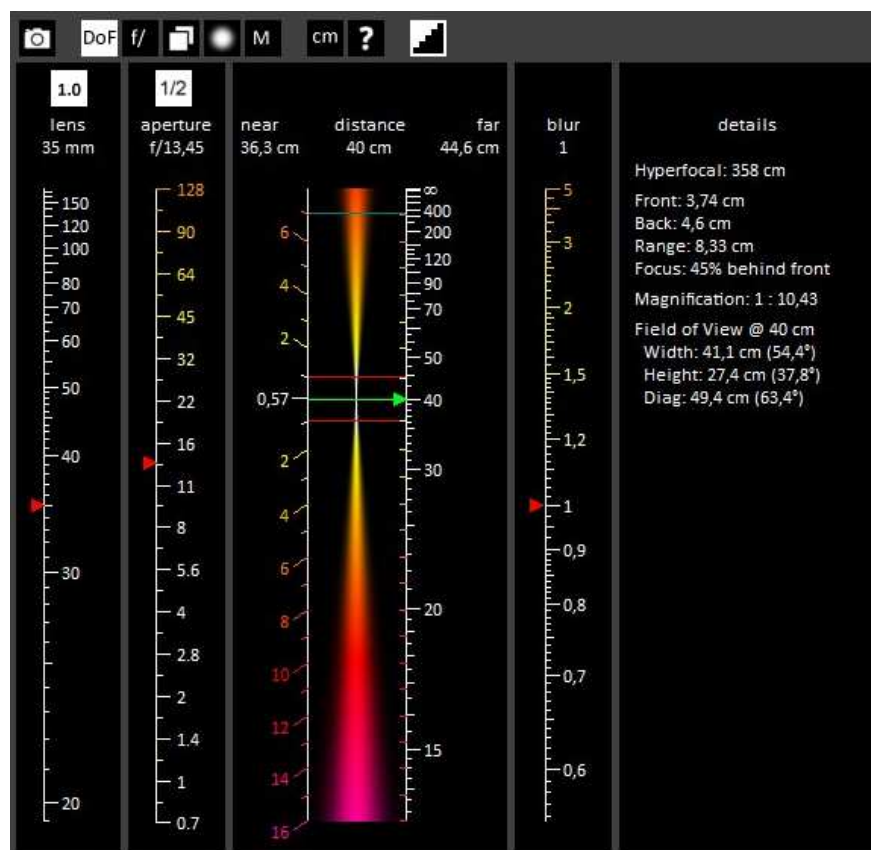
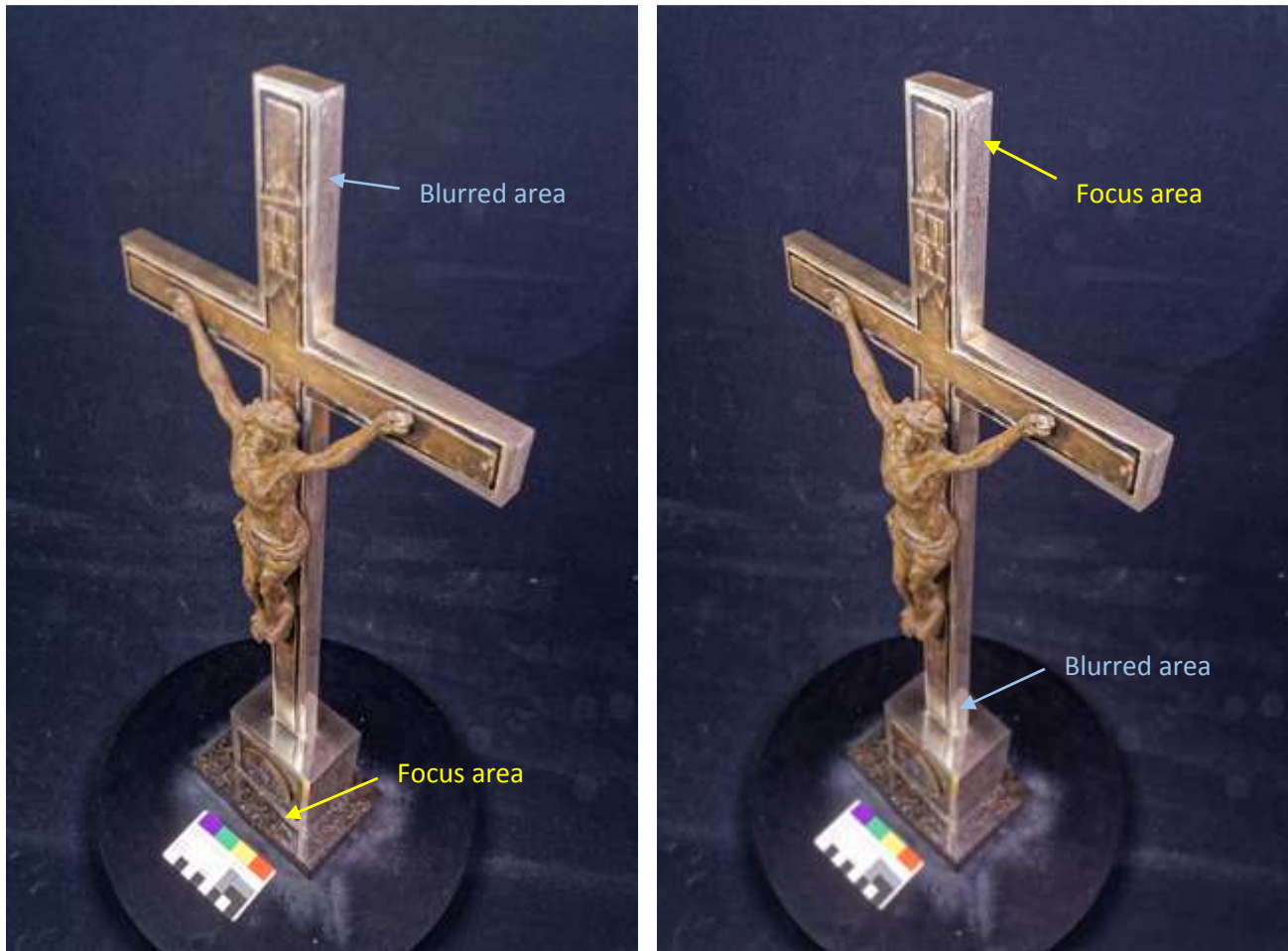


Fig. 17: Depth of Field Calculator for Windows

In the picture is a setting of focal length 35 mm, aperture  $f/13$  and distance 40 cm. The calculated depth of field, where the image is still sharp is from 36,3 to 44,6 cm.

On the Fig. 18 is a comparison of two photos in the same position but with different focus. On the left, the camera was focused on the bottom of the object and the top is blurred. On the right photo, camera was focused on the top of the object while the bottom of the object is blurred.



**Fig. 18:** Examples of short depth of field on object 2

Small depth of field can increase errors in alignment and noise level in the final mesh models, as matching of the points out of focus is more difficult.

Due to the small depth of field, it was necessary to shoot several sets of photos with different focus distance. In the Tab. 5 and Tab. 6 is an overview of the number of photo sets (one rotation is 36 photos) with different focus for each photo acquisition and elevation of both objects:



**Tab.5: Number of photos for each elevation for Object 1:**

Elevation	Diffused light	Cross-polarization	Scanning spray
top 0°	2x36	2x36	2x36
top 20°	5x36	5x36	5x36
top 40°	6x36	6x36	6x36
top 60°	5x36	6x36	6x36
top 80°	3x36	3x36 + 2x36 details	3x36 + 2x36 details
bottom 0°	2x36	2x36	2x36
bottom 20°	5x36	5x36	5x36
bottom 40°	6x36	6x36	6x36
bottom 60°	6x36	5x36	5x36
bottom 80°	3x36	3x36	3x36
<b>Total</b>	<b>1548</b>	<b>1620</b>	<b>1620</b>

**Tab.6: Number of photos for each elevation for Object 2:**

Elevation	Diffused light	Cross-polarization	Scanning spray
top 0°	2x36 +3x36 details	2x36 +3x36 details	2x36 +3x36 details
top 20°	4x36 + 3x36 details	4x36 + 3x36 details	4x36 + 3x36 details
top 40°	4x36 + 3x36 details	5x36 + 3x36 details	4x36 + 3x36 details
top 60°	4x36	4x36	4x36
bottom 0°	2x36	2x36	2x36
bottom 20°	2x36	2x36	2x36
bottom 40°	2x36	2x36	2x36 +15 detail
bottom 60°	3x36	3x36	2x36
<b>Total</b>	<b>1476</b>	<b>1512</b>	<b>1434</b>

### 2.5.2 Data Acquisition Variants

#### Diffused Light, No Polarization

The best lighting conditions can be achieved with a light source generating diffuse light. This can be attained either outside during a cloudy day or in the studio using various diffusers, i.e. translucent plastic sheets. The light has to be even with no big differences in luminance, such as sharp shadows or highlights. Used LED lights created favourable diffused light which illuminated the objects evenly.

The photo shooting was taken in a completely dark studio, with two LED lights used as the only source for the illumination of the object, as can be seen on the scheme in Fig. 13. This allowed avoiding any other light sources on the specular surface.

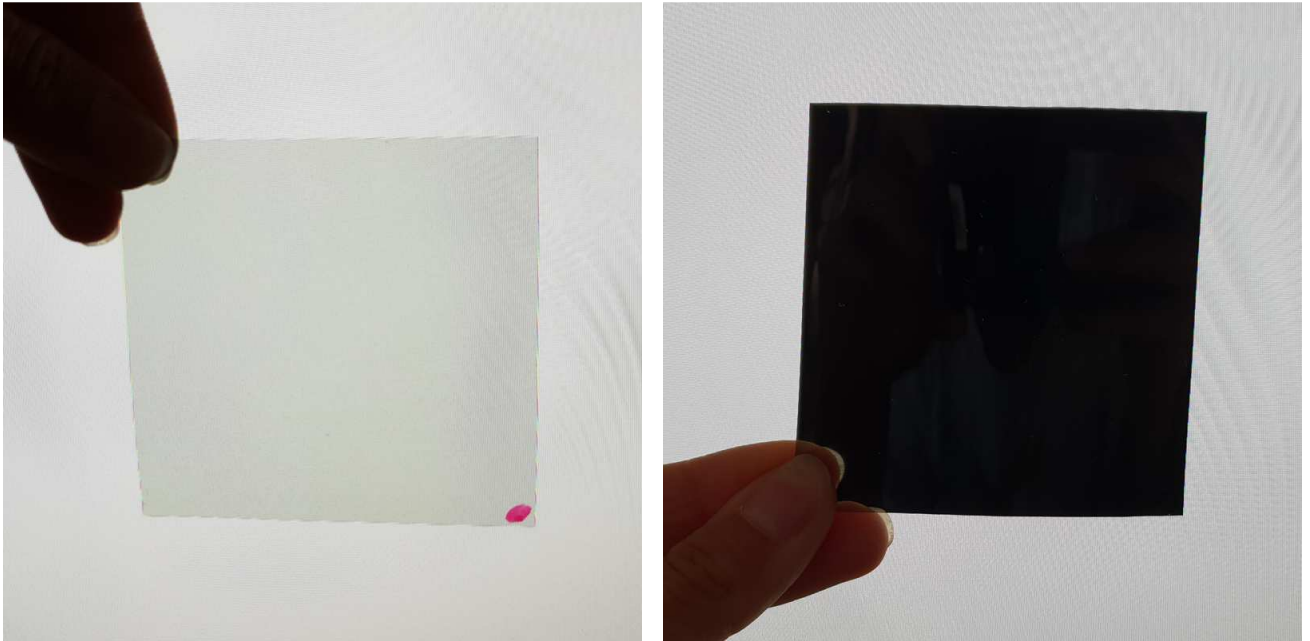


Fig. 19: Object 1 and 2 with diffused light

### Cross-polarization

Cross polarized photography is a technique used to filter the specular reflectance from the object in the photo. To minimize specular highlights, circular polarizers were applied to camera lens and linear polarizers were applied to LED lights.

Linear polarization filters allow the transmission of one axis of polarization but either reflect or absorb the perpendicular axis. If a second linear polarizer is placed in series, the maximum transmission of light occurs when the polarization axes of the two polarizers are parallel and minimal transmission occurs when their axes are perpendicular. This can reduce almost all specular reflected light.



**Fig. 20: Orientation of the polarizing filter**

On Fig. 20 is the example of the orientation of the polarizing filter in front of LCD screen. LCD screens use linear polarizing filters. If another filter is added with an angle of  $0^\circ$ , the light passes through, but if the filter is rotated  $90^\circ$ , the light is blocked.

Cross polarization increases saturation and contrast, however some reflection can still remain in the spots of strong specular reflection in the form of blue colour, as can be seen on the aluminium foil in Fig. 21 on the right photo, where the filters are crossed, while on the left photo, the filters are parallel.



**Fig. 21: Comparison of parallel and crossed filters**

Fig. 22 and 23 shows the effect of the photos taken with and without cross polarization on both objects. Specular reflection is suppressed, colours are more saturated and lighting more homogeneous all over the object.



**Fig. 22: Comparison of the photos of object 1 with diffused light and cross-polarization**

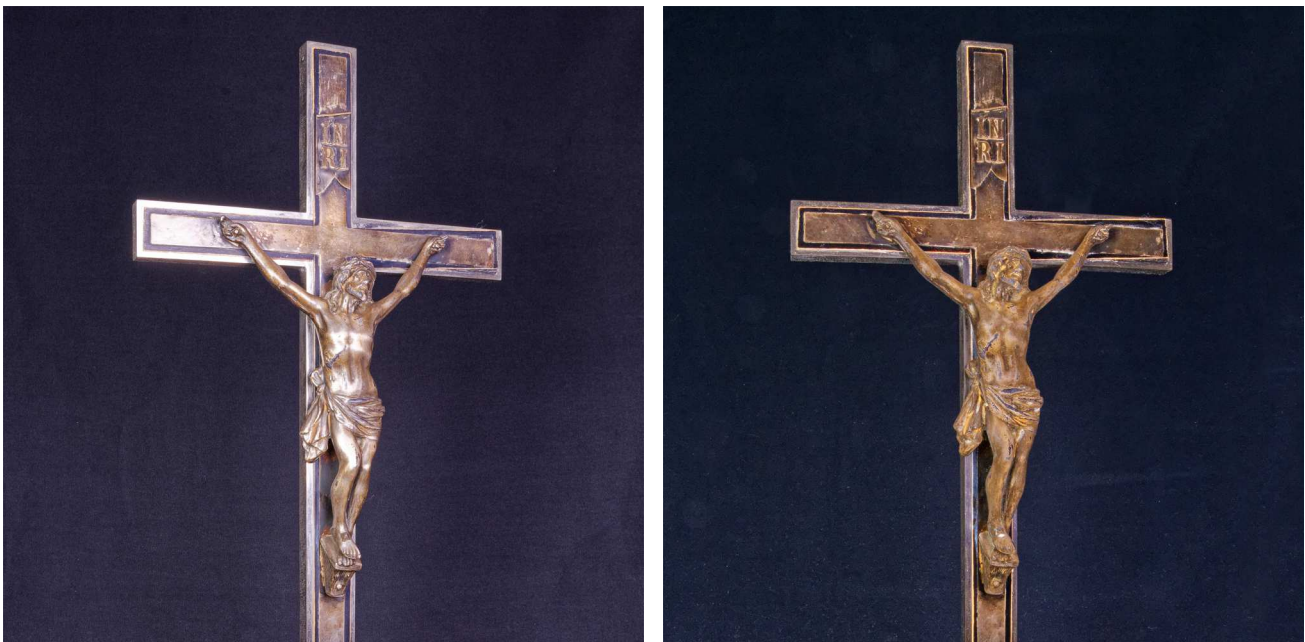


**Fig. 23: Comparison of the photos of object 2 with diffused light and cross-polarization**

Polarization reduces the amount of light passing through the lens to the sensor, about 3 f-stops, thus longer exposure time or smaller aperture number has to be used.

## Coatings

Coatings are used to change shiny surface of the object to matt. They help to create the model, however for texturing, it's necessary to take another set of photos without the coating. This is not necessary, if just the geometry without the texture is required.

Very important is not to move the item between the photo shooting with and without the coating. Any slight movement could render it impossible to align both sets of photos together.

For this purpose, various coatings are used, such as talc dust, scanning spray, anti-fungal foot spray, chalk spray, baby powder.

For this work, only scanning spray was allowed to be used on the surface of the objects, as it should disappear after certain time without leaving any residues on the surface. Other materials would require cleaning after the photo shooting.

On Fig. 24 and 25 is the comparison of the photos of both objects with diffused light and covered with the scanning spray.



**Fig. 24:** Comparison of the photos of Object 1 with diffused light (left) and covered with the scanning spray (right)

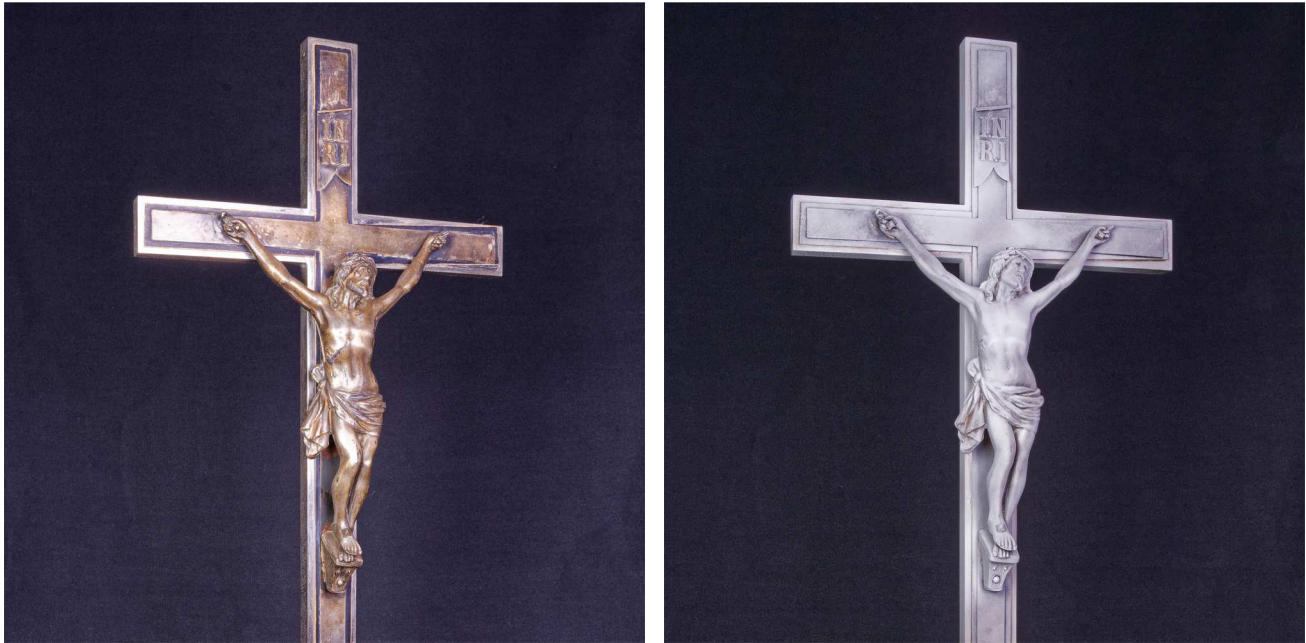


Fig. 25: Comparison of the photos of Object 2 with diffused light (left) and covered with the scanning spray (right)

## 2.6 Photo Processing

The RAW files from the camera were converted into JPEG format using the DxO Photolab software. Specific settings were applied to all photos.

Setting the white balance is important for getting the true colour for texturing. The colour temperature of used lights was 5500 K which was set in DxO. Corrections can be also done using colour charts.

For good alignment and mesh calculation it is important to recover the information in highlights and shadows. Selective tone mapping allows to recover details by selective adjustments of highlights, midtones, shadows and blacks. The option *Highlights* recovers, as the name suggests, the highlights of the image, *Midtones* controls the brightness of the levels located in the middle of the histogram, while *Shadows* controls the brightness of dark areas and *Blacks* sets the black point, which represent the left end of the histogram (dxo.com).

DXO Smart Lighting optimizes the dynamic range of the photo and unblocks the shadows by preserving the light areas and recovers details. *MicroContrast* improves the contrast of small details of the photo which looks like sharpness adjustment, without getting the artefacts around the edges as is usual when sharpening. Noise reduction decreases the noise – colour artefacts and grain.

On Fig. 26 is the screenshot from the DxO Photolab with the selected photo displayed before and after adjustments for comparison. It is important to apply the same adjustments for all photos in one processing batch.



**Fig. 26: Comparison of the photo before and after adjustments in DxO Photolab**

Also very important is not to apply the lens distortion corrections. The photos have to be undistorted for the aligning and mesh calculations.

For the workflows of the diffused light and cross-polarization photos, two sets of photos were made from RAW files. One set for alignment and reconstruction and the second set for texturing. The set for alignment had increased contrast for better process, the set for texturing had lowered brightness of the highlights and added brightness to the shadows and darks, in order to eliminate ambient shadows.

For the workflow of scanning spray photos, there were two sets of photos, one with the object covered with the scanning spray and the other without. The set with scanning spray was processed with increased contrast, while the second set was processed only for texturing.

## 2.7 Data Processing Workflow using Reality Capture

Processing of photos with Reality Capture Software (RC) covers the following main steps:

- aligning photos
- mesh reconstruction
- simplification
- generating texture
- exporting results

These steps were used for each object and method (diffused light, cross-polarization and scanning spray).

RC uses a system Temp folder for all temporary files created during the processing and for speeding up the calculations, it is better to set a cache location to a separate SSD. The amount of temporary data is about 350-450 GB for a project, so it's suggested to have at least 512 GB SSD. After one project is finished, it is necessary to clear the cache before starting next project.

### 2.7.1 Aligning

Aligning photos is a process during which the software analyses a set of photos and calculates the position and orientation of the camera in each photo with regard to the position of the scanned object. When the images are aligned (registered), the result is the sparse point cloud and also it's possible to see the position of all cameras or the path when moving and taking the photos. The point cloud is a visualization of grid points that carries information about the metric component of the model in space.

Aligning was the same process for both objects, while the two methods of diffused light and cross polarization had the same workflow, the difference was only with scanning spray photos.

For the diffused light and cross polarization method workflows, two sets of photos were prepared in DxO Photolab, as was described in the chapter 2.6. One set for alignment and reconstruction and the second set for texturing.

For the scanning spray method workflow, two sets of photos were taken, one white sprayed set for alignment and reconstruction and second non-sprayed set for texturing (set of CPL photos were used).

In RC, aligning of the photos is, after importing the photos, simply done by clicking on Align images button. The default Alignment settings are suitable for most projects, but they can be tweaked up to get better results.

*Max features per mpx* defines how many feature points can be detected per 1 Mpix, for smaller objects it can be set to 20000.

*Max features per image* was set to 80000 in order to detect more features on each photo.

*Preselector features* was set to 40000 (half of the max features per image, so the half of the best detected features was used for alignment process).

*Image overlap* – by default it is set to Medium and defines how the object is covered by the photos and in what area size the features will be recognized, for our workflow it was set to Low.

*Detector sensitivity* defines how the features of the object are fine and how RC will detect them. For textures with enough contrast features, eg. granite surface, Low sensitivity can be used, for textures with low amount of features, eg. blank surface of the pottery, High sensitivity can be used.





Fig. 27: Alignment settings used for the workflows

If the photos are taken correctly, RC can align all images as one single component which contains all aligned photos. If there are more components (usually the others contain just a few photos), it's better to run alignment again, so RC will refine the main component, or manually enter the control points and run alignment again. Control points can be defined manually, each control point has to be on at least 3 photos.

Aligning of the photos for each object was split into two separate parts – top part and bottom part of the object. Each part was aligned separately and later both parts were aligned together. Each part (top and bottom part) was after alignment exported as a separate component. Then, both components were imported and aligned together while in the Alignment settings, *Merge components only* was set to Yes. Aligning components separately and joining them later together shortened the alignment process.

### Aligning of the diffused light photos

#### Object 1:

On Fig. 28 are the screenshot from alignment of top and bottom parts and on Fig. 29 are both top and bottom components aligned together:

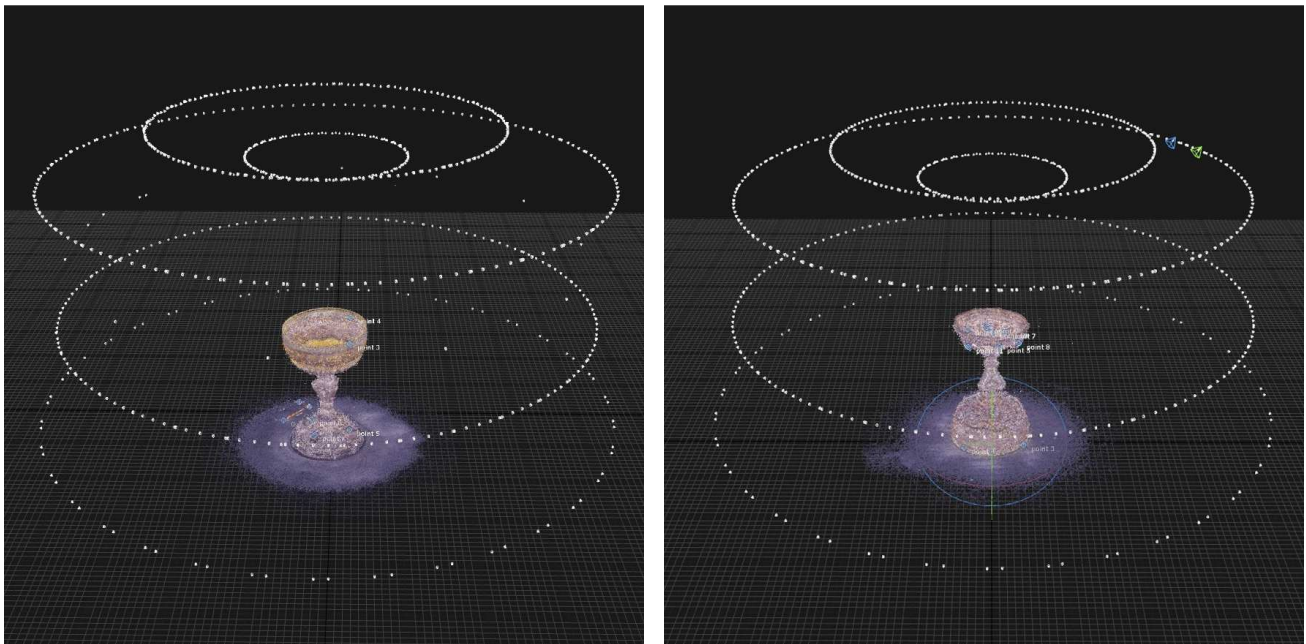


Fig. 28: Alignment of top and bottom parts of Object 1

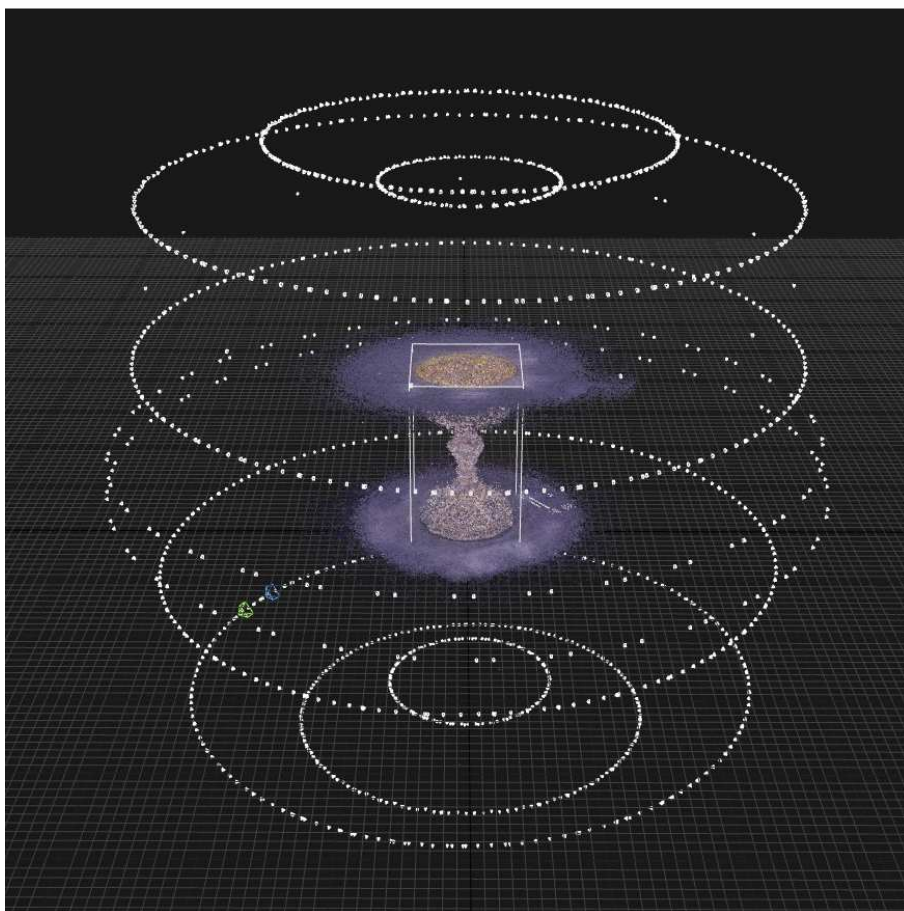


Fig. 29: Alignment of the top and bottom components of Object 1

The quality of the alignment can be checked in RC in the Alignment report, the results are displayed in Tab. 7:

**Tab.7: Alignment report for the object 1**

Number of aligned photos	1526
Point count	6 877 467
Total projections	27 088 383
Average track length	3.937551
Median error (pixels)	0.210109

*Point count* represents the number of generated points of a model during the alignment. The higher number, the better.

*Total projections* number shows how many times are 3D points seen in images.

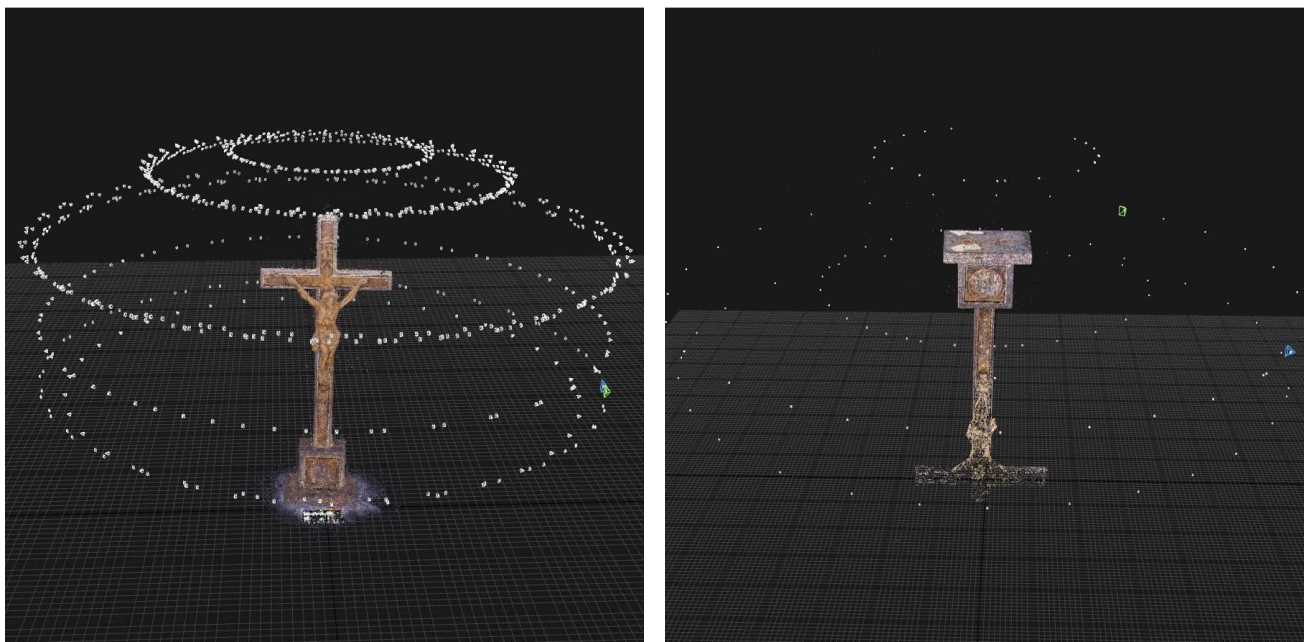
*Average track length* shows, in how many photos a point appears. The higher the number, the better, anything over 3 is considered as a good result.

*Median error* indicates that half of the point projection error is better than the shown number of pixels. Ideally, the number under 0,6 px is considered as a good result.

### Object 2:

Object 2 was a little bit tricky when taking the photos of the bottom side. As it was not standing by itself on the top of the cross, it was necessary to attach it in the vice which was covered with black cloth so that it is not visible. The whole assembly was too heavy for automatic rotating of the turntable, so the rotation and photo shooting was performed manually. Some additional photos of the bottom of the base were added during alignment of both components together.

On Fig. 30 are the screenshot from alignment of top and bottom parts and on Fig. 31 are both top and bottom components aligned together:

**Fig. 30: Alignment of top and bottom parts of Object 2**

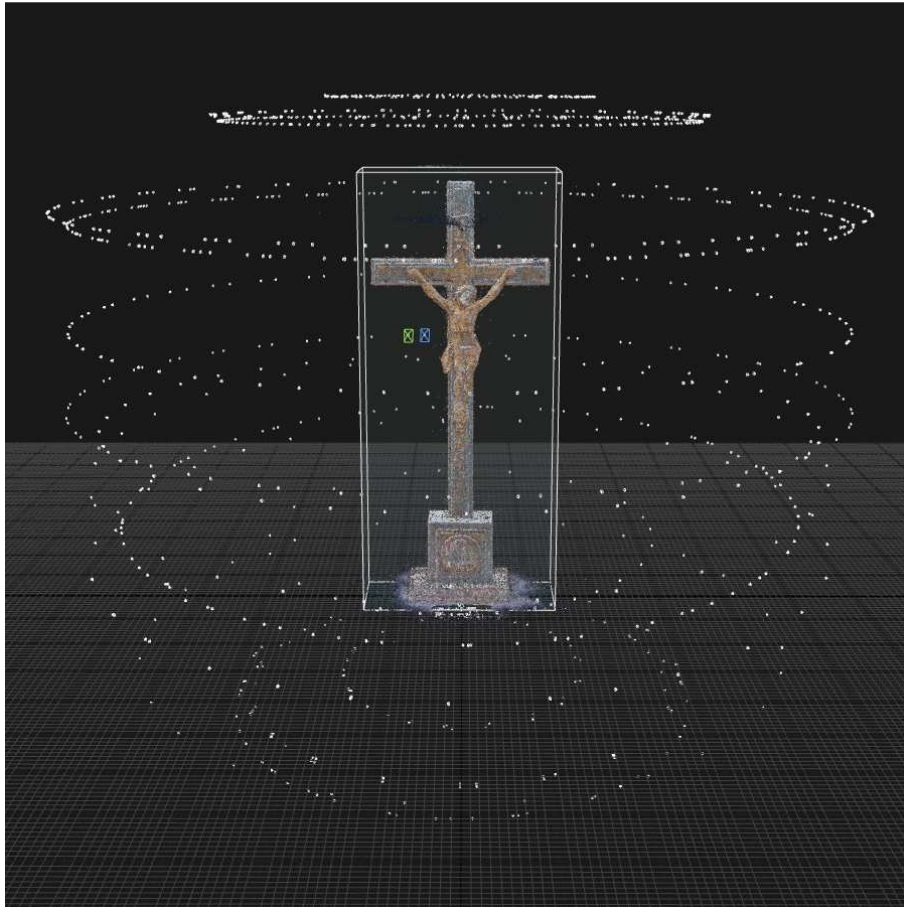


Fig. 31: Alignment of the top and bottom components of Object 2

Tab.8: Alignment report for Object 2

Number of aligned photos	1426
Point count	4103806
Total projections	14166000
Average track length	3,451676
Median error (pixels)	0,313502

### Aligning of Cross-polarization Photos

#### Object 1:

On Fig. 32 is the screenshot from alignment of both top and bottom components aligned together:

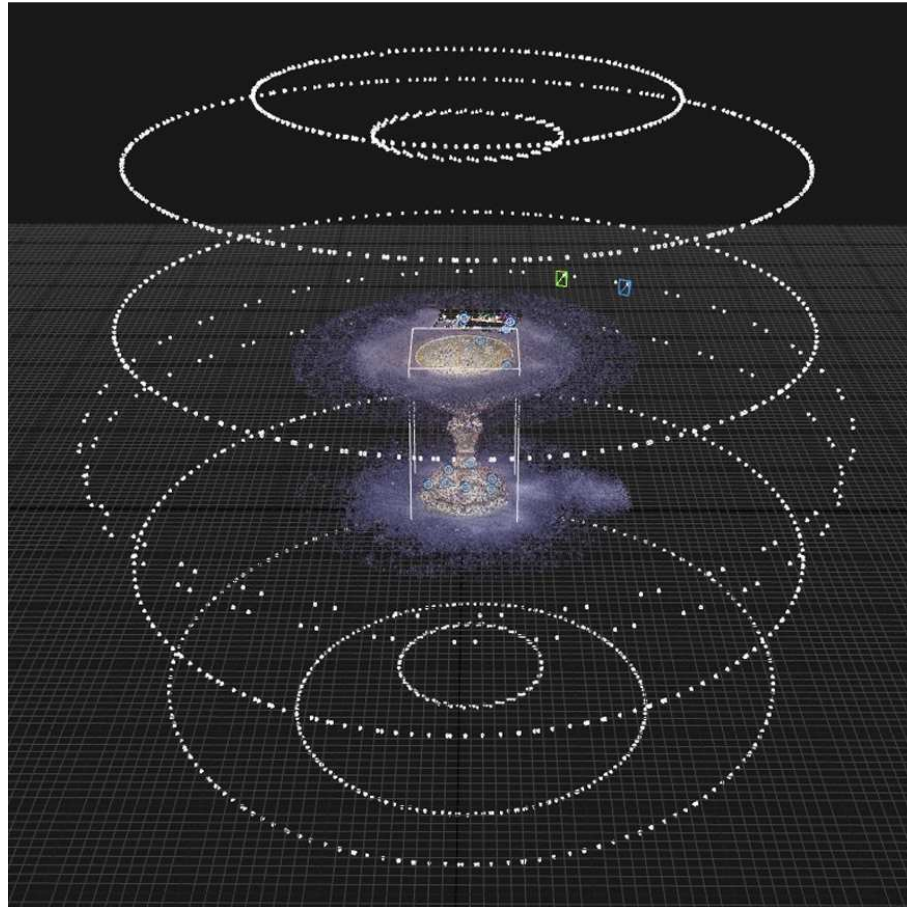


Fig. 32: Alignment of the top and bottom components of Object 1

Tab.9: Alignment report for Object 1

Number of aligned photos	<b>1605</b>
Point count	4763828
Total projections	18944949
Average track length	3,976832
Median error (pixels)	0,401359

### Object 2:

On Fig. 33 is the screenshot from alignment of both top and bottom components aligned together:

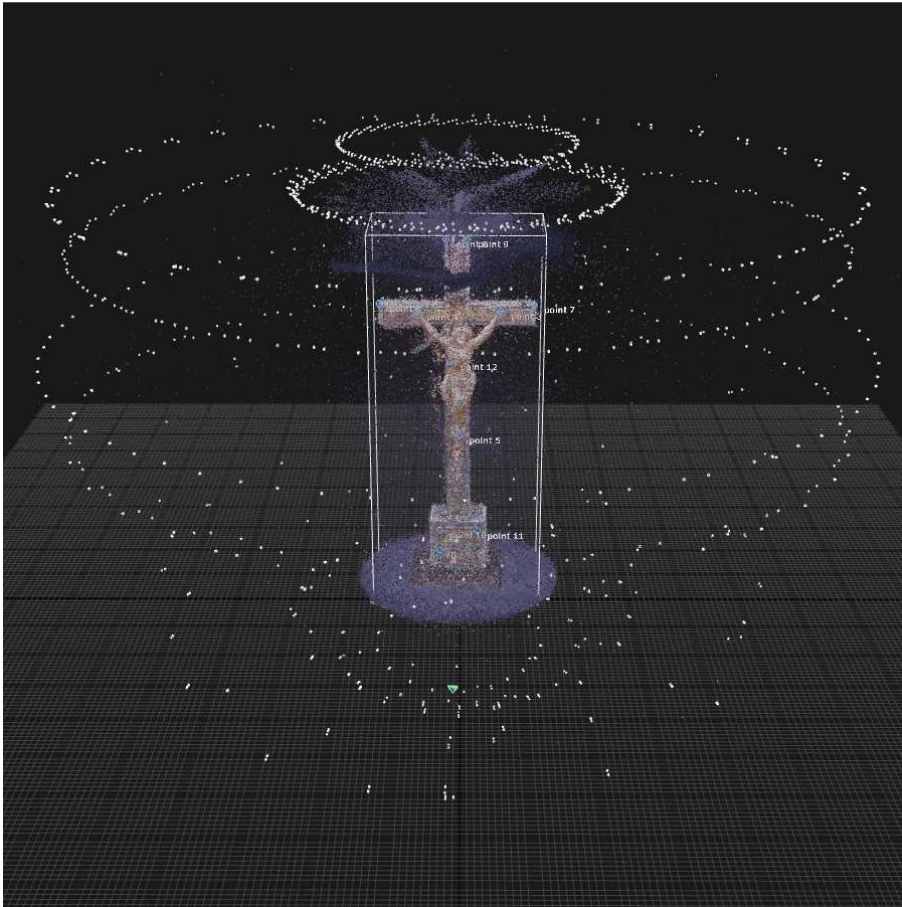


**Fig. 33:** Alignment of the top and bottom components of Object 2

**Tab.10:** Alignment report for Object 2

Number of aligned photos	1483
Point count	1493644
Total projections	5055303
Average track length	3,381866
Median error (pixels)	0,265721

### Aligning of the Scanning Spray Photos

In this option, there were two sets of photos of the objects (top and bottom) sprayed with the scanning spray, with white surface. After the scanning spray disappeared from the surface, the set of cross-polarization photos was taken, without any movement of the object on the turntable. This allowed to use the cross-polarization photos for texturing the mesh from scanning spray photos.

From the cross-polarization photos, 99 photos were selected for texturing. All photos (scanning spray and CPL) were aligned together, while before the reconstruction, the scanning spray photos were selected for mesh calculation and the cross-polarization photos were selected only for texturing. In case the texture is not necessary, this step can be left out.

In RC, while selecting only the scanning spray images, in the "Selected inputs", "Enable meshing" was set to "Enable" and "Enable texturing and colouring" to "Disable". Then, with only selected cross-polarization photos, "Enable meshing" was set to "Disable" and "Enable texturing and colouring" to "Enable" so only these photos were used for texturing.

**Object 1:**

On Fig. 34 is the screenshot from alignment of both top and bottom components aligned together:

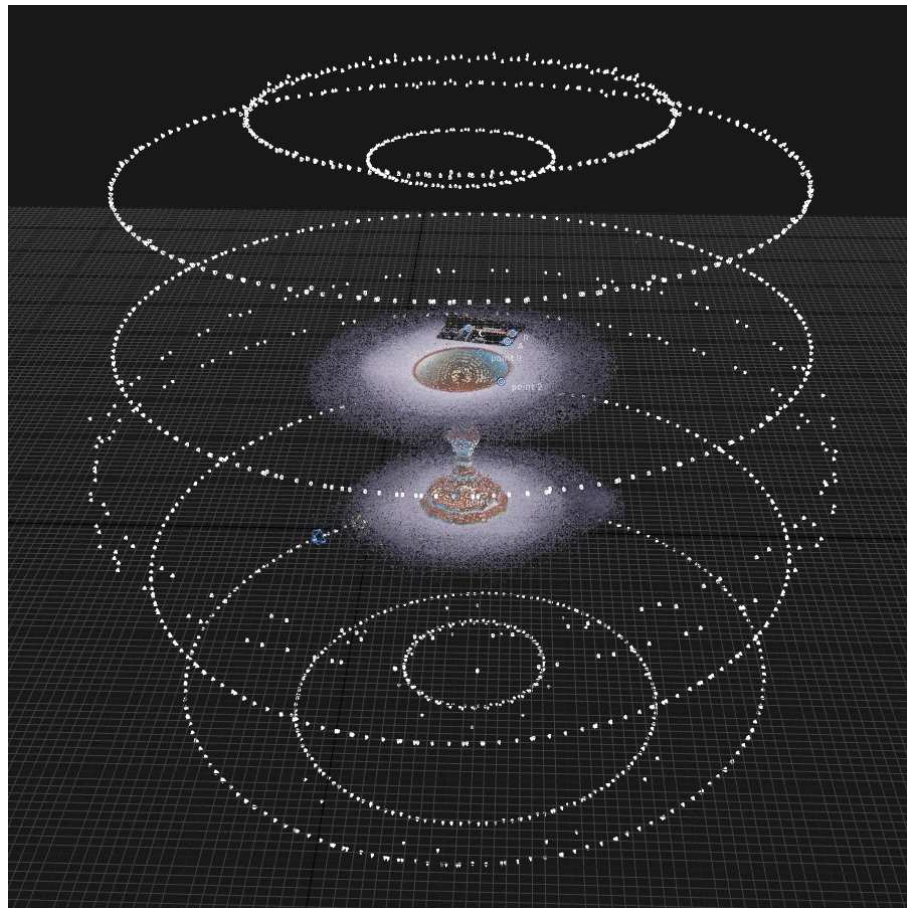


**Fig. 34: Alignment of the top and bottom components of Object 1**

**Tab.11: Alignment report for Object 1**

Number of aligned photos	<b>1584</b>
Point count	6567173
Total projections	27233999
Average track length	4,146837
Median error (pixels)	0,236184

**Object 2:**

On Fig. 35 is the screenshot from alignment of both top and bottom components aligned together:

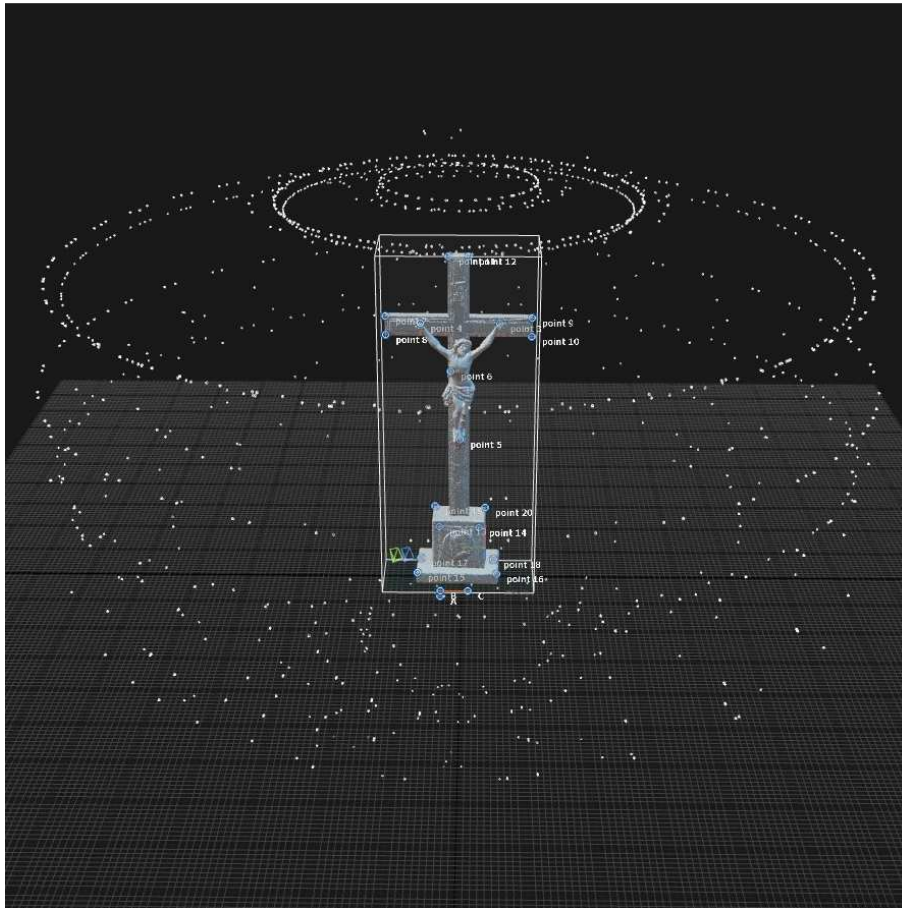


Fig. 35: Alignment of the top and bottom components of Object 2

Tab.12: Alignment report for Object 2

Number of aligned photos	<b>1399</b>
Point count	1061818
Total projections	3466404
Average track length	3,263651
Median error (pixels)	0,239218

### Setting the Distance Constraints

After aligning both top and bottom components, it's necessary to set at least two control points and define the distance between them. Three control points A, B and C were created in several photos containing the scale bar recticules and the distance constraints were defined (in meters) – 0,02 m between the points A and B and 0,05 m between the points B and C, as can be seen in Fig. 36 (RC displays the numbers with one decimal number).





**Fig. 36: Defining the distance constraints on both objects**

After defining the distances, the alignment was updated, so the coordinate system and scale was changed.

### 2.7.2 Mesh Reconstruction

After the alignment is done, the point cloud goes through the meshing, i.e. the phase of generating a geometric grid, in which the individual points of a point cloud are connected into triangles by triangulation. These form the grid itself - mesh, which defines the surface of the object.

*Set reconstruction region* - After the alignment is done, it's good to set up the reconstruction region of certain area with an object, so the areas which are not necessary will not be reconstructed. This speeds up the reconstruction.

Reconstruction settings were kept as default.

There are three option for model calculation – Preview, Normal quality and High quality. The difference is in downscaling setting of the photos for the reconstruction. It's better to start with Normal quality to see if the model is calculated okay and then to use High quality.

### Reconstruction of the Diffused Light Photos

On Fig. 37 is a result of the reconstruction of Object 1 from diffused light photos. The mesh contains 38,7 million of triangles.

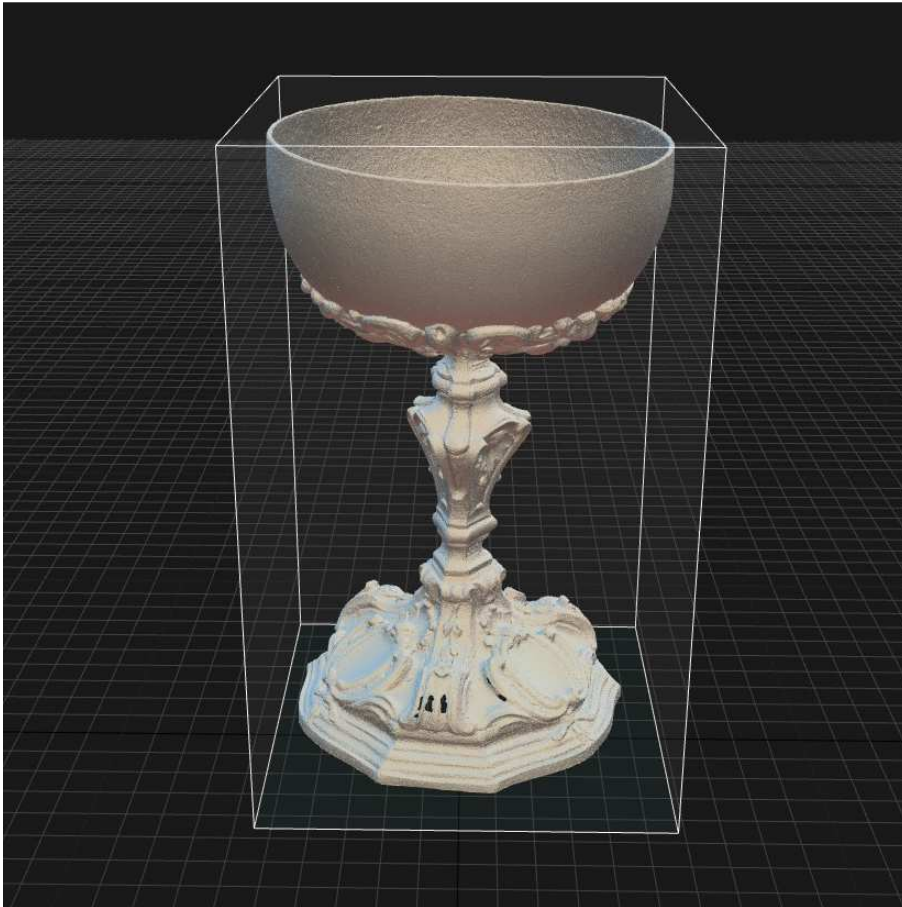


**Fig. 37: Reconstruction of Object 1 from diffused light photos**

As can be seen in the detail on Fig. 38, in the bottom part of the object there are holes. It shows some limitations of photogrammetry. This part of the object is made from pressed metal sheet and the thickness in these places is about 0,5 mm. Due to this small wall thickness, during the alignment of both point clouds of top and bottom parts, intersections between them in some places occurred which software interpreted as holes

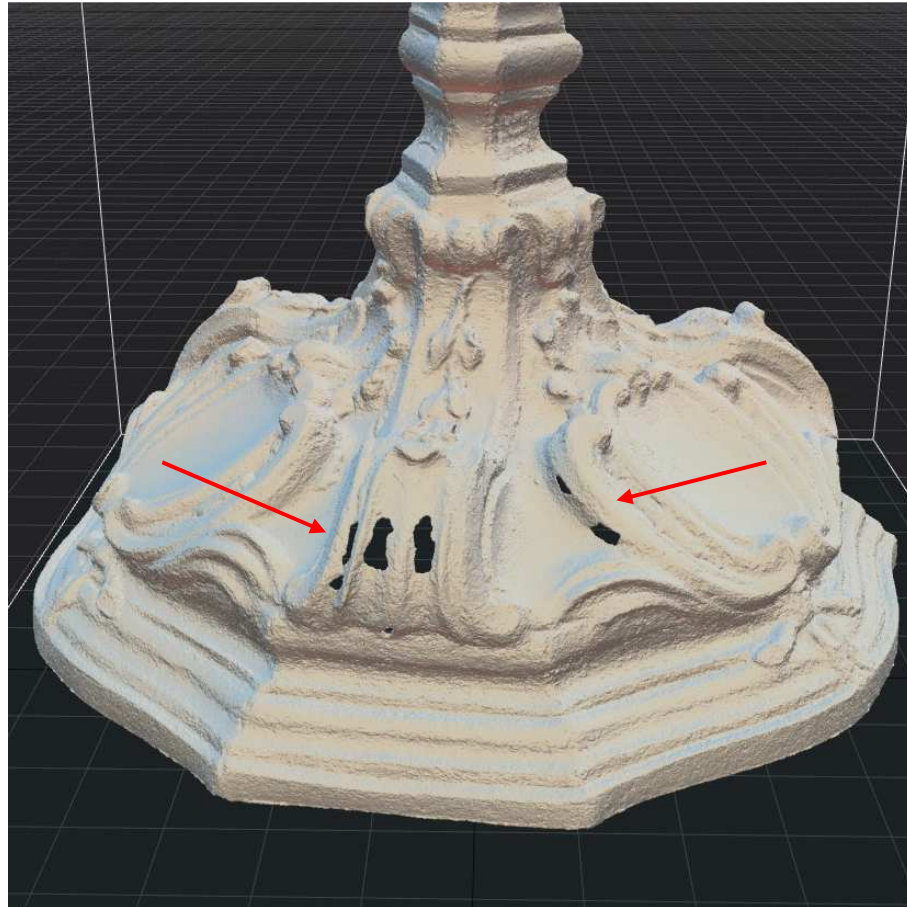


**Fig. 38: Detail of the object**

Although there were attempts to add more detailed photos of this part of the object from both sides as well as control points in another alignment and reconstruction, it was not possible to close the holes. The holes can be closed in an external software, such as Blender and imported back to RC before texturing. This operation is out of the scope of this work and budget for additional software.

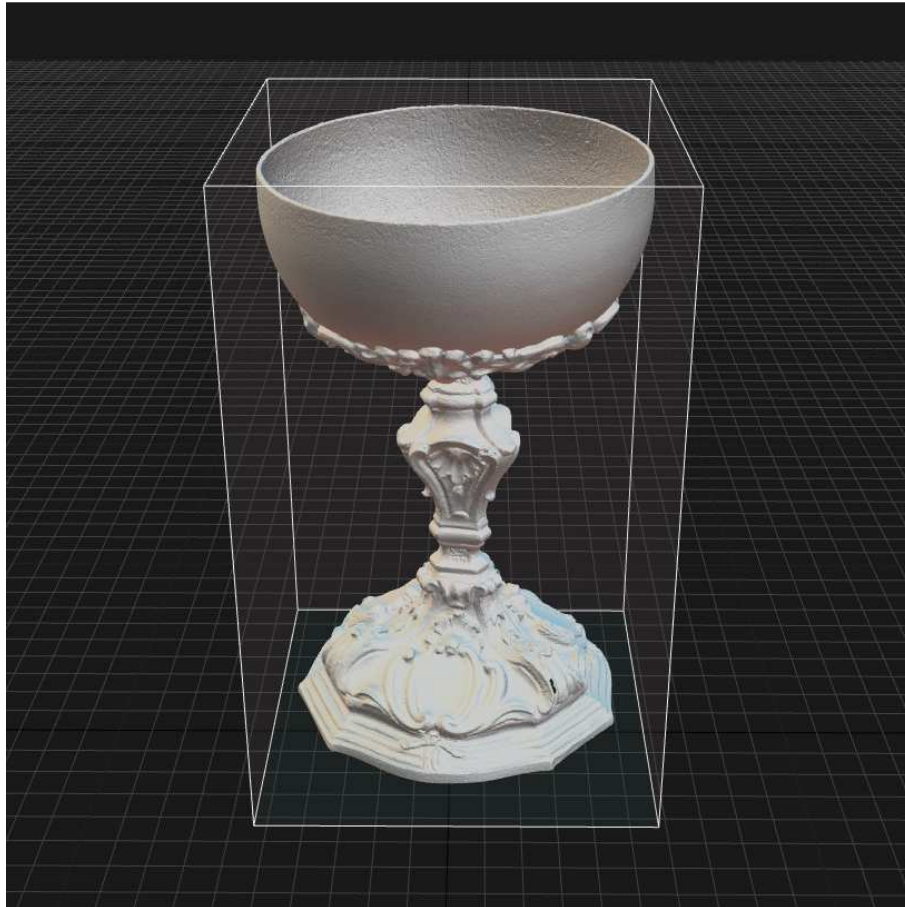
On Fig. 39 is a result of the reconstruction of Object 2 from diffused light photos.



Fig. 39: Reconstruction of Object 2 from diffused light photos

#### Reconstruction of Cross-polarization Photos

On Fig. 40 is the result of the reconstruction of Object 1 from cross-polarization photos. The mesh contains 41,8 million of triangles.



**Fig. 40: Reconstruction of Object 1 from cross-polarization photos**

Similarly as in previous reconstruction, in the bottom part of the object there are holes.

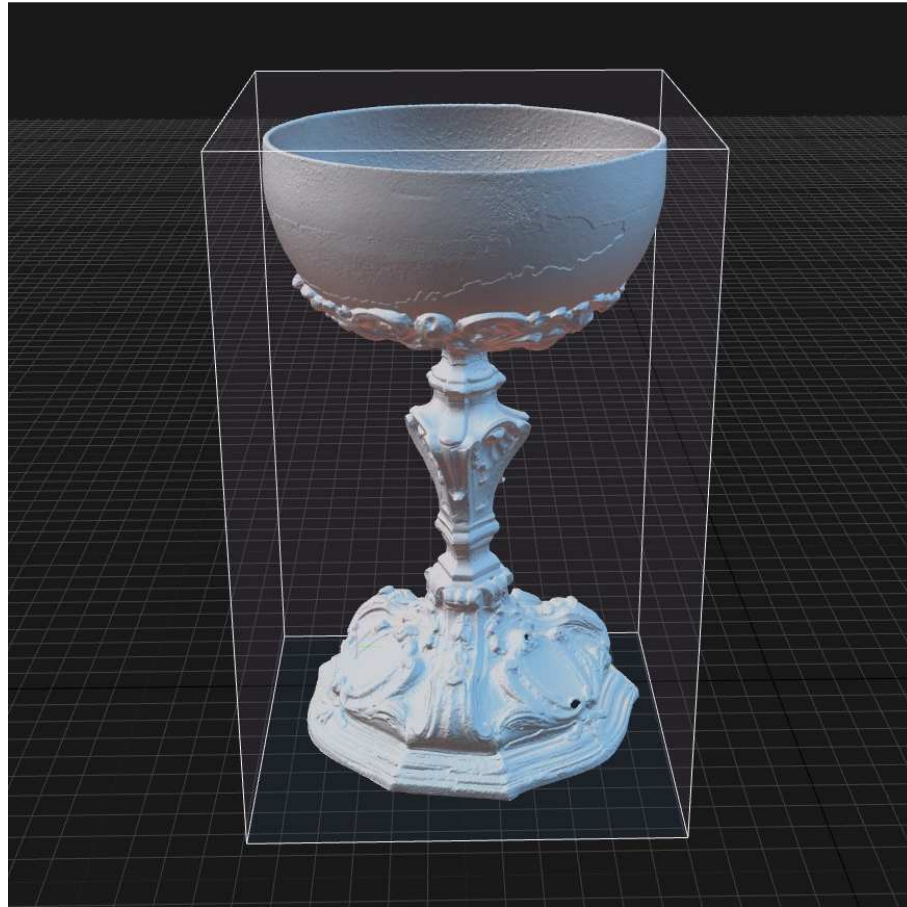
On Fig. 41 is a result of the reconstruction of Object 2 from cross-polarization photos.



Fig. 41: Reconstruction of Object 2 from cross-polarization photos

#### Reconstruction of the Scanning Spray Photos

On Fig. 42 is the result of the reconstruction of Object 1 from scanning spray photos.



**Fig. 42: Reconstruction of Object 1 from scanning spray photos**

When looking closer at this mesh, it's possible to see the seams on the surface, Fig. 43.



**Fig. 43: Seams on the surface**

The seams are caused by not very good alignment. The problem is that top and bottom set of photos were taken with two spraying processes, each position was covered with the scanning spray separately, thus the

scanning spray coating created additional surface with different thickness, texture and characteristic points. Therefore, both parts are very similar, but they don't have the same surfaces which created the seams in aligning.

Also, as in previous reconstructions, in the bottom part of the object there are holes.

On Fig. 44 is a result of the reconstruction of Object 2 from scanning spray photos.



**Fig. 44:** Reconstruction of Object 1 from scanning spray photos

Also as on Object 1, the seams on the surface are visible, Fig. 45:



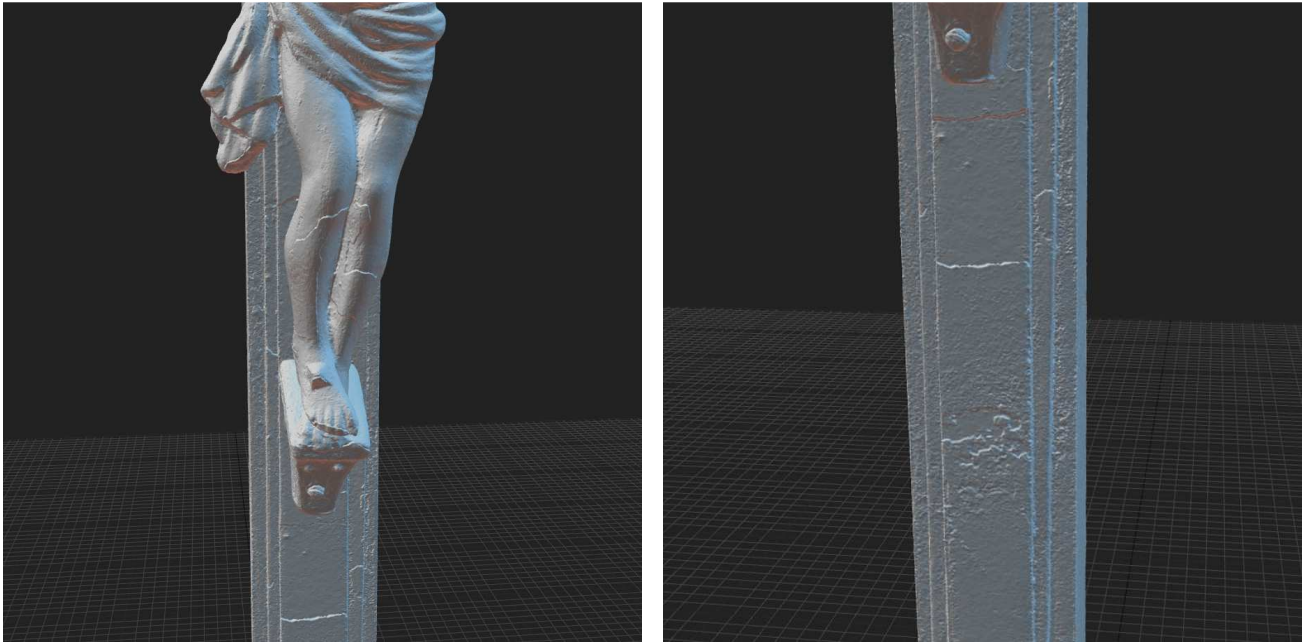


Fig. 45: Seams on the surface

### 2.7.3 Simplification

The created mesh usually contains tens of millions triangles which is difficult to open and edit in any software later. Therefore it's beneficial to reduce the number of triangles, as flat surfaces can be equivalently defined with a few triangles instead of thousands.

On Fig. 46 for comparison is an example of simplification, on the left photo is a model 1 with 10 M triangles, while on the right is a simplified model with only 10 K triangles.

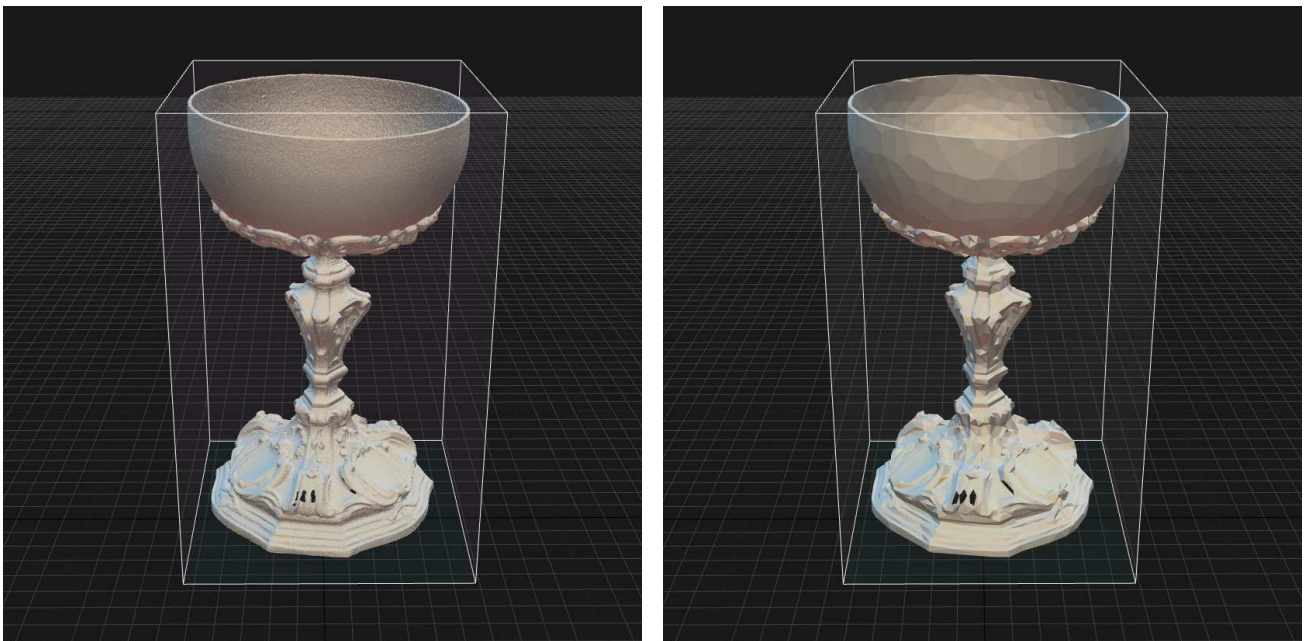


Fig. 46: Comparison of 10 M mesh and 10 K mesh

In RC, the simplification is done using the Simplify tool. It is suggested to do the simplification to a half of the number of original triangles and then repeat again to the target count (50 % increments). In this project, the target number of triangles was 10M for object 1 and 20M for object 2, which is detailed enough for archiving, as the details are maintained and it is possible to process the model further e.g. in Meshlab.

#### 2.7.4 Texturing

The polygon mesh represents only the spatial model of the object. In order for this model to be a true visual representation of the original, it is necessary to assign light and colour information to this mesh.

After the polygon mesh is created, UV coordinates (also known as texture coordinates) are generated for each vertex in the mesh. UV mapping is the process of projecting a 2D image to a 3D model's surface for texture mapping. In other words, a UV map is the flat representation of the surface of a 3D model. The process of creating a UV map is called UV unwrapping. The letters "U" and "V" denote the axes of the 2D texture because "X", "Y", and "Z" are already used to denote the axes of the 3D object in model space (UV mapping 2020). An example of mapping a globe, depicting the object in both XYZ and UV spaces is shown in Fig. 47 (UV mapping 2020):

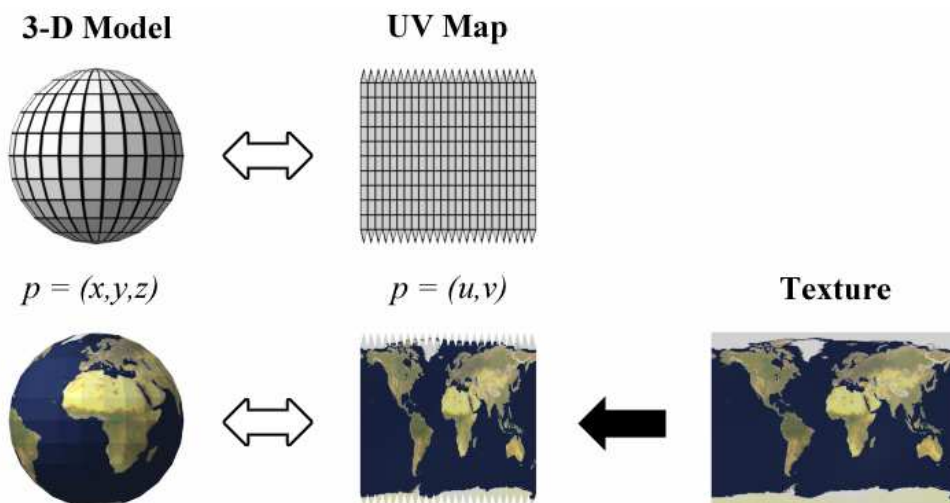


Fig. 47: UV mapping a globe

The Unwrap parameters were kept basically default. *Large triangle removal* was set to 1000. *Maximum texture resolution* was set to 8K. *Texel size* was set to Optimal (texel represents a single unit of measurement in texture space in real world scale). The *Maximum texture resolution* was set to 8K.

After unwrapping, RC will cover the model with a checkerboard texture for the preview the unwrap (Fig. 48 and Fig. 49). One black or white square should theoretically represent one texel.

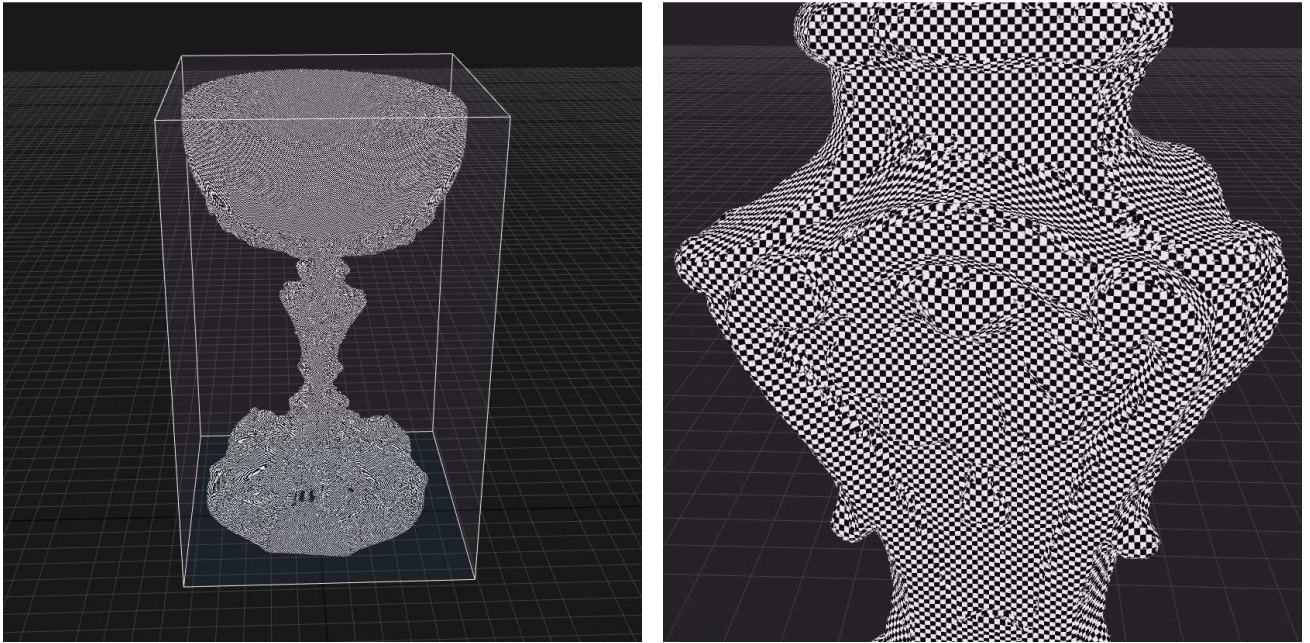


Fig. 48: Unwrapped model 1

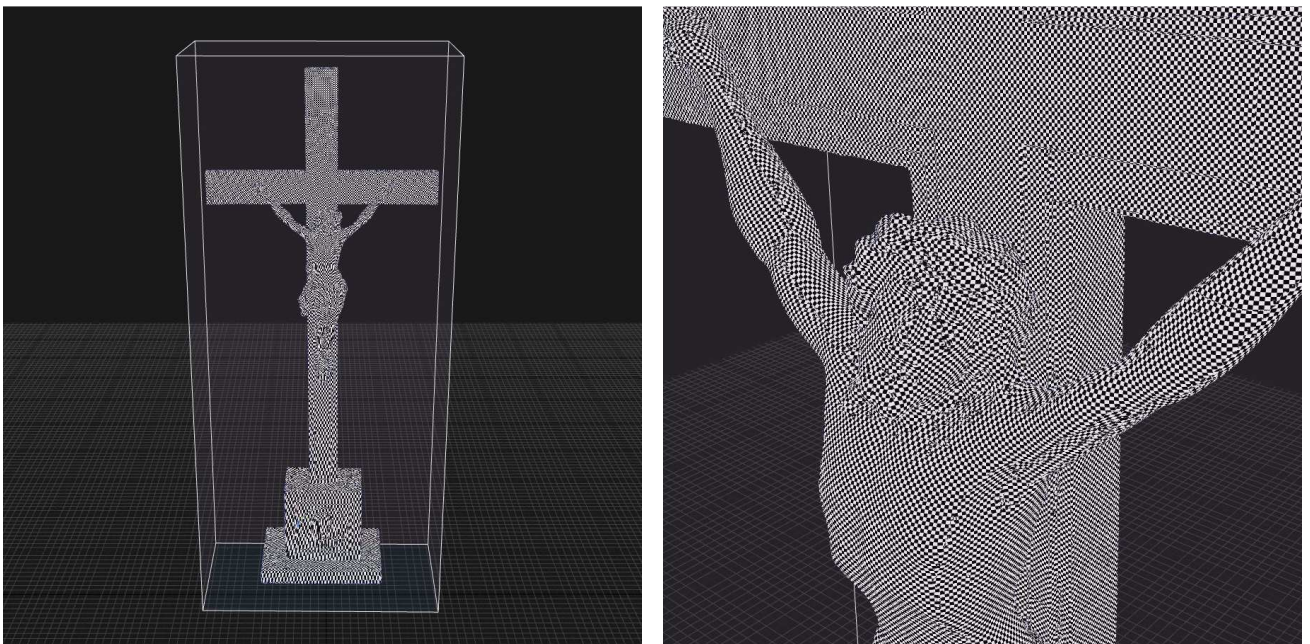
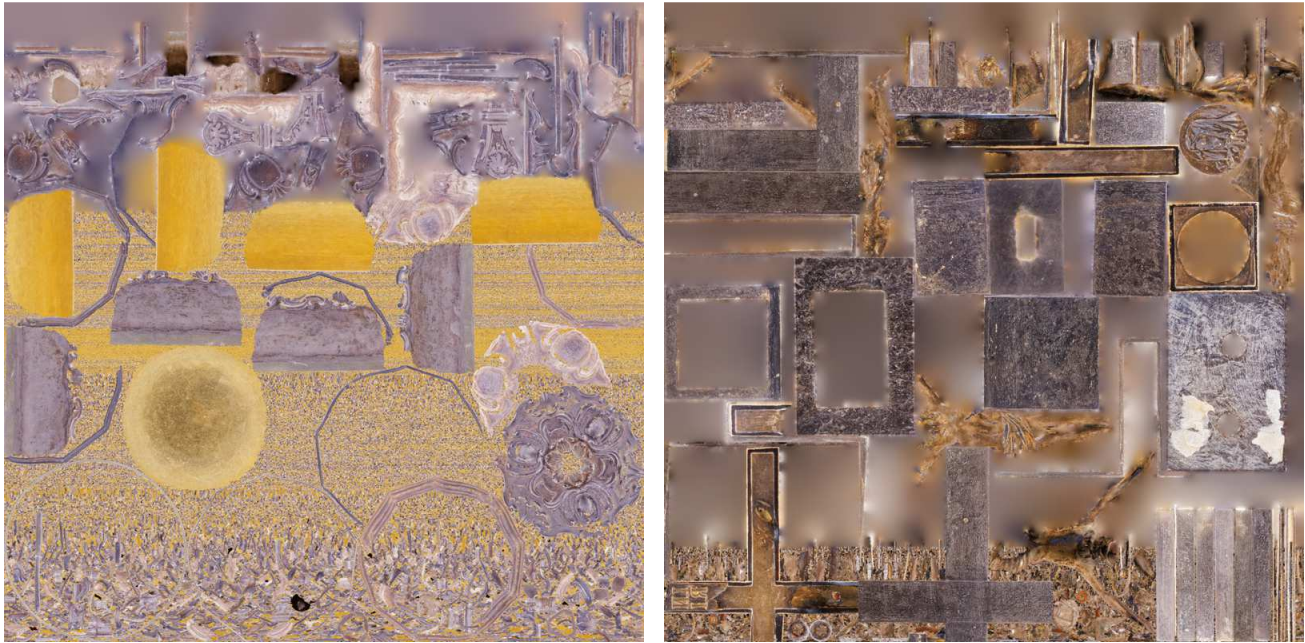


Fig. 49: Unwrapped model 1

Once the model is unwrapped, the software creates the texture and applies it on each triangle individually, so each triangle will map to the appropriate texture from the "decal sheet". On Fig. 50 are textures for Object 1 and 2 (for CP):



**Fig. 50: Exported texture of Object 1 and 2**

This texture can be exported and edited e.g. in Photoshop, to correct the colours or retouch some small details and then import back to RC.

In the following tables 13 and 14 is the texturing report:

**Tab.13: Texturing report for Object 1**

	<b>Diffused light model</b>	<b>CPL model</b>	<b>Scanning spray model</b>
Texture resolution	8192x8192	8192x8192	8192x8192
Texel size (units per texel)	0,000043	0,000041	0,000041
Texture quality	100 %	100 %	100 %

**Tab.14: Texturing report for Object 2**

	<b>Diffused light model</b>	<b>CPL model</b>	<b>Scanning spray model</b>
Texture resolution	8192x8192	8192x8192	8192x8192
Texel size (units per texel)	0,000069	0,000063	0,000063
Texture quality	100 %	100 %	100 %

The texel size represents the dimension of a texture image pixel in meters and corresponds to the minimal detail captured. It means, that for Object 1, the minimal detail in the texture is 0,041-0,043 mm while for Object 2, the minimal detail in the texture is 0,063-0,069 mm. (Note: for CPL model and scanning spray model, the same set of photos was used for texturing, thus there is the same texel size).

The texture quality equals to the percentage of a texel size with regard to the optimal texel size. It describes how the texture is detailed with regard to the maximal detail that you can get from images.

On Fig. 51 is displayed the textured model of Object 1, the details are on Fig. 52.

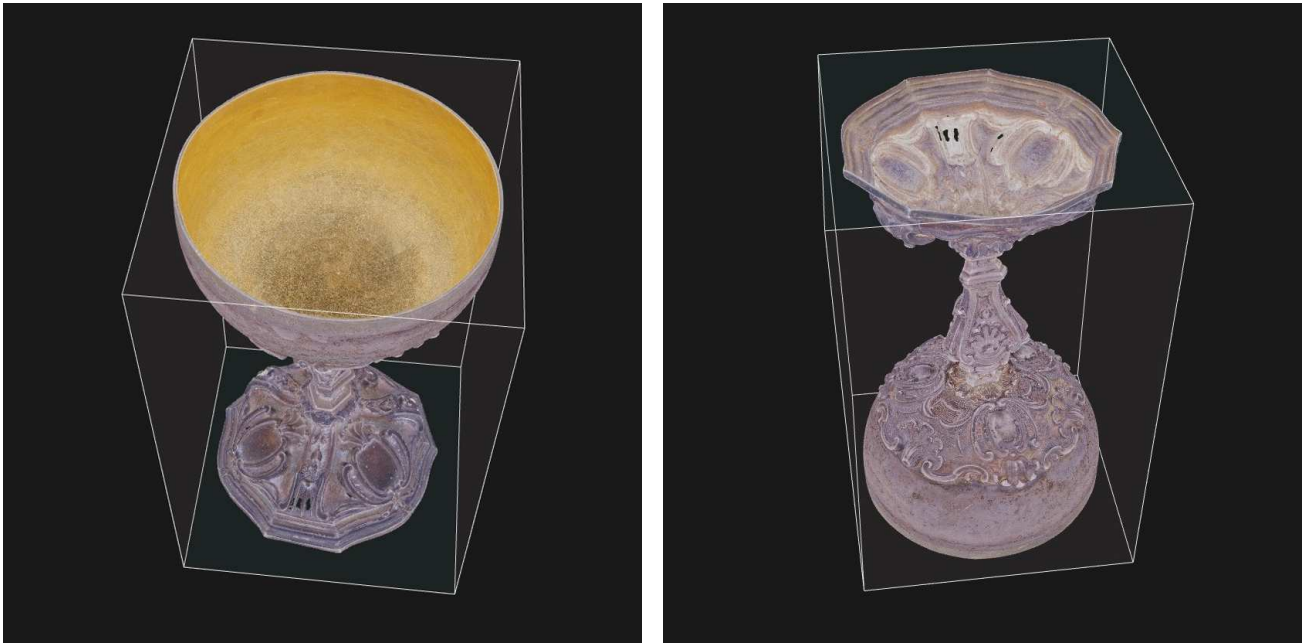


**Fig. 51: Textured model 1**

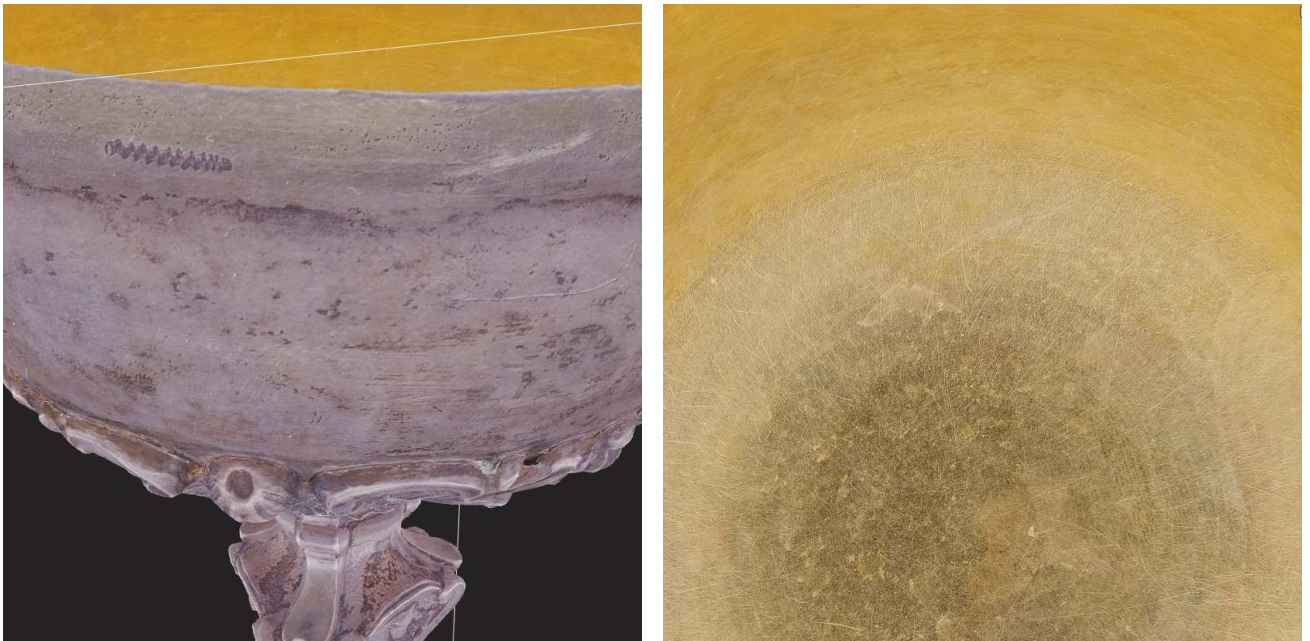


**Fig. 52: Details of the texture of the model 1**

On Fig. 53 is displayed the textured model of Object 2, the details are on Fig. 54.

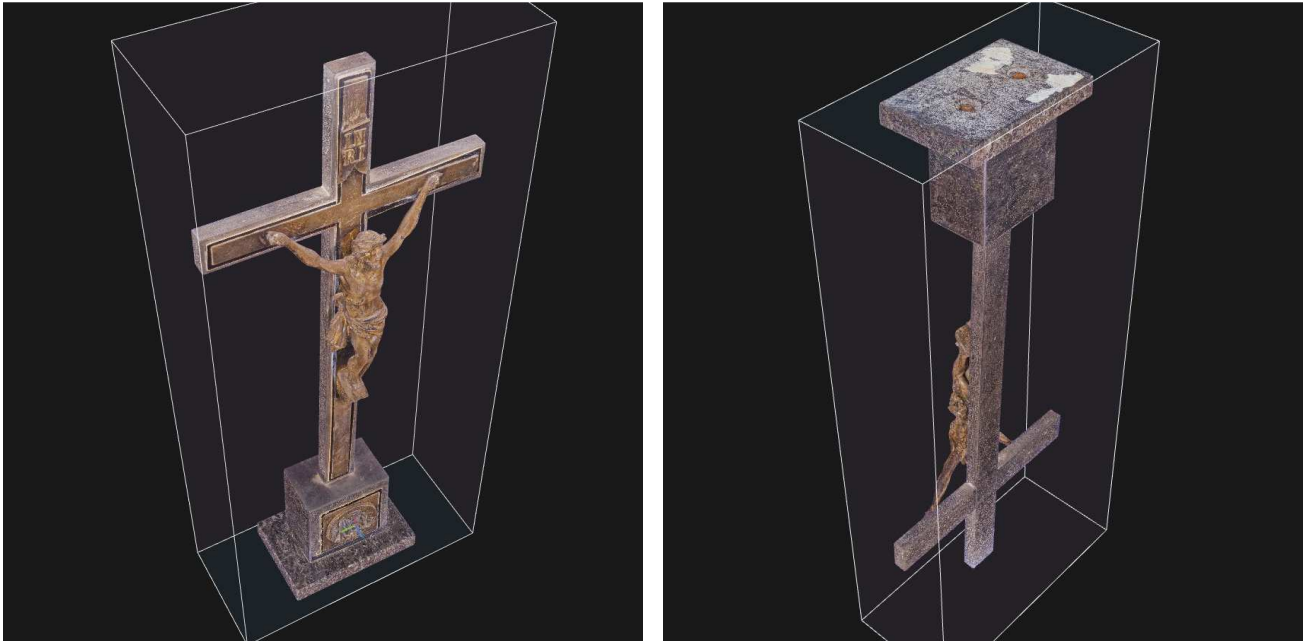


Fig. 53: Textured model 2

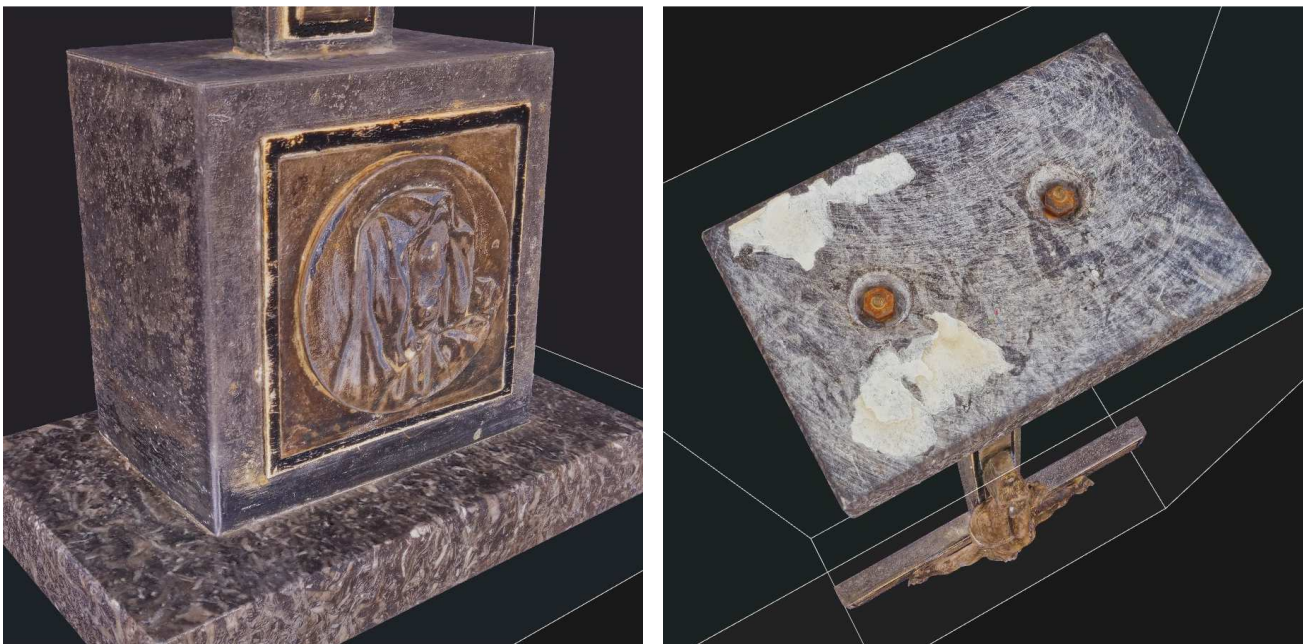


Fig. 54: Details of the texture of the model 2

### 2.7.5 Exporting

There are several ways how to export the final model. It's possible to make a render, a fly-through video, or export triangular model to Polygon File Format (PLY) and Wavefront Format (OBJ), or export a dense point cloud in XYZ format. PLY format doesn't contain texture, thus is suitable for 3D printing, while OBJ also contains texture.

## Renderings

Another option is using the *Render* tool to render the chosen 3D view into an image. In Fig. 55 and Fig. 56 are examples of renderings, left (a) are displayed just the vertices of the model, in the middle (b) is the shaded model and on the right (c) is the textured model.

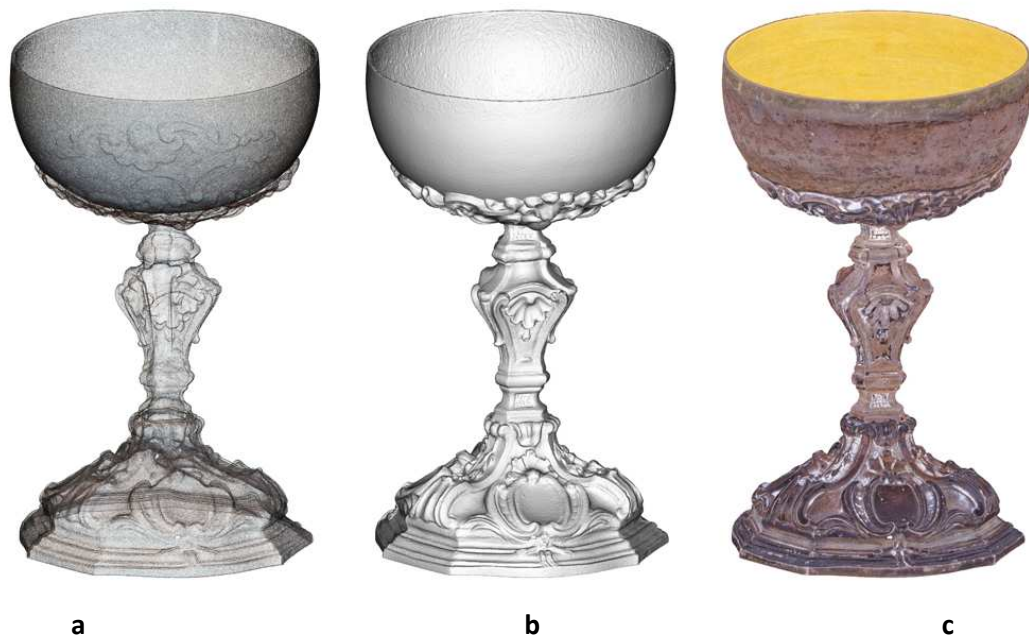


Fig. 55: Examples of renderings of Object 1



Fig. 56: Examples of renderings of Object 2

## Orthographic Projections

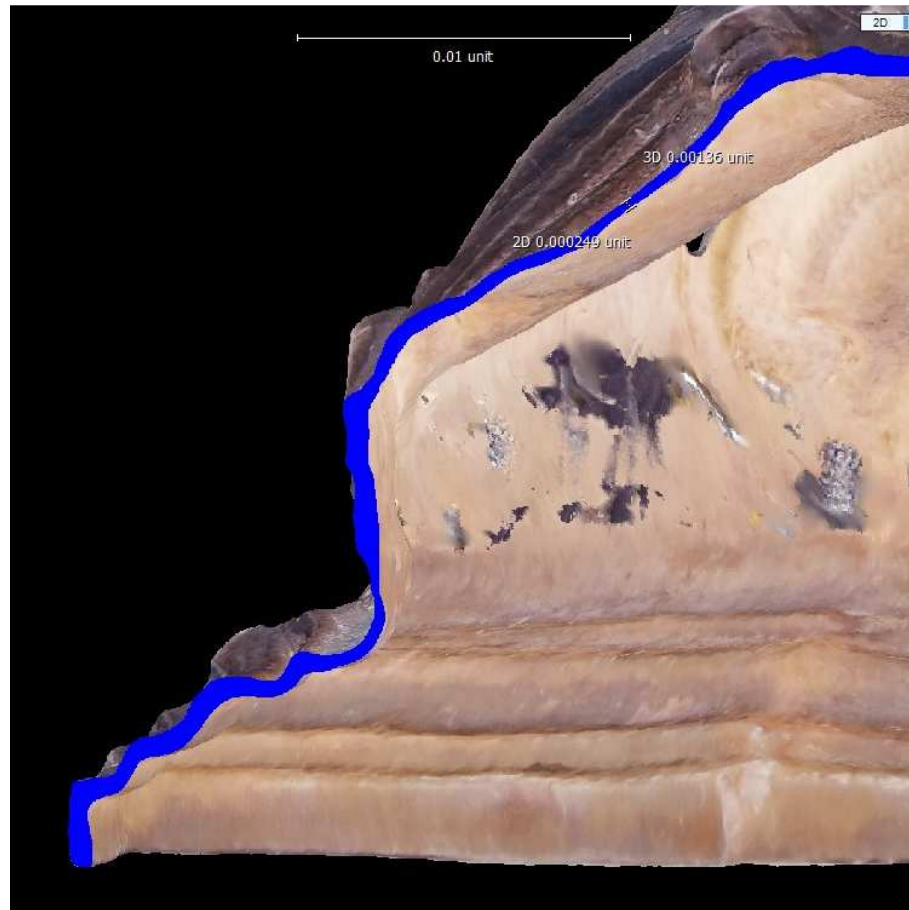
RC offers the possibility to create ortho projections from a reconstruction region. It's also possible to create sections of the model by changing the reconstruction region, as can be seen in Fig. 57. In the right image is visible, how "deep" inside it was possible to see with the camera during the photo shooting and how the inner surface was reconstructed.



Fig. 57: Ortho projections of Object 1

In the ortho projection it's also possible to use the *Distance* tool to measure the distance between two points. In Fig. 58 is an example of measuring the thickness of the wall in the central section of Object 1, where the measured thickness is 0,249 mm (unit is in RC defined as 1 m).





**Fig. 58: Measuring the distance**

Another example is the measuring of the diameter of the top part of Object 1, as can be seen in Fig. 59. The diameter is 99,3 mm.



Fig. 59: Measuring the distance

### Exporting to Sketchfab

Sketchfab (sketchfab.com) is one of many online platform for publishing, sharing, buying and selling 3D content. It contains a viewer that allows to display 3D models on the web.

RC has a directly integrated export function to Sketchfab. When the 3D model is finished, *Share* button is in the Export part of the WORKFLOW tab, after clicking on which a window asking to specify how the user wants to share the content will appear. When selecting '*Upload To Sketchfab*', the user is prompted to (log in into a Sketchfab account and) authorize RC to list and display your models, upload, and update model. When the process is finished, it's possible to view the model on Sketchfab, edit 3D settings, publish, and share.

In Fig. 60 and Fig. 61 are QR codes which after their scanning show the model of Object 1 and 2 in Sketchfab.



<https://skfb.ly/6UyD>

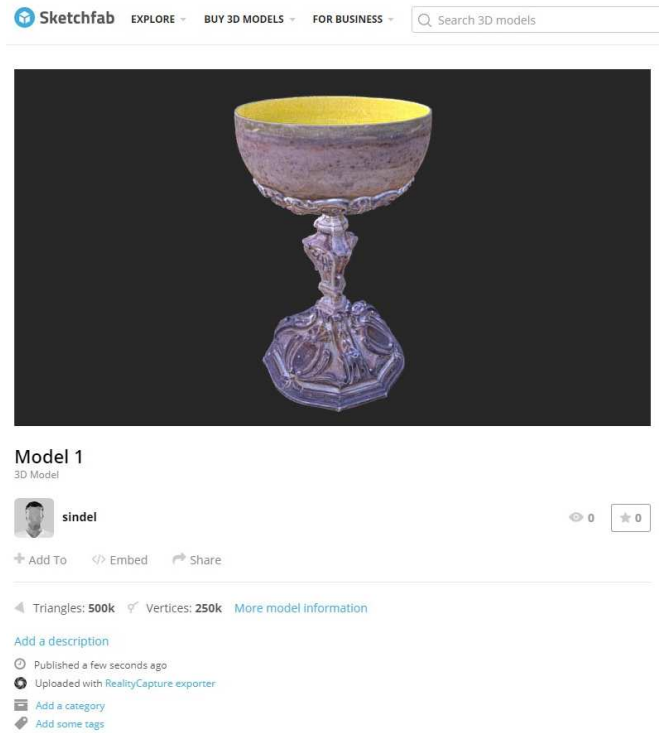


Fig. 60: QR code for Object 1 in Sketchfab



<https://skfb.ly/6VnqG>

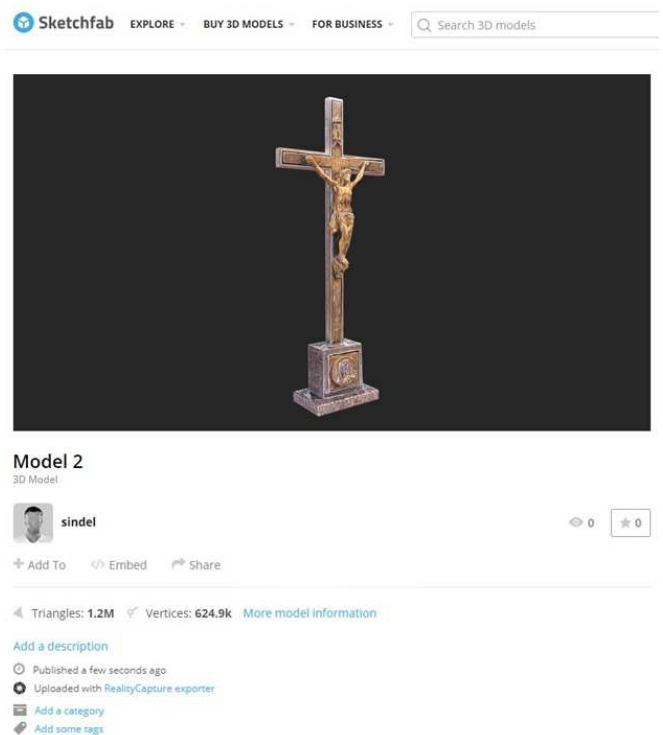


Fig. 61: QR code for Object 2 in Sketchfab

## 3 Results and Discussion

### 3.1 Comparison of Applied Methods

The calculated 3D models were compared in terms of their quantitative and qualitative properties in order to establish the accuracy of each reconstruction method.

#### 3.1.1 Comparison with CT scan

In order to perform a comparative analysis using difference models, it is necessary to have a reference model created by at least one grade of more accurate method than the test models. For this purpose, the X-ray computed tomography (CT) was chosen. CT enables to investigate non-destructively the objects of cultural heritage, the scanning is non-invasive as X-rays cannot cause any harm to studied inanimate objects.

CT scanning of both models was performed in the Laboratory of computed tomography at the Earth Science Institute of the Slovak Academy of Sciences in Banská Bystrica, Slovakia. The models were scanned by the GE phoenix v|tome|x L240 (micro-CT-L240), a high-resolution microfocus system with protective cabinet for 2D and 3D computed tomography.

This micro-CT system is generally used for non-destructive X-ray inspection of highly absorbent materials, eg. in the field of geology, archaeology, metallurgy, biology or material sciences. Unlike a classic clinical CT scanner in the hospital, this industrial micro-CT is based on rotation of the object between fixed X-ray tube and fixed detector and on X-ray energy  $> 12,4$  keV. It is particularly suitable for massive, radioscopic denser and larger samples as well as for small objects and provides detailed resolution up to  $1 \mu\text{m}$ . On Fig. 62 and Fig. 63 are photos from scanning of Objects 1 and 2 in the micro-CT-L240:



Fig. 62: Scanning of the object 1 in the micro-CT-L240

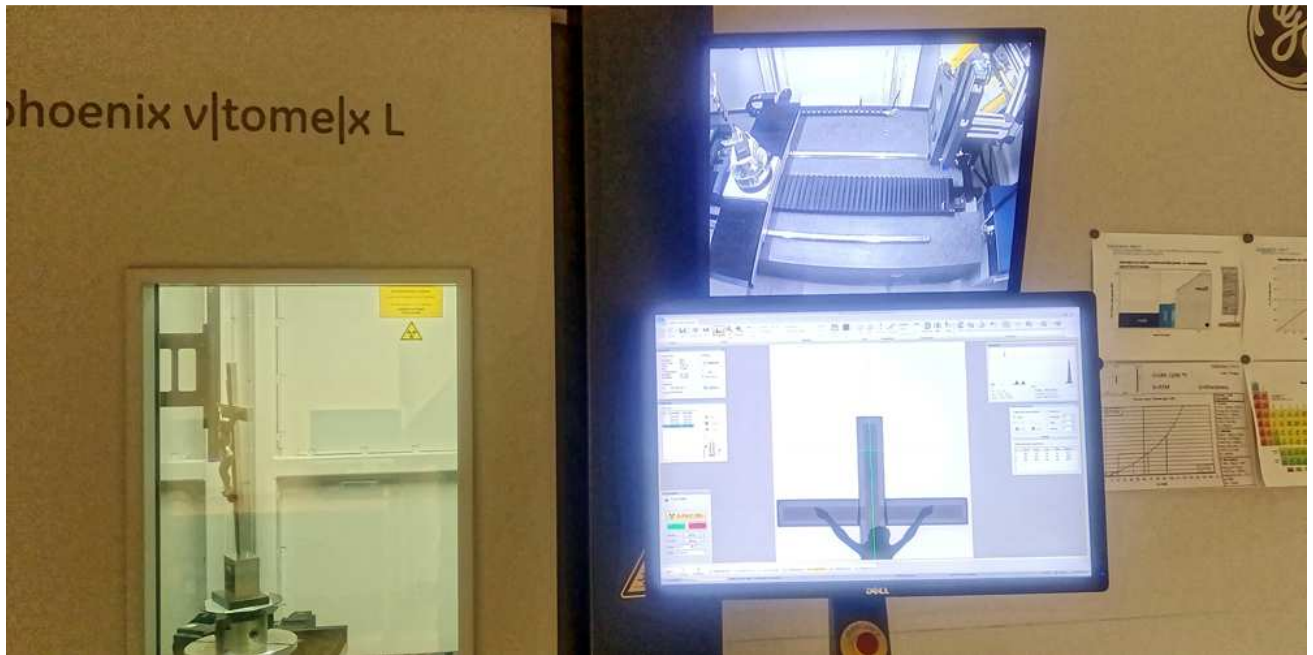


**Fig. 63: Scanning of the object 2 in the micro-CT-L240**

The output of the scanning were digital images in DICOM (Digital Imaging and Communications in Medicine) standard and the data were processed on the local reconstructive workstation using VGStudio MAX 2.2 .

Both objects are made of high attenuation materials which, although some filters were used to prevent this during scanning, caused the scattering of the X-ray radiation and brought various artefacts into the images in the form of bright or dark streaks, marked with arrows in Fig. 64.

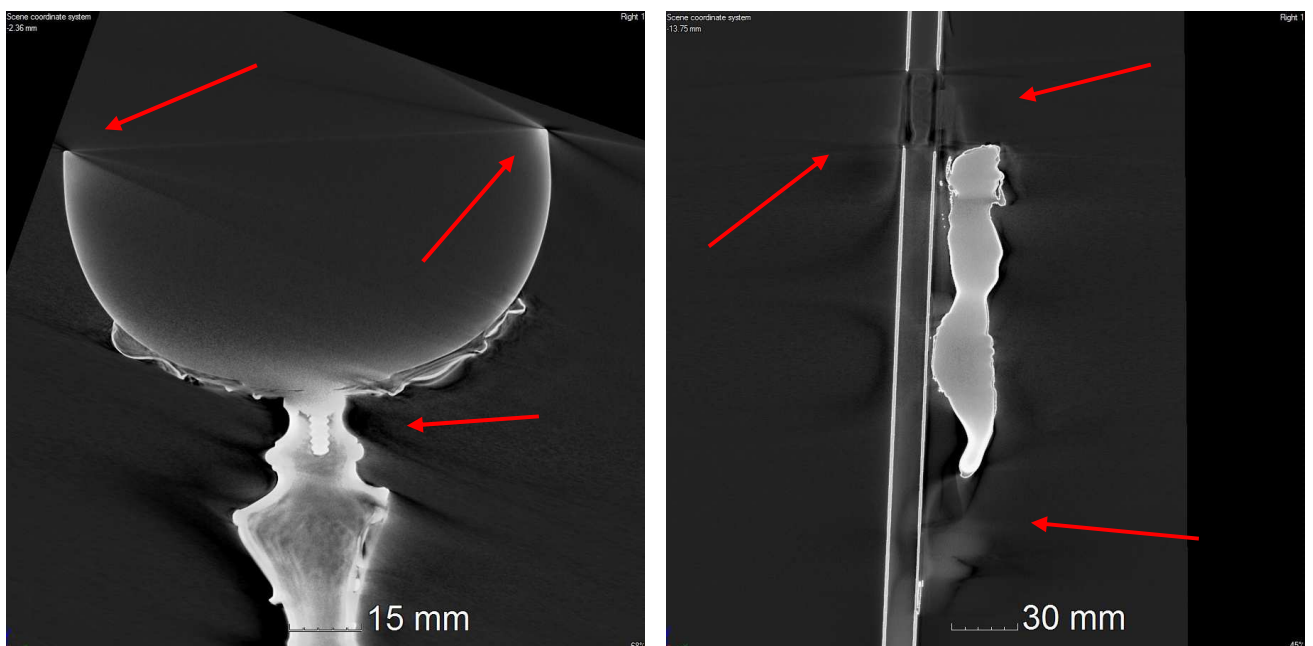


**Fig. 64: Examples of bright and dark streaks in Object 1 and 2**

These artefacts caused a problem to determine the boundaries (surface determination) of the actual object (what is still material and what is not). It was not possible to establish the surface determination, either noise and artefacts appeared, which appeared like material or the material decreases and holes are formed). In Fig. 65 and Fig. 66 is an example of both situations in Object 1, in Fig. 67 and Fig. 68 is an example of both situations in Object 2:

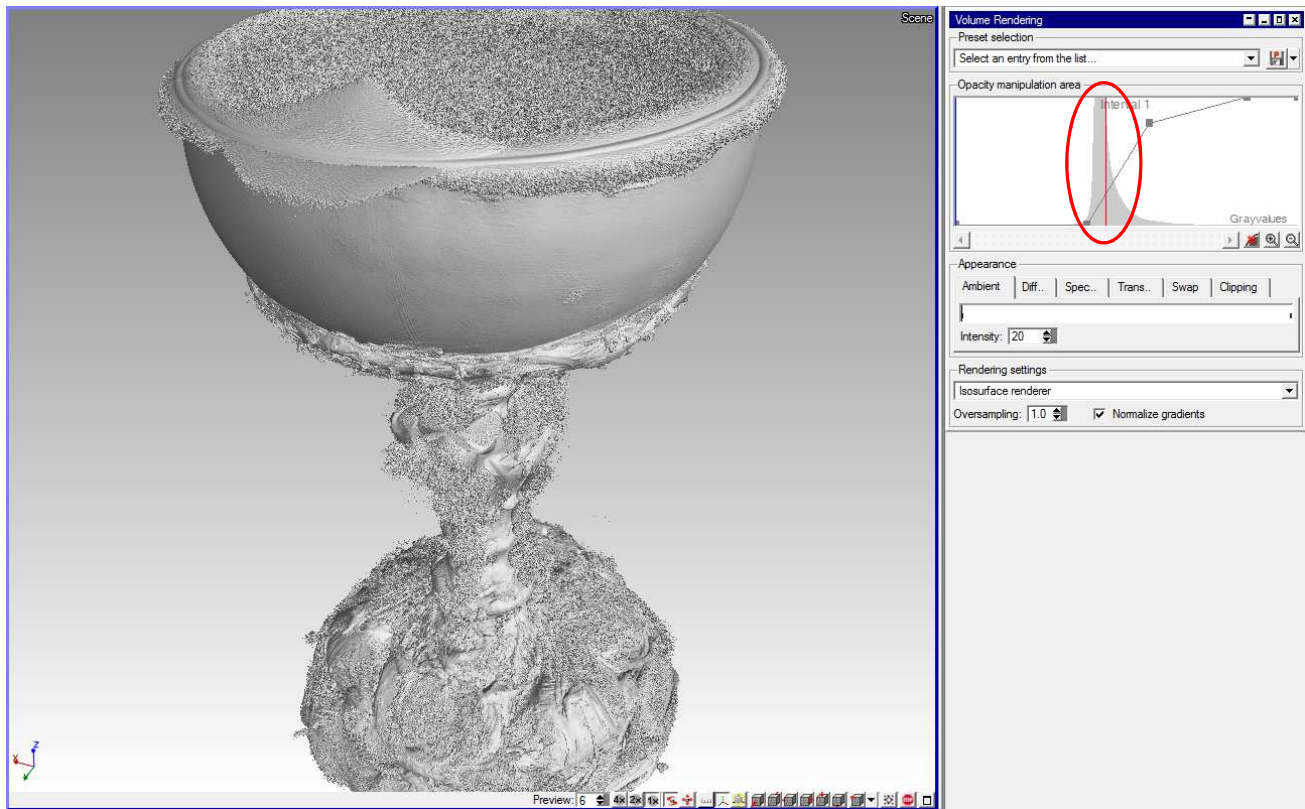


Fig. 65: Surface determination settings 1 of Object 1

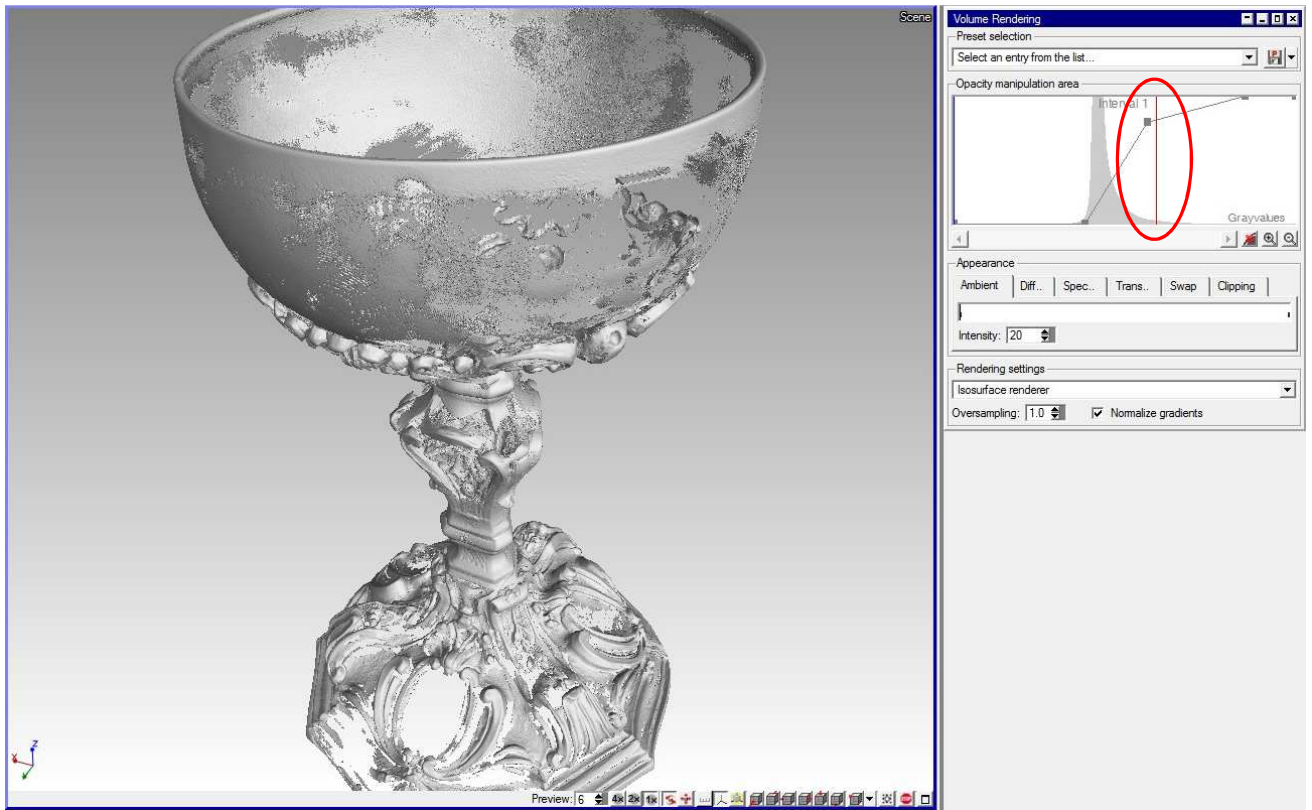


Fig. 66: Surface determination settings 2 of Object 1

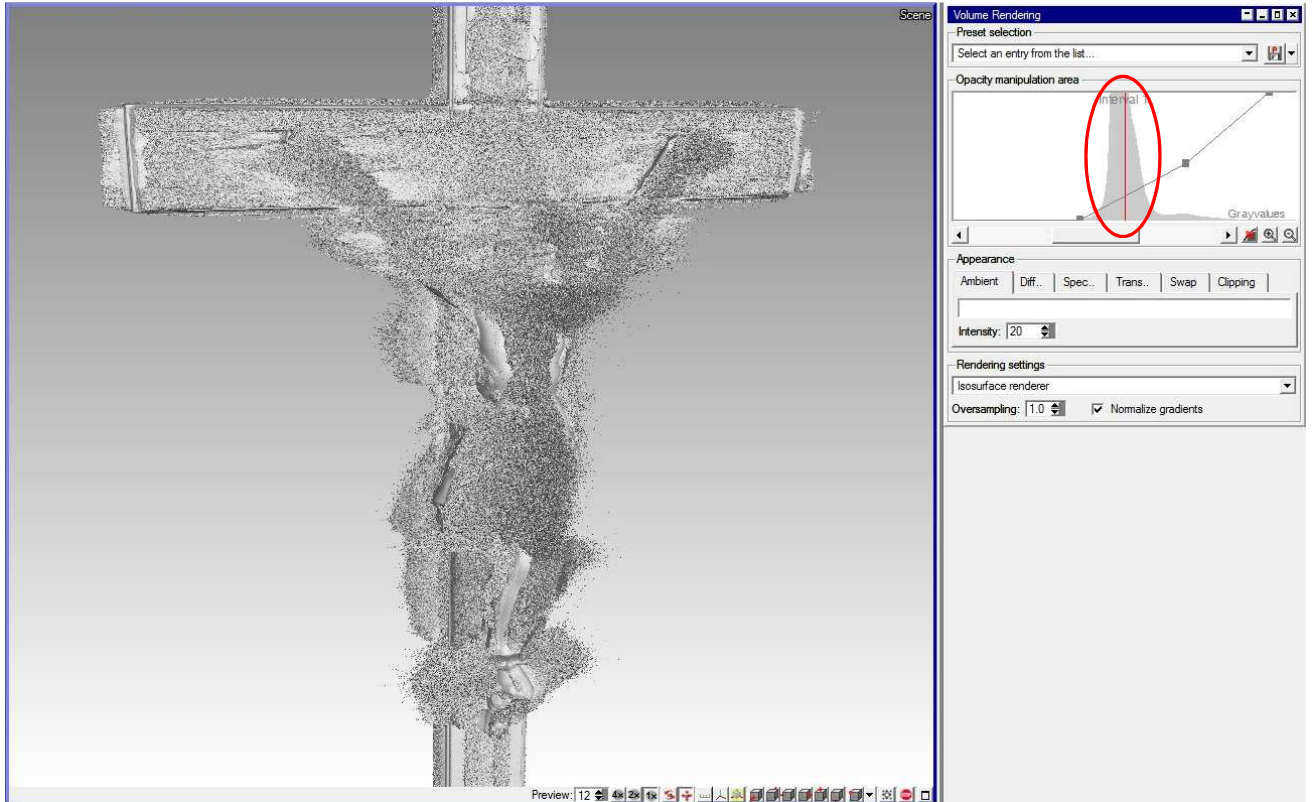


Fig. 67: Surface determination settings 1 of Object 2

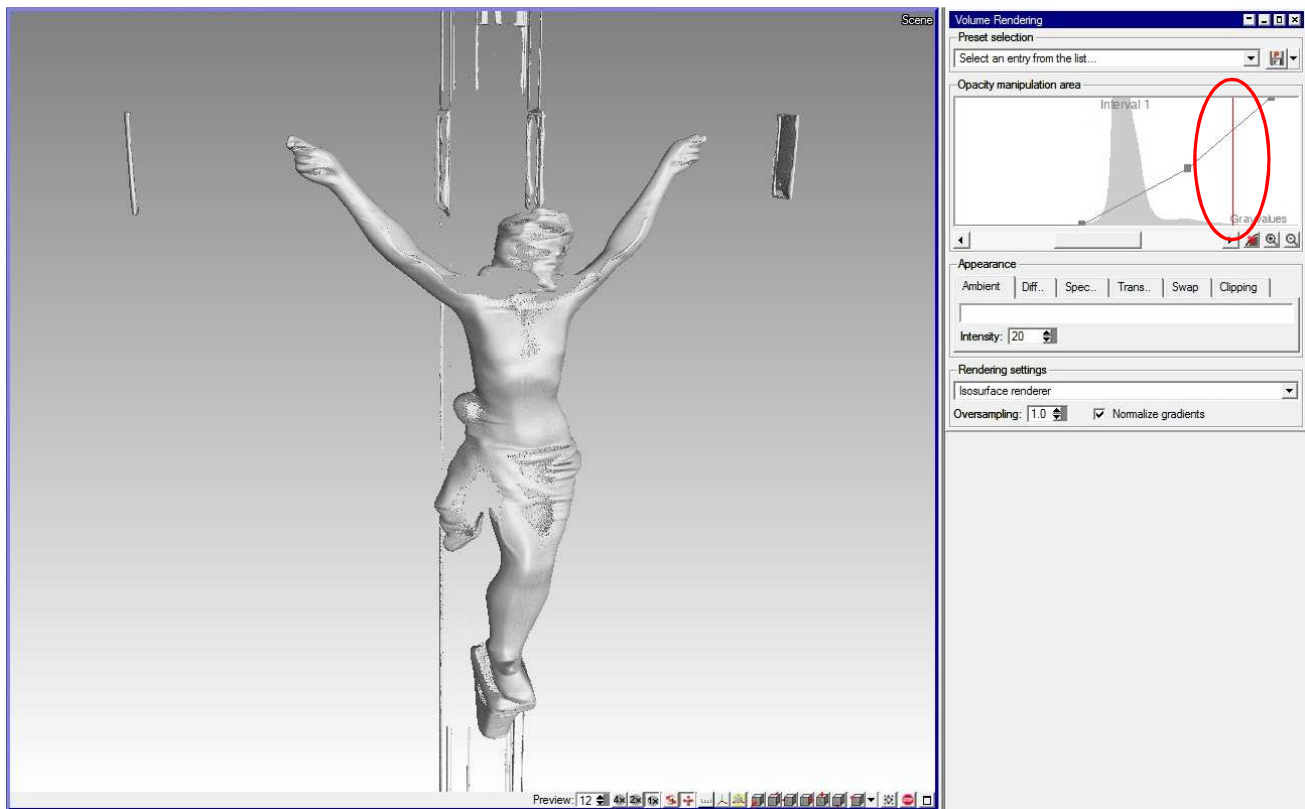


Fig. 68: Surface determination settings 2 of Object 2

The reasons for this according to the Institute lies in the material from which the objects are made (if they were made out of e.g. aluminium, the scan would have been successful) as well as in the shape or edges of the objects. Based on the aforementioned results, the models from micro-CT turned out not to be useable for the comparison.

### 3.1.2 Comparison of Volume and Surface Deviations in CloudCompare

Although the reference 3D models from micro-CT could not have been used, all created models of both Objects 1 and 2 were compared between each other in CloudCompare software (cloudcompare.org). CloudCompare is a 3D point cloud and triangular mesh processing Open Source tool designed to perform 3D surface deviation analysis between points clouds. The results will help in the general evaluation of individual methods of model creation.

For the comparison of two variants of the models (e.g. model of the Object 1 created from diffused light and cross-polarization photos), these were imported in OBJ or PLY formats into the software (OBJ was used for the Object 1 as it contains the texture which helped in manual aligning of the models; PLY was used for Object 2, where the shapes were clearly defined).

Before the comparison, two point clouds have to be aligned. CloudCompare offers a few ways of registration (aligning) - manually, *align the bounding boxes*, automatic alignment, or alignment based upon manually selection of corresponding points pairs in each point cloud. The *Points pair picking* with 6 corresponding points (3 are minimum, the more the better alignment) was used as it resulted in better alignments.



After detailed registration of the models, comparison or difference raster of both point clouds (models) was calculated using the *Cloud/Cloud Distance (C2C)* function. C2C method is the computation of the nearest neighbouring distances between the reference cloud and the compared cloud. The result of the chosen Least Square Plane C2C method was the visualization of surface deviation analysis using a colour scale. The colours represent the distance between both point clouds and it's possible to see the colour scale that shows the value of the C2C distance computation. The blue colour represents zero or minimal distance, while red colour represent maximum distance on the selected scale.

For the analysis results, CloudCompare computes the mean distance and the standard deviation. These results are shown in the tables in each comparison below.

## Object 1

### Diffused Light vs. CPL Models Comparison

On Fig. 69 is an axonometric view of the Object 1 showing the absolute difference between the point clouds of the models made from diffused light and CPL method.

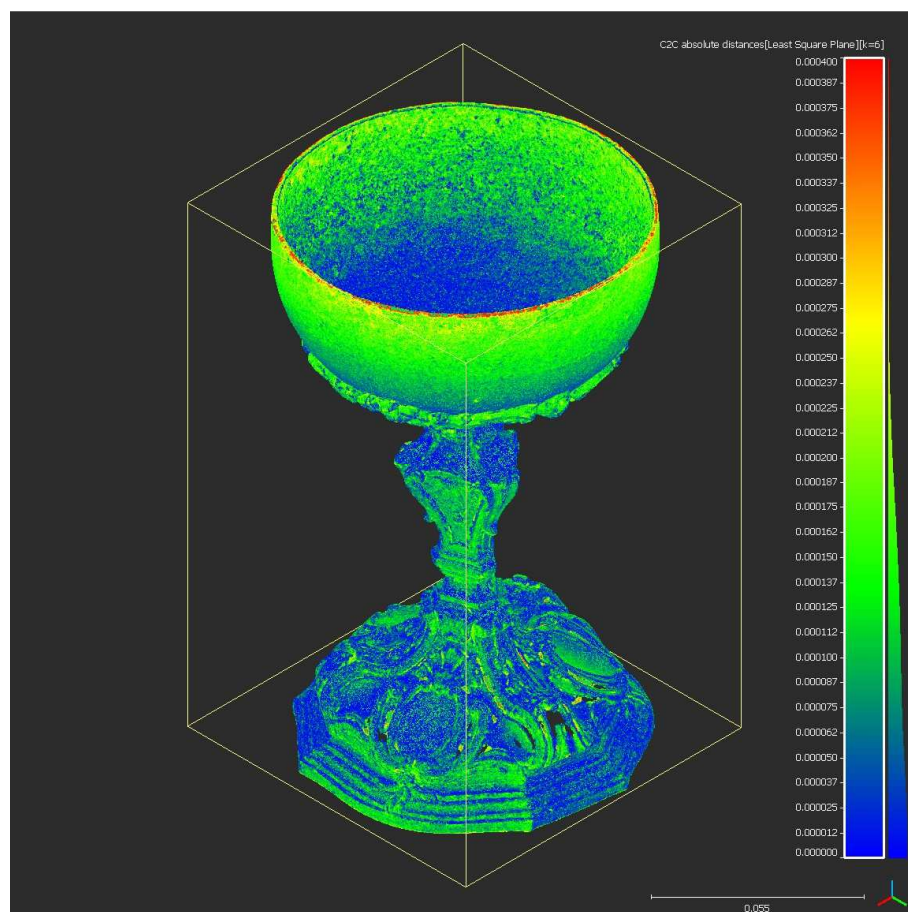


Fig. 69: Visualization of surface deviation

The maximum value on the scale was set to 0,0004 m (0,4 mm). These values can be seen only on the top of the object. Generally there is a good match between both models, below 0,2 mm.

The following Fig. 70 shows a multiview of all sides of the model.

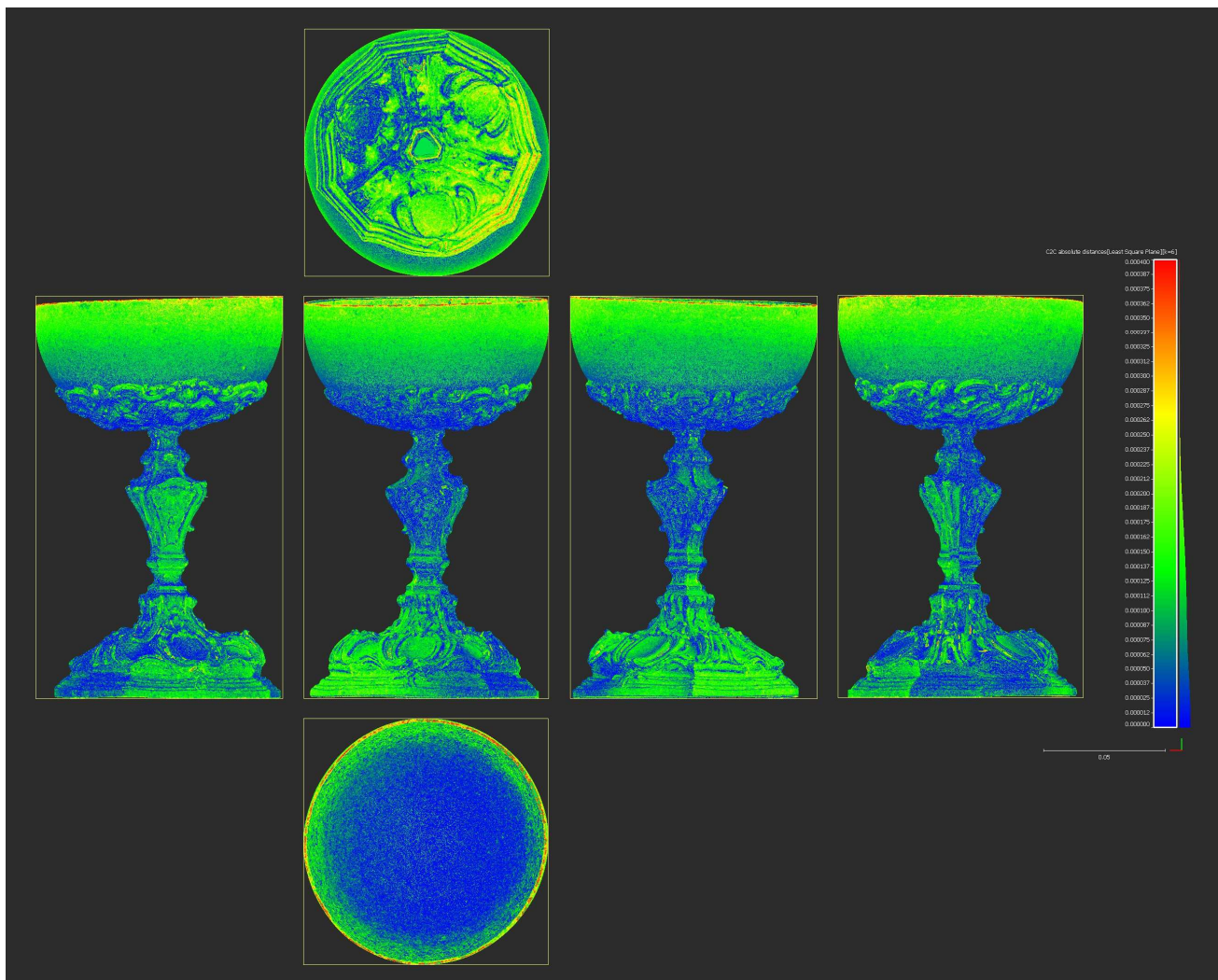


Fig. 70: Visualization of surface deviation

In Tab. 15 are the statistical results from the comparison of both models in CloudCompare:

Tab.15: Analysis results

**Diffused light vs. CPL models comparison**

<b>Mean distance</b>	0,000094
<b>Standard deviation</b>	0,000072
<b>Number of points</b>	4997123

Histogram on Fig. 71 shows the distribution of the points according to the absolute distance:

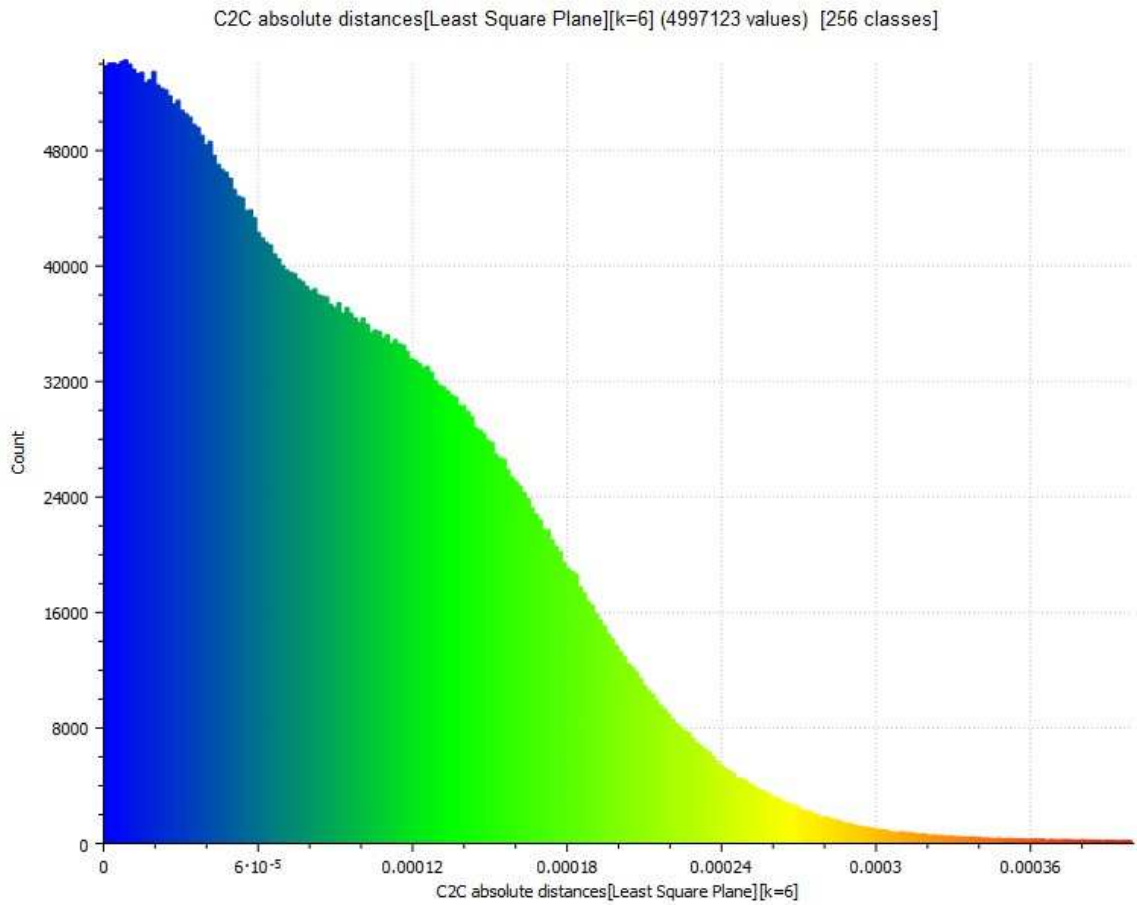


Fig. 71: Histogram of the points distribution according to the absolute distance

### Diffused Light vs. Scanning Spray Models Comparison

On Fig. 72 is an axonometric view of the object 1 and on Fig. 73 a multiview showing the absolute difference between the point clouds of the models made from diffused light and scanning spray method.

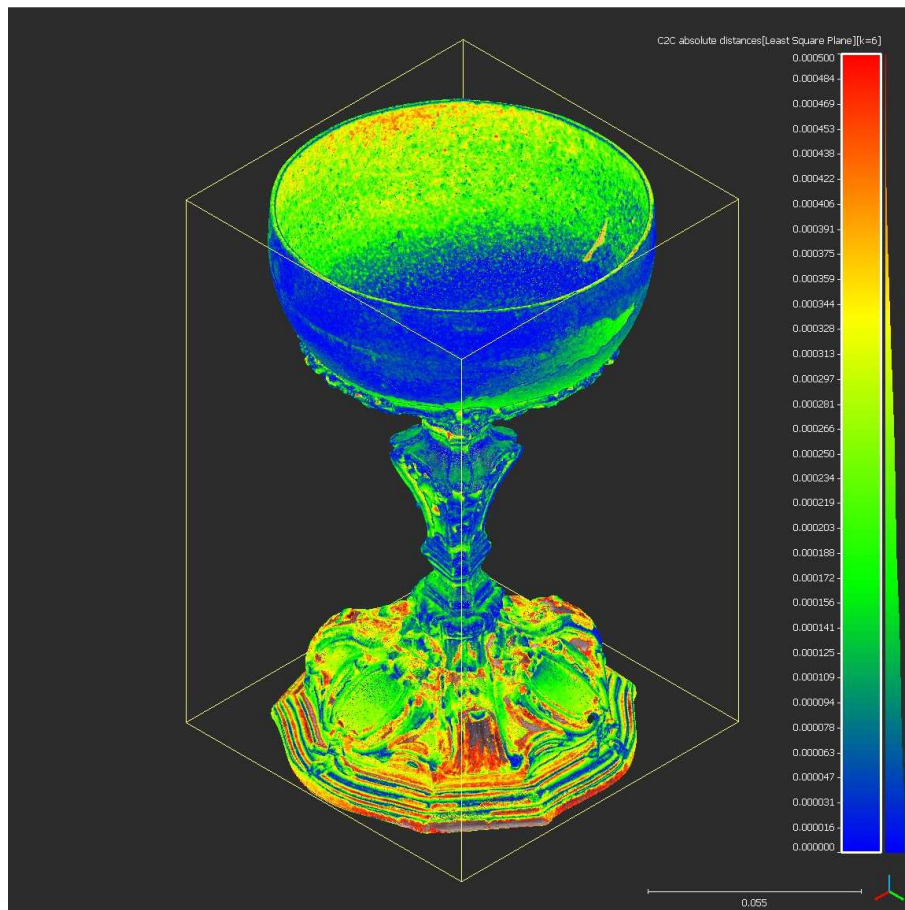


Fig. 72: Visualization of surface deviation

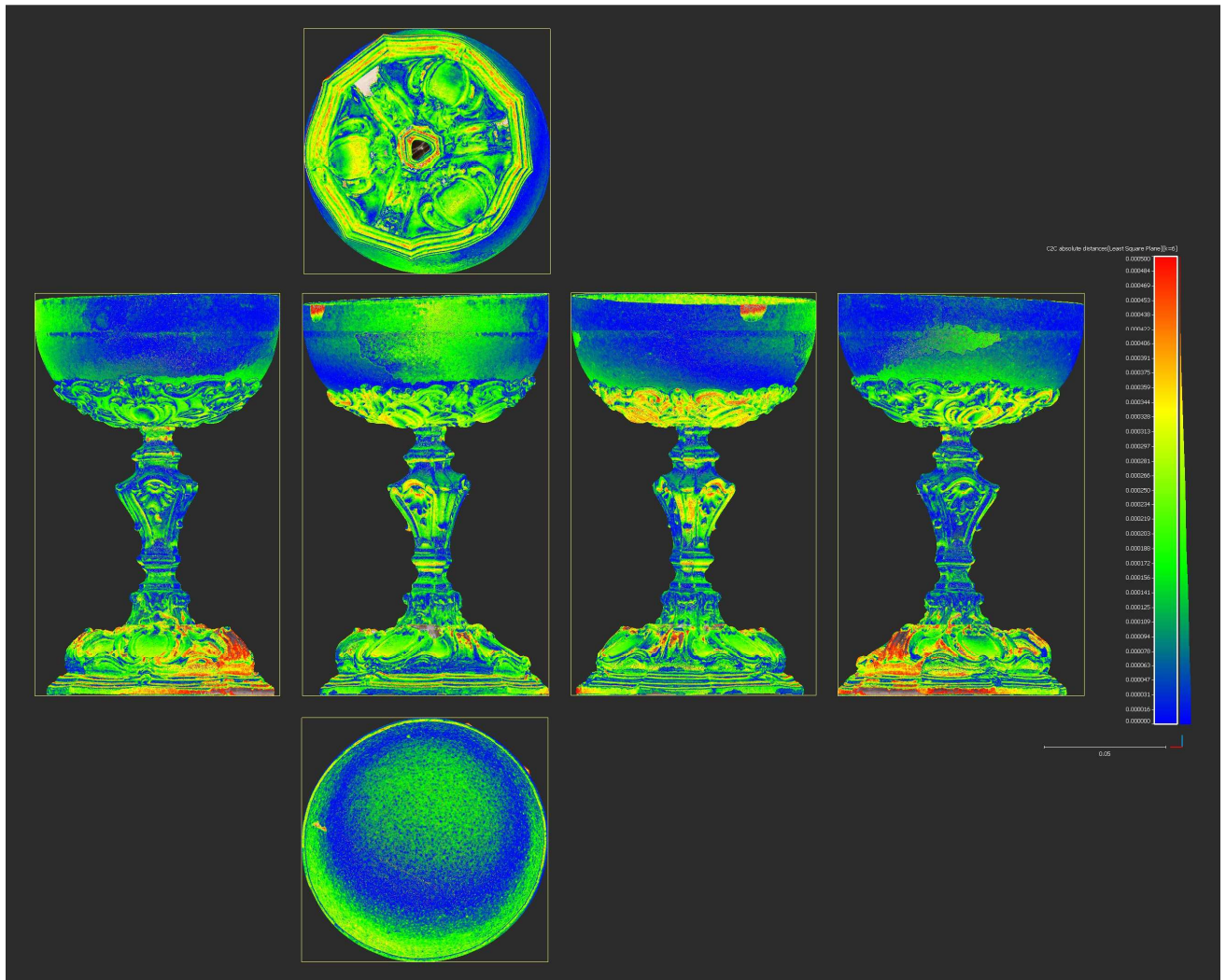


Fig. 73: Visualization of surface deviation

It is visible that on certain spots of the bottom part of the model, the difference is more than 0,5 mm.

In Tab. 16 are the statistical results from the comparison of both models in CloudCompare:

Tab.16: Analysis results

**Diffused light vs. scanning spray models comparison**

<b>Mean distance</b>	0,000159
<b>Standard deviation</b>	0,000117
<b>Number of points</b>	5000428

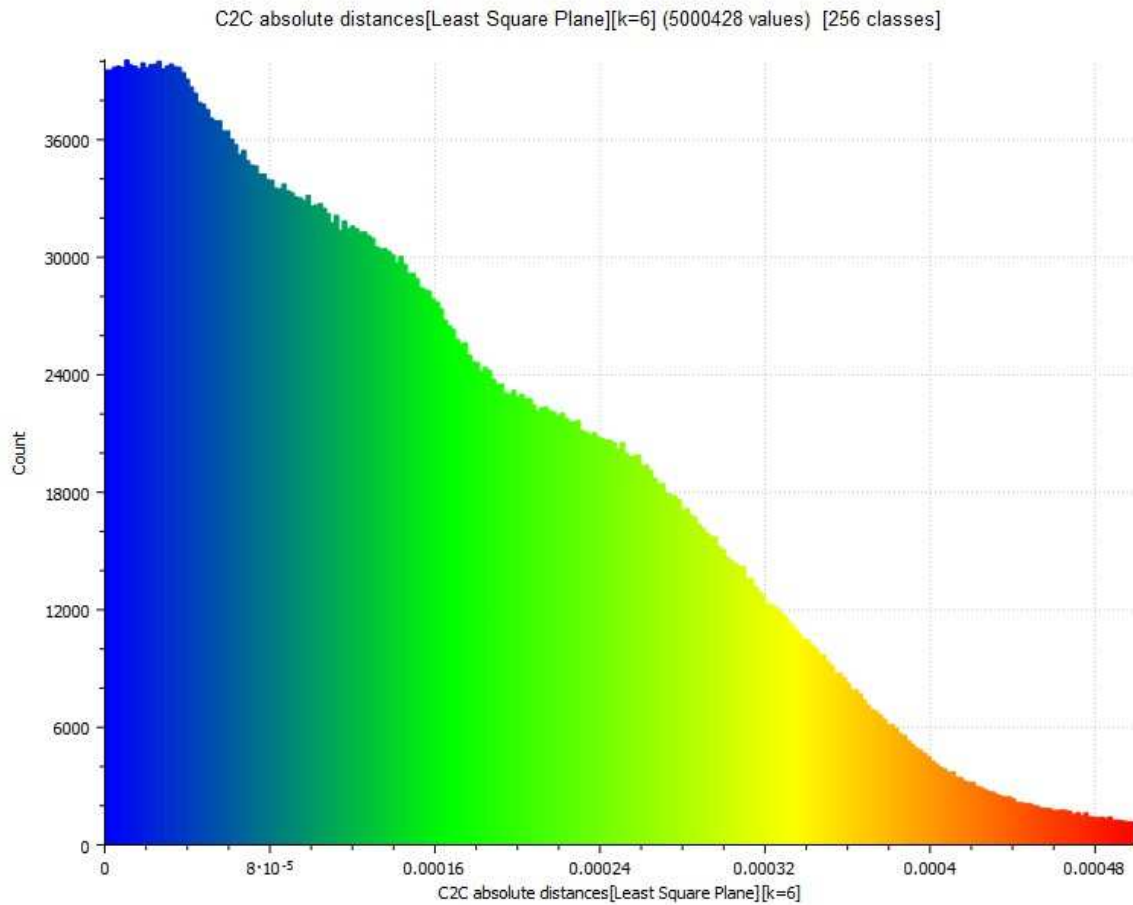


Fig. 74: Histogram of the points distribution according to the absolute distance

### CPL vs. Scanning Spray Models Comparison

On Fig. 75 is an axonometric view of Object 1 while Fig. 76 displays a multiview showing the absolute difference between the point clouds of the models made from CPL and scanning spray method.

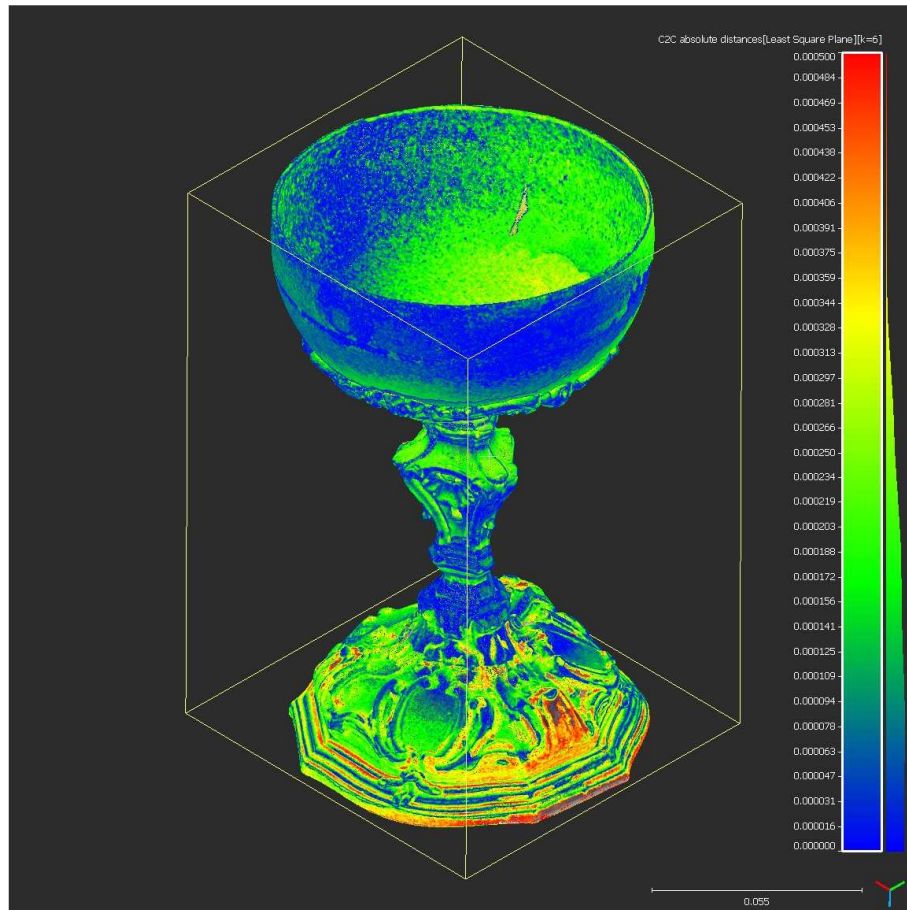


Fig. 75: Visualization of surface deviation

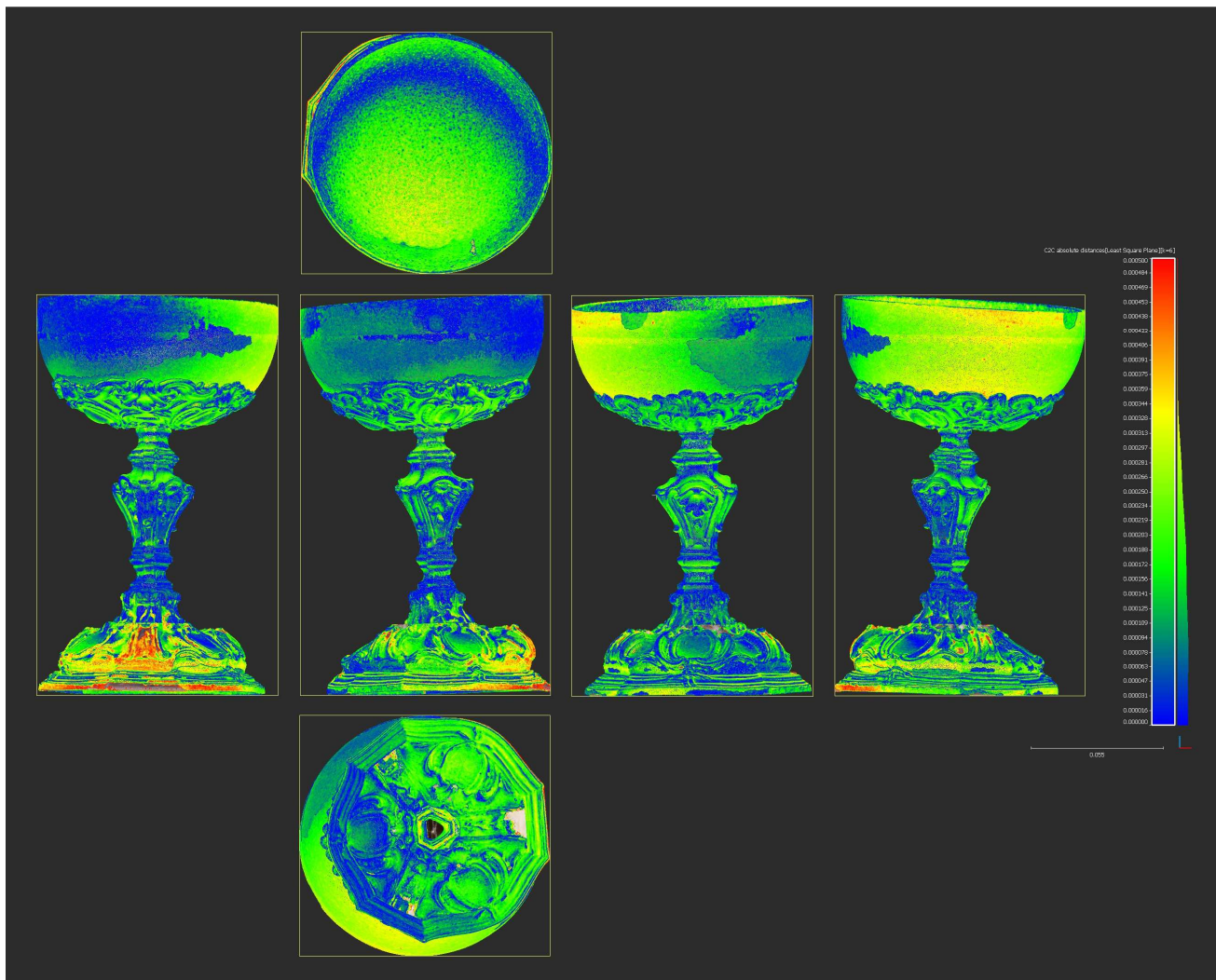


Fig. 76: Visualization of surface deviation

Also here is visible higher deviation in the bottom part of the model.

In Tab. 17 are the statistical results from the comparison of both models in CloudCompare:

Tab.17: Analysis results

**CPL vs. scanning spray models comparison**

<b>Mean distance</b>	0,000141
<b>Standard deviation</b>	0,000096
<b>Number of points</b>	5000428



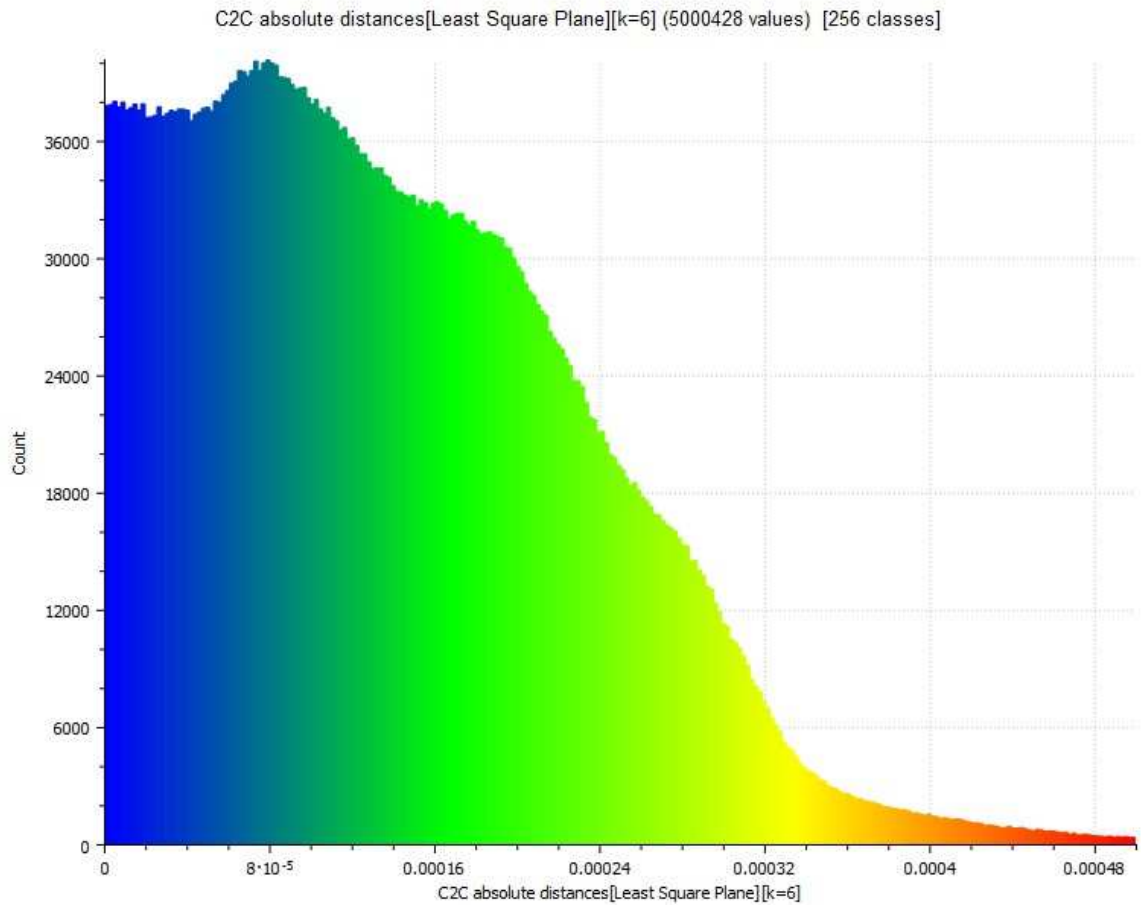
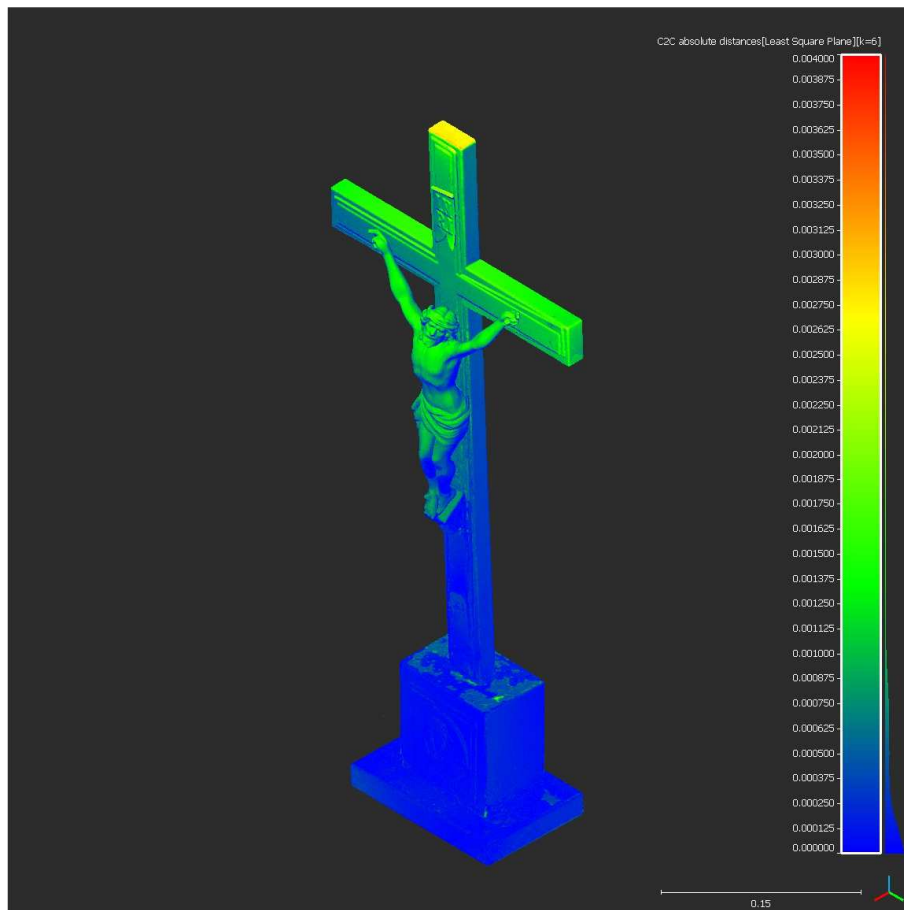


Fig. 77: Histogram of the points distribution according to the absolute distance

## Object 2

### Diffused Light vs. CPL Models Comparison

On Fig. 78 is an axonometric view of Object 2 showing the absolute difference between the point clouds of the models made from diffused light and CPL method.



**Fig. 78: Visualization of surface deviation**

During the comparison of the models it was found that there is a big difference between them, more than 3 mm on the top of the cross. The reason is that the cross was not firmly connected with the base, allowing some movement (with no possibility to repair it) and there was a difference in angle of the cross between two photo sessions (taking photos of the top and bottom parts) which caused the big deviation, as can be seen on the Fig. 79.



**Fig. 79:** Schematic visualisation of the movement and difference in the angle of the cross

For this reason, the base and the cross was aligned and compared separately.

On Fig. 80 is an axonometric view of the bottom part of Object 2 showing the absolute difference between the point clouds of the models made from diffused light and CPL method.

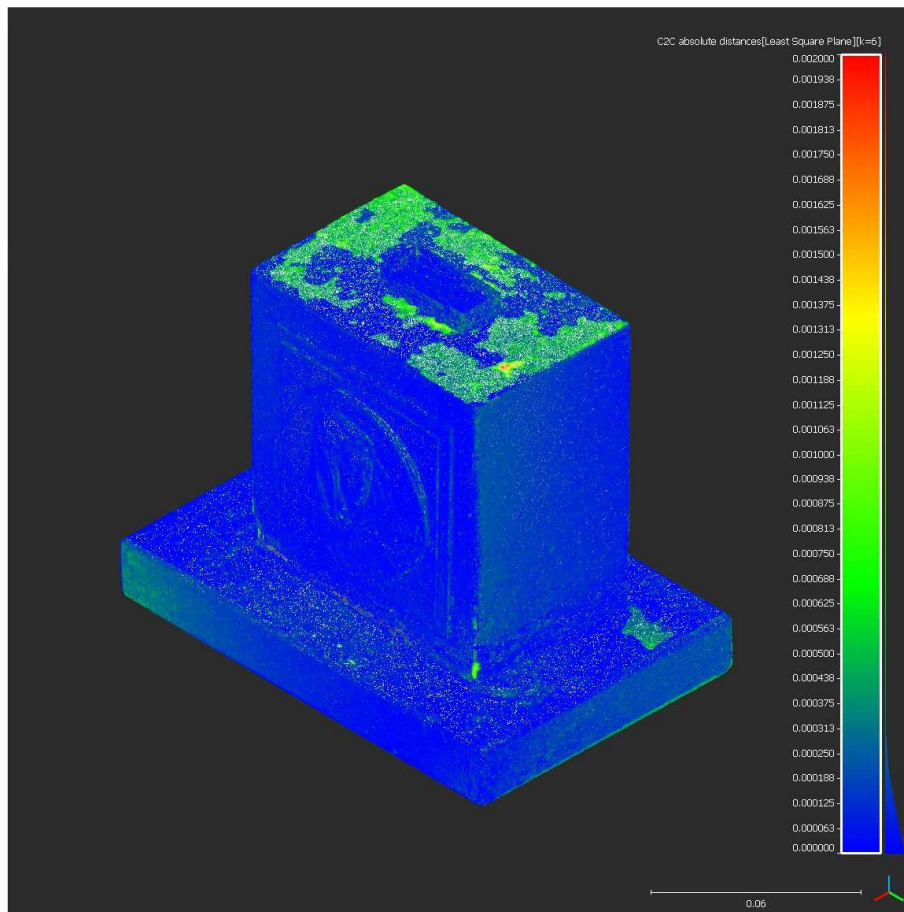
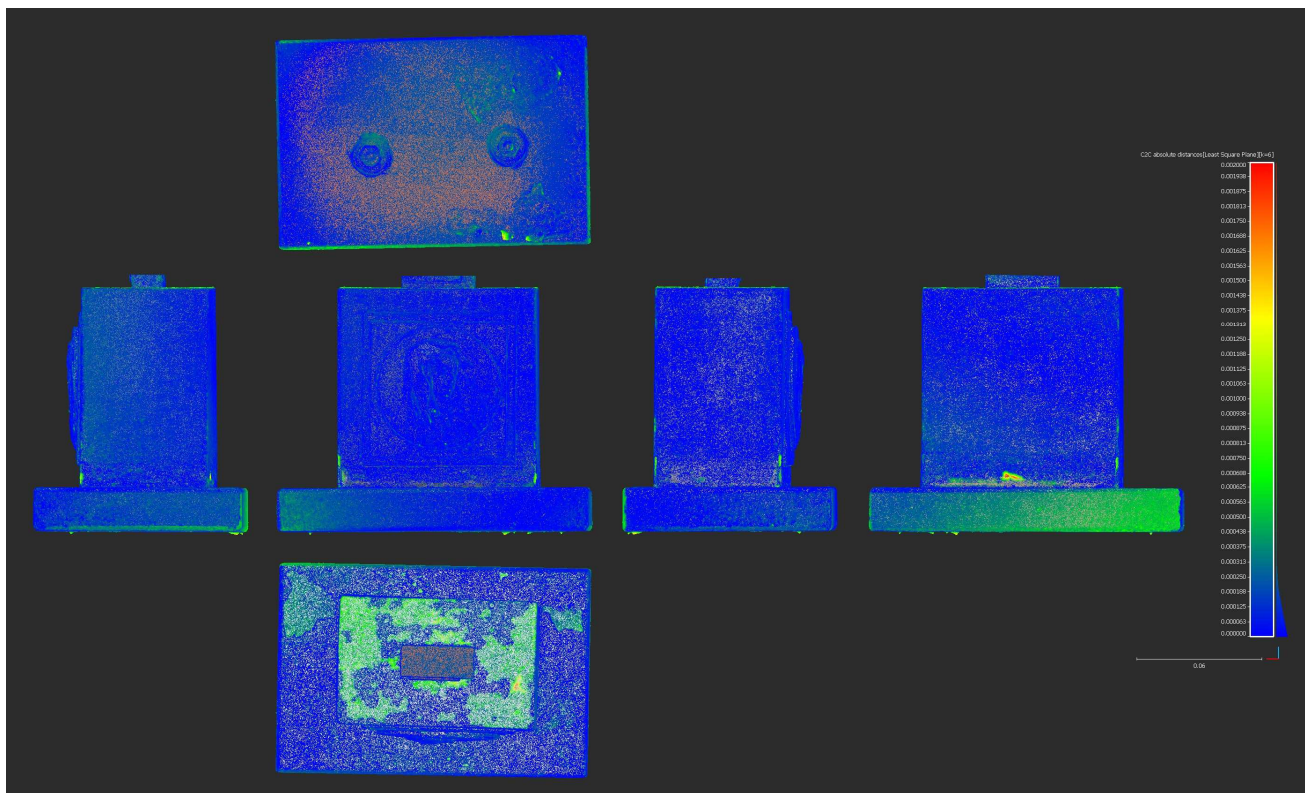


Fig. 80: Visualization of surface deviation



**Fig. 81: Visualization of surface deviation**

In Tab. 18 are statistical results from the comparison of both models in CloudCompare:

**Tab.18: Analysis results**

**Diffused light vs. CPL models comparison**

<b>Mean distance</b>	0,000127
<b>Standard deviation</b>	0,000146
<b>Number of points</b>	3729267

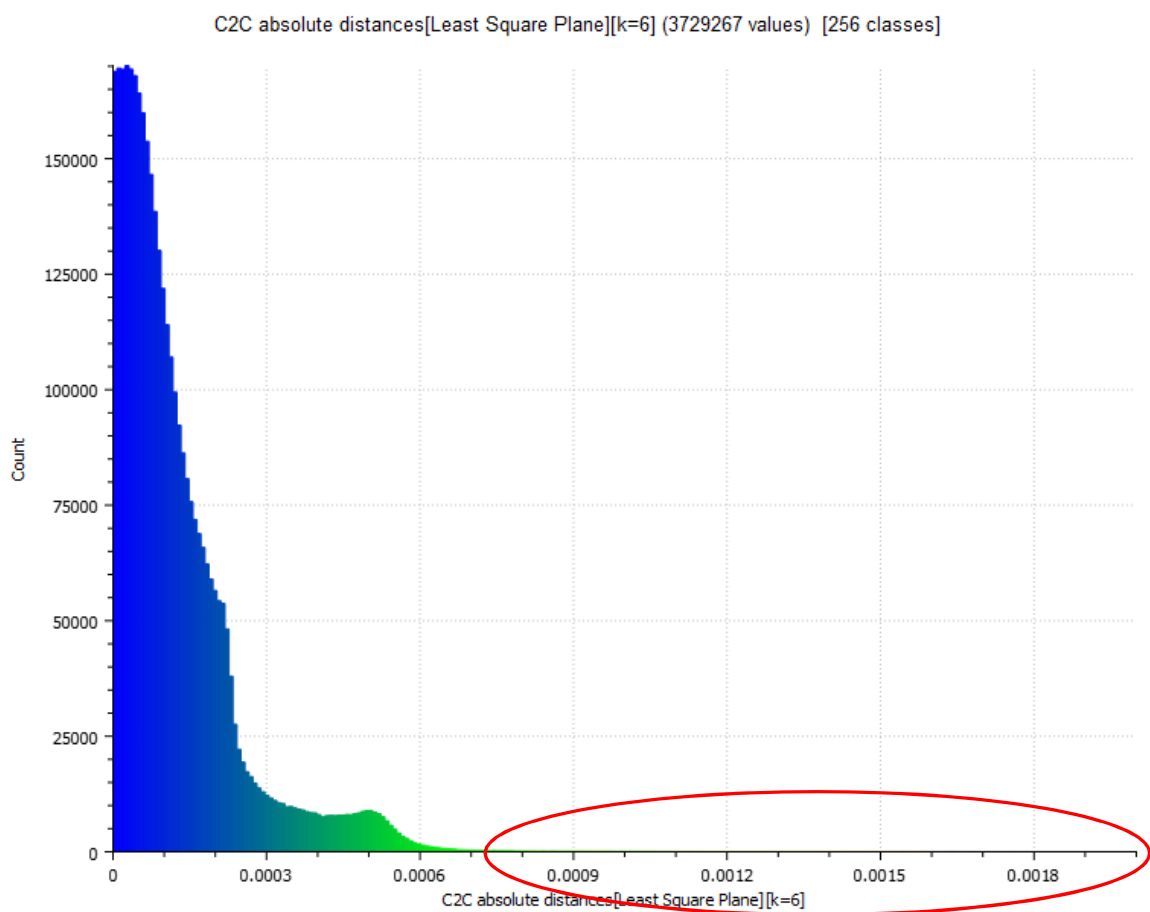


**Fig. 82: Histogram of the points distribution according to the absolute distance**

Fig. 82 shows a small number of points in bigger distance, as marked within the ellipse. They probably represent lonesome points outside of the object, which were not noticed and deleted. Even upon detailed examination of the point clouds they could not have been found.

On Fig. 83 is an axonometric view of the top part of the Object 2 showing the absolute difference between the point clouds of the models made from diffused light and CPL method.

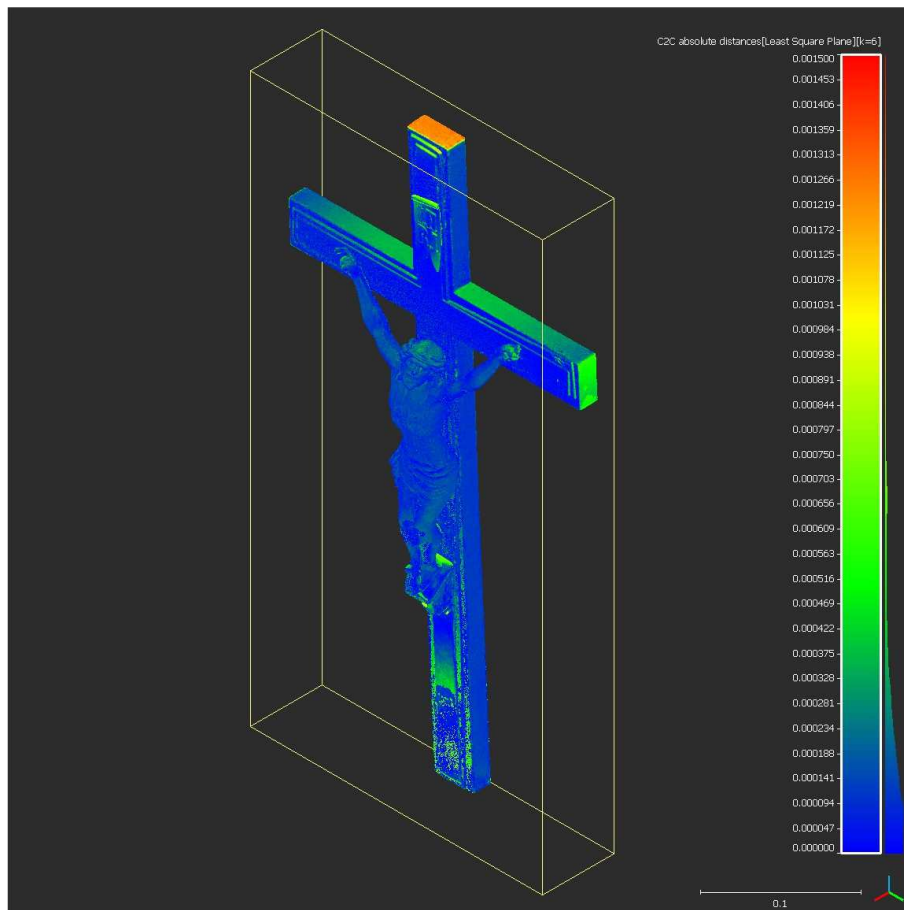


Fig. 83: Visualization of surface deviation

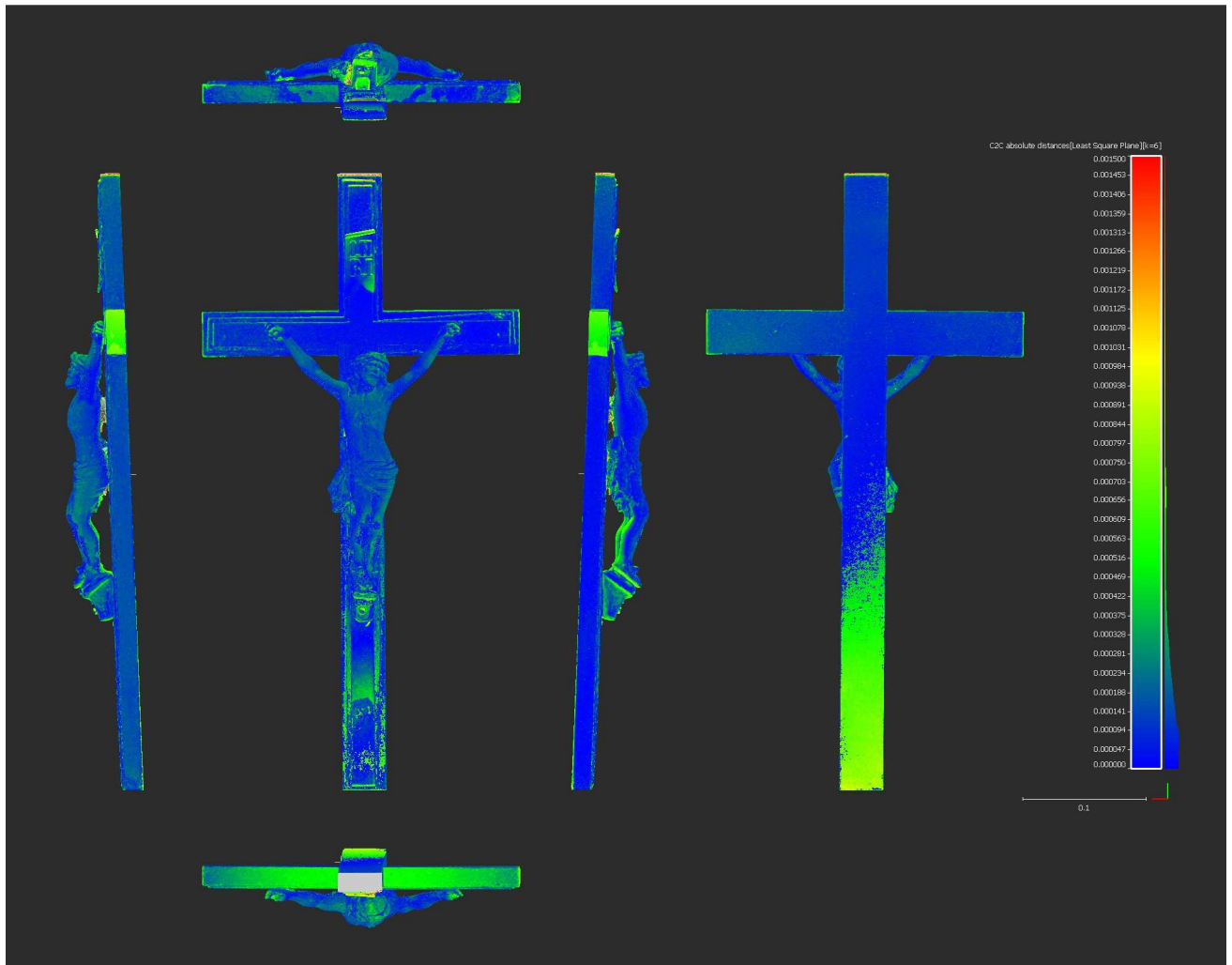


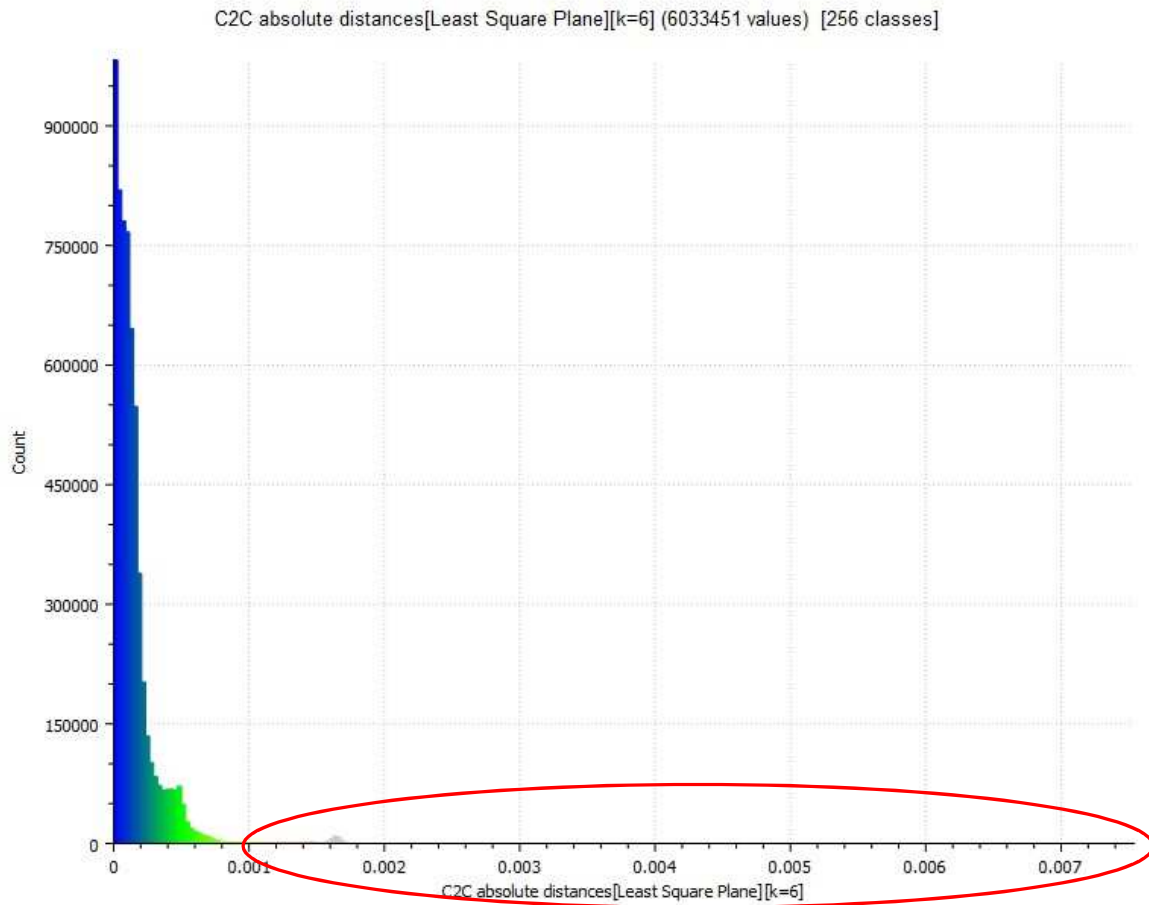
Fig. 84: Visualization of surface deviation

In Tab. 19 are the statistical results from the comparison of both models in CloudCompare:

Tab.19: Analysis results

**Diffused light vs. CPL models comparison**

<b>Mean distance</b>	0,000149
<b>Standard deviation</b>	0,000184
<b>Number of points</b>	6033451



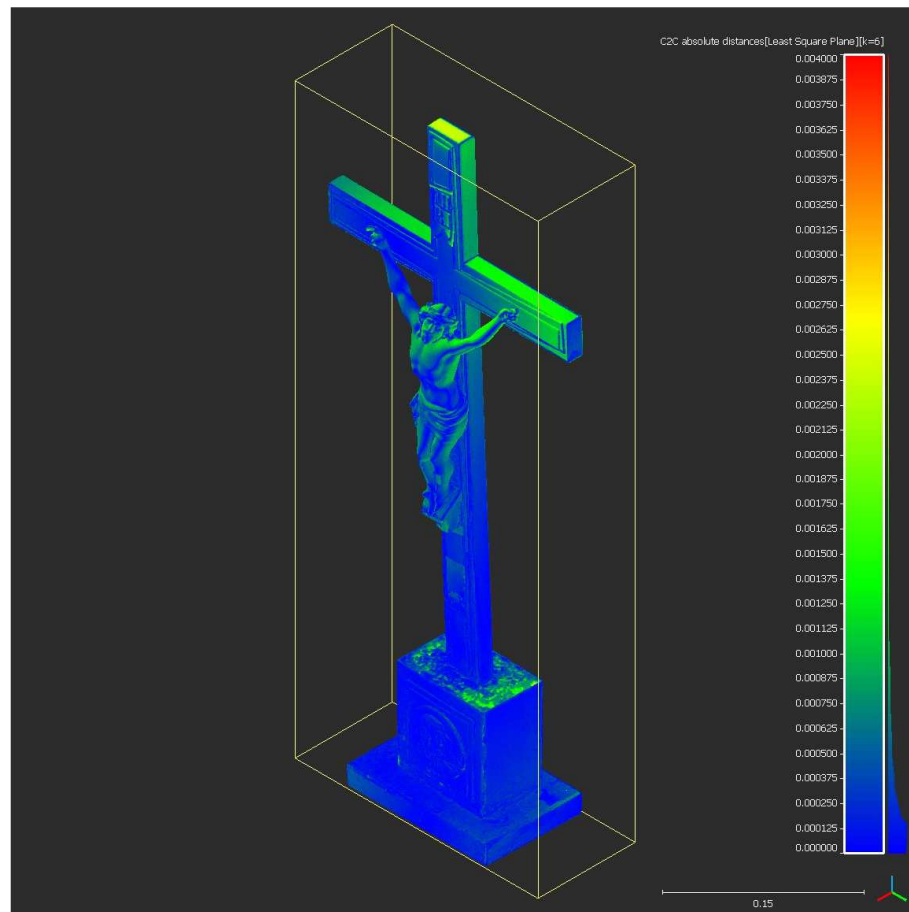
**Fig. 85: Histogram of the points distribution according to the absolute distance**

Fig. 85 again shows a small number of points in bigger distance, as marked within the ellipse.

### Diffused Light vs. Scanning Spray Models Comparison

On Fig. 86 is an axonometric view of Object 2 showing the absolute difference between the point clouds of the models made from diffused light and scanning spray method.





**Fig. 86: Visualization of surface deviation**

Similarly as in previous comparison, there is a deviation of the angle of the cross with the base. Although the difference is not as big as before (Fig. 78), the base and the cross were split and compared separately.

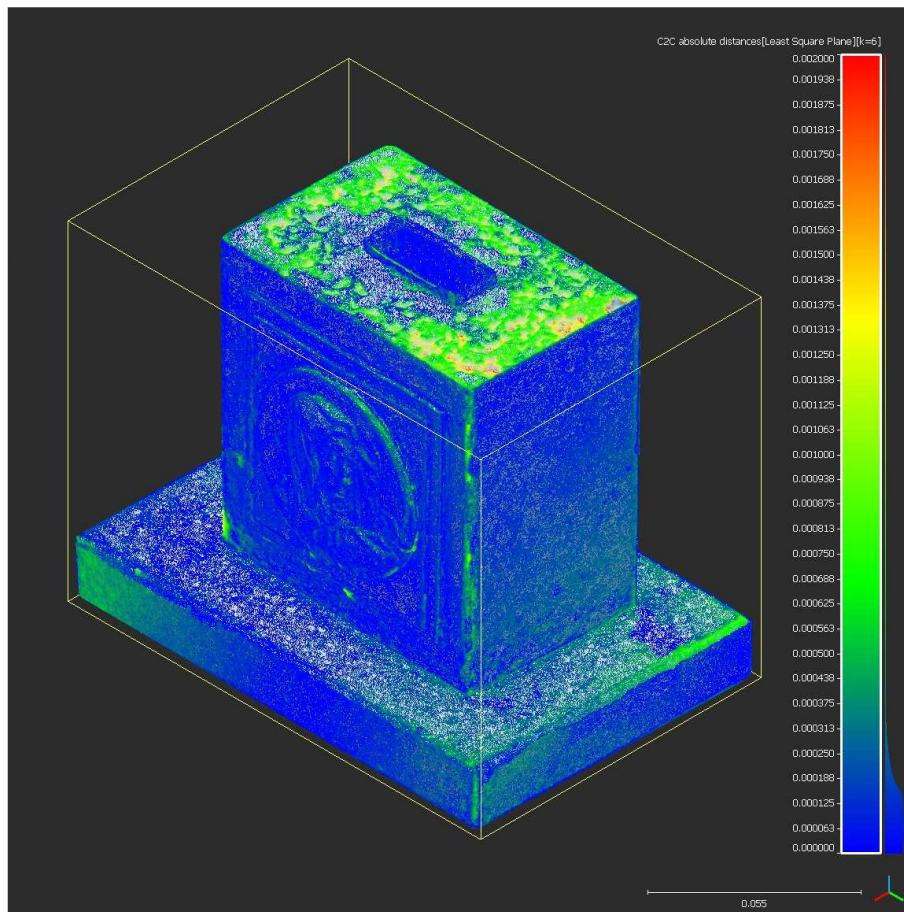
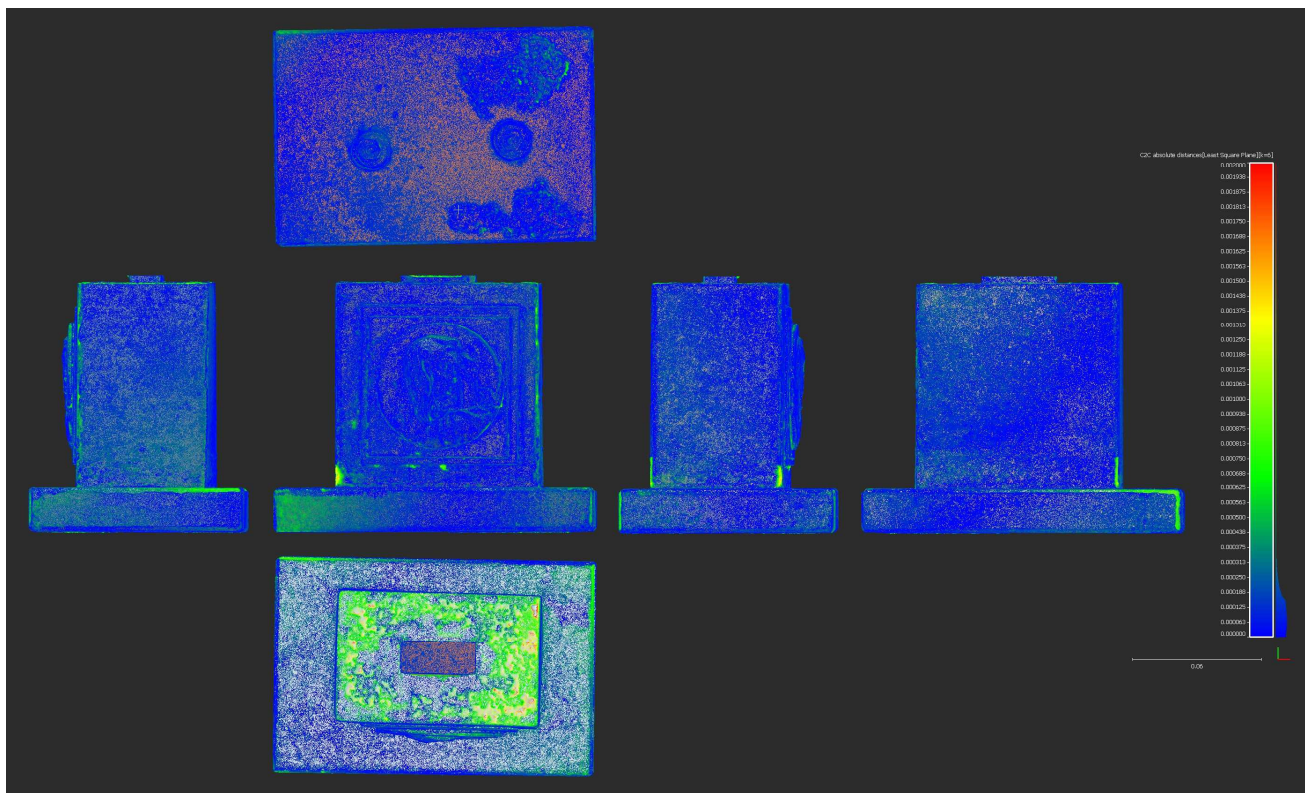


Fig. 87: Visualization of surface deviation



**Fig. 88: Visualization of surface deviation**

In Tab. 20 are the statistical results from the comparison of both models in CloudCompare:

**Tab.20: Analysis results**

**Diffused light vs. scanning spray models comparison**

<b>Mean distance</b>	0,000140
<b>Standard deviation</b>	0,000146
<b>Number of points</b>	3407564

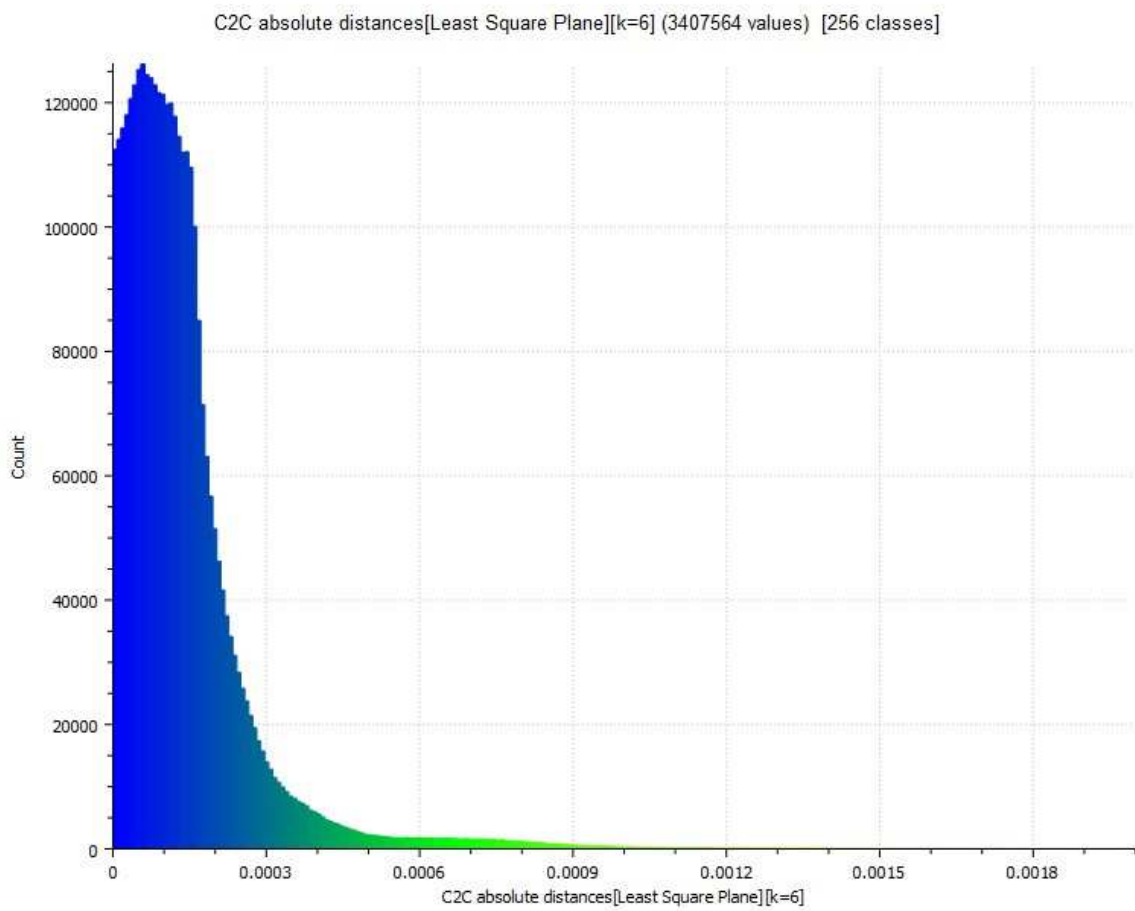


**Fig. 89: Histogram of the points distribution according to the absolute distance**

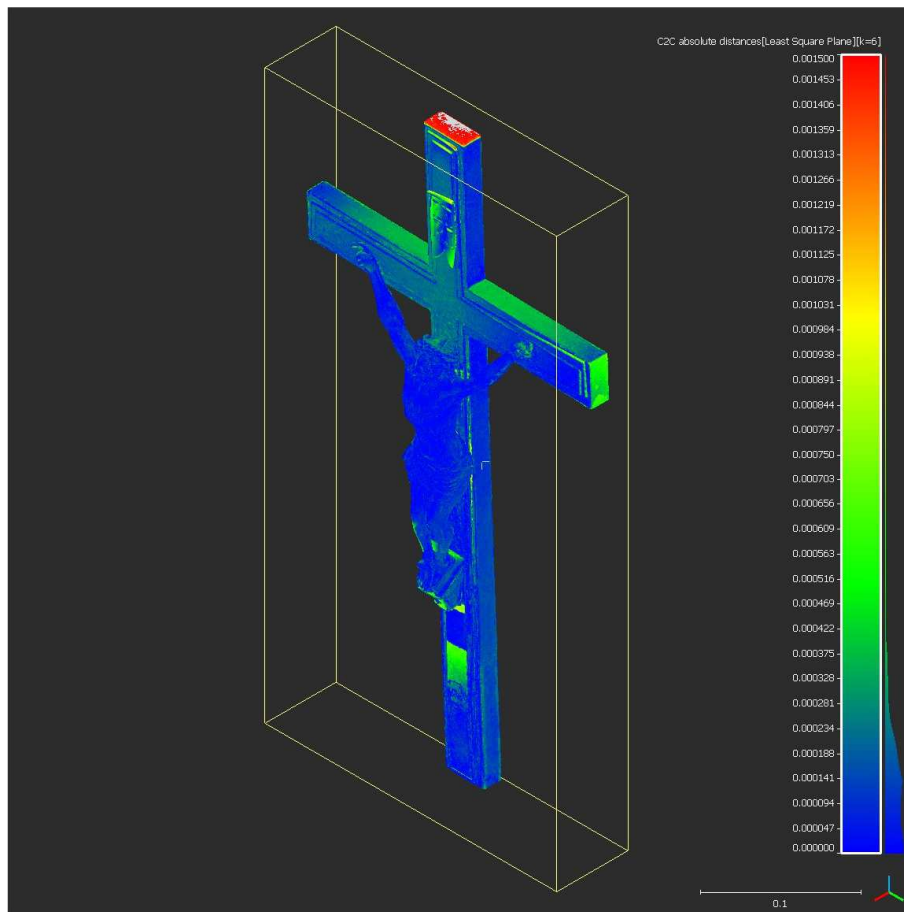


Fig. 90: Visualization of surface deviation

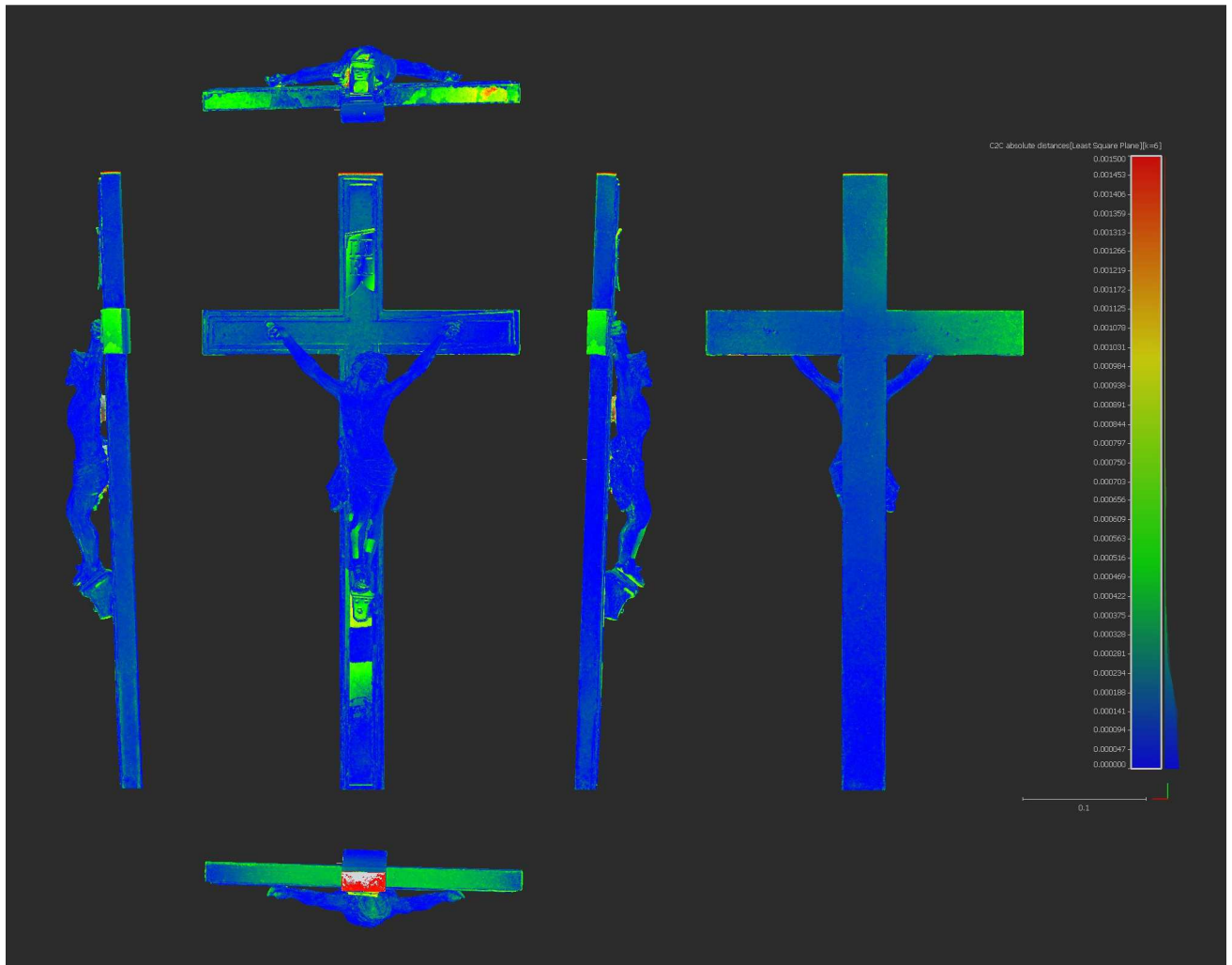


Fig. 91: Visualization of surface deviation

In Tab. 21 are the statistical results from the comparison of both models in CloudCompare:

Tab.21: Analysis results

**Diffused light vs. scanning spray models comparison**

<b>Mean distance</b>	0,000169
<b>Standard deviation</b>	0,000189
<b>Number of points</b>	6035080

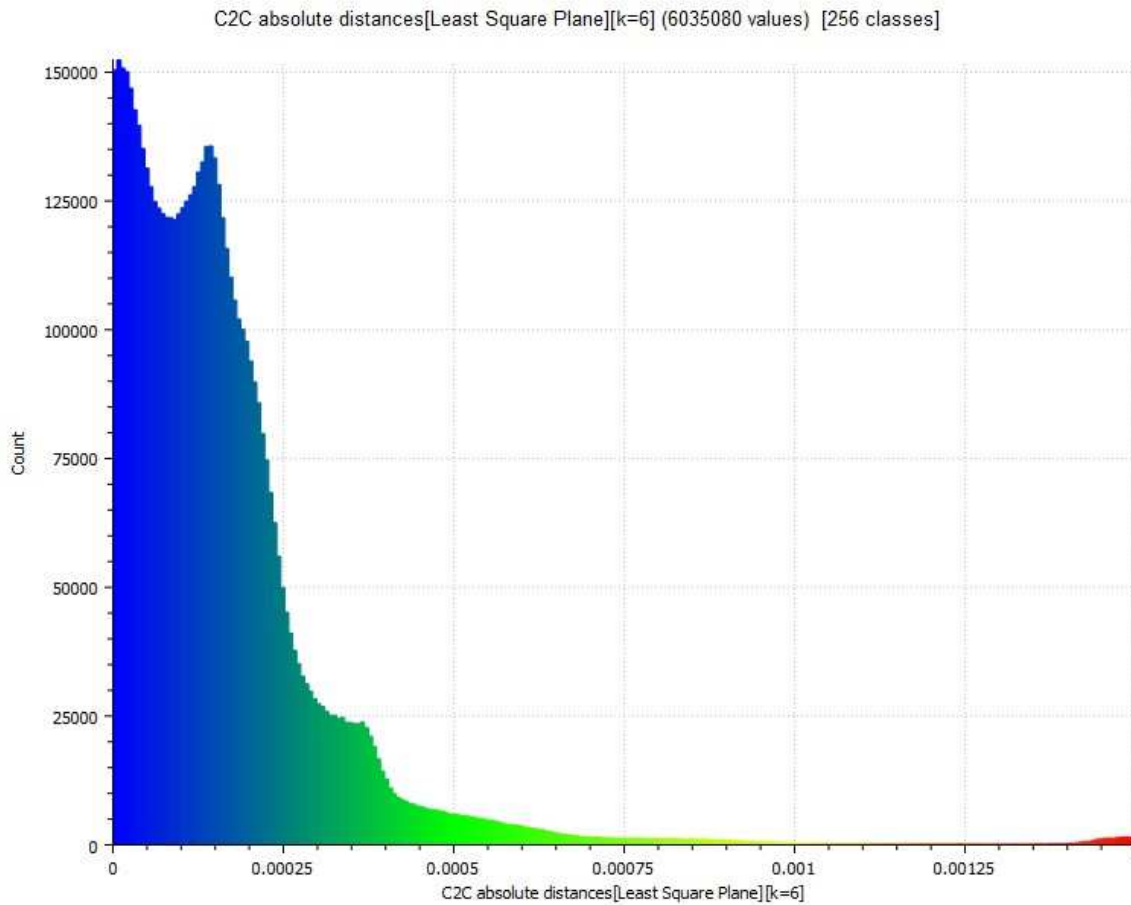
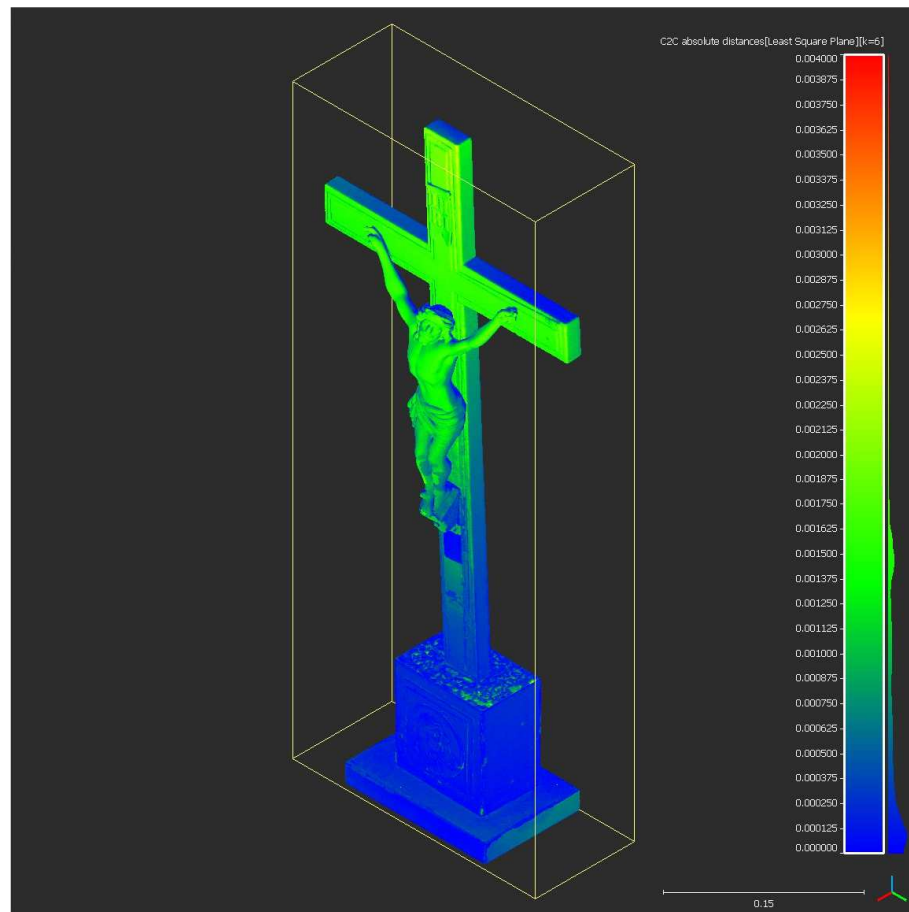


Fig. 92: Histogram of the points distribution according to the absolute distance

### CPL vs. Scanning Spray Models Comparison

On Fig. 93 is an axonometric view of Object 2 showing the absolute difference between the point clouds of the models made from CPL and scanning spray method.



**Fig. 93: Visualization of surface deviation**

The deviation of the angle of the cross with the base is visible again therefore both parts were split also in this case and compared separately.

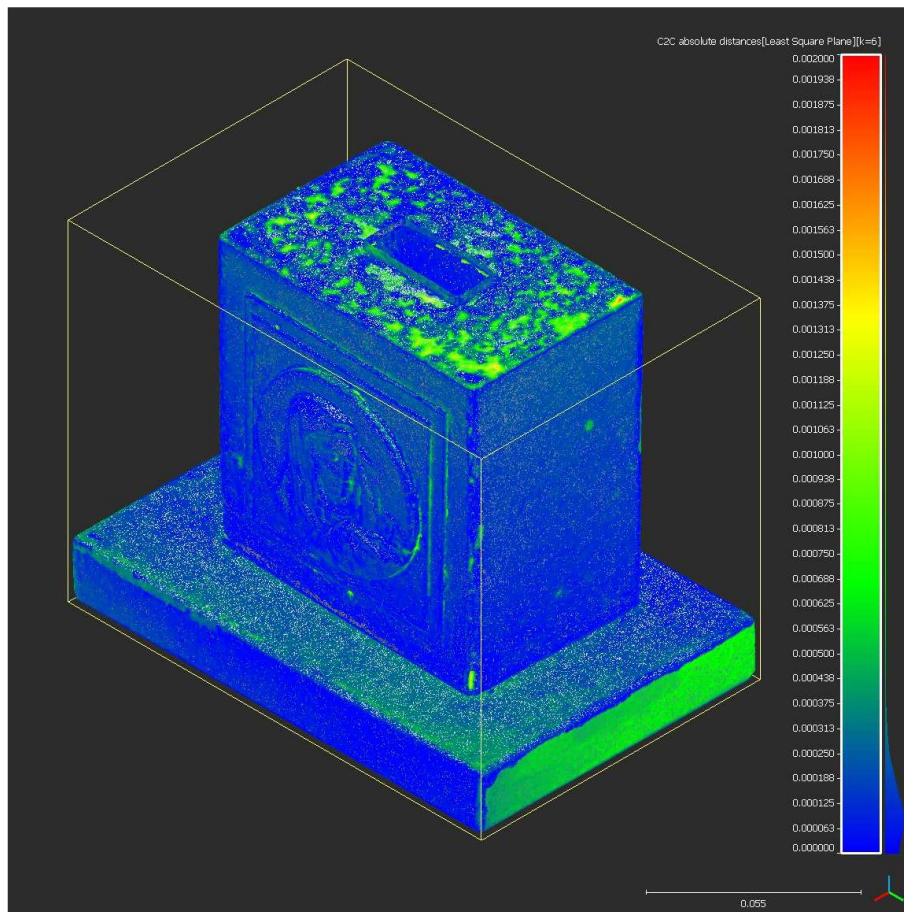
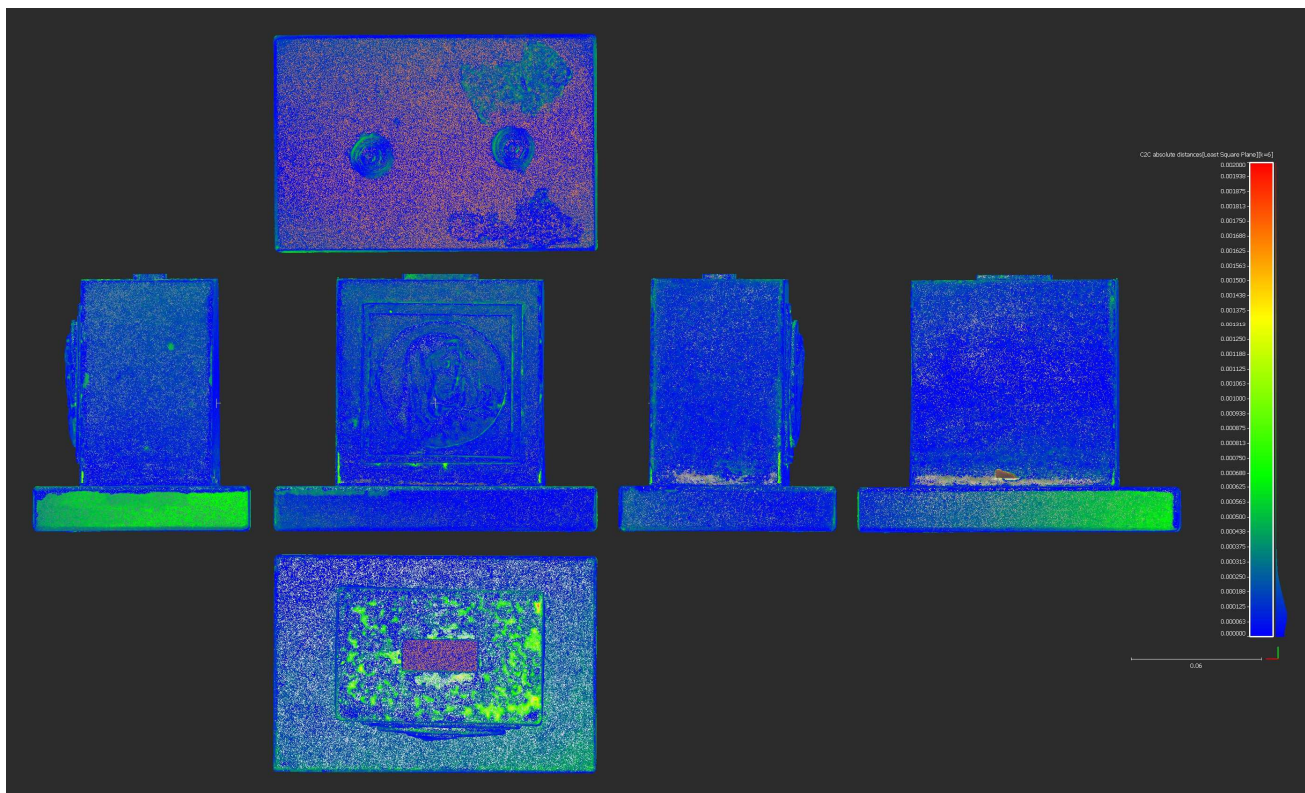


Fig. 94: Visualization of surface deviation





**Fig. 95: Visualization of surface deviation**

In Tab. 22 are the statistical results from the comparison of both models in CloudCompare:

**Tab.22: Analysis results**

**CPL vs. scanning spray models comparison**

<b>Mean distance</b>	0,000160
<b>Standard deviation</b>	0,000159
<b>Number of points</b>	3702516

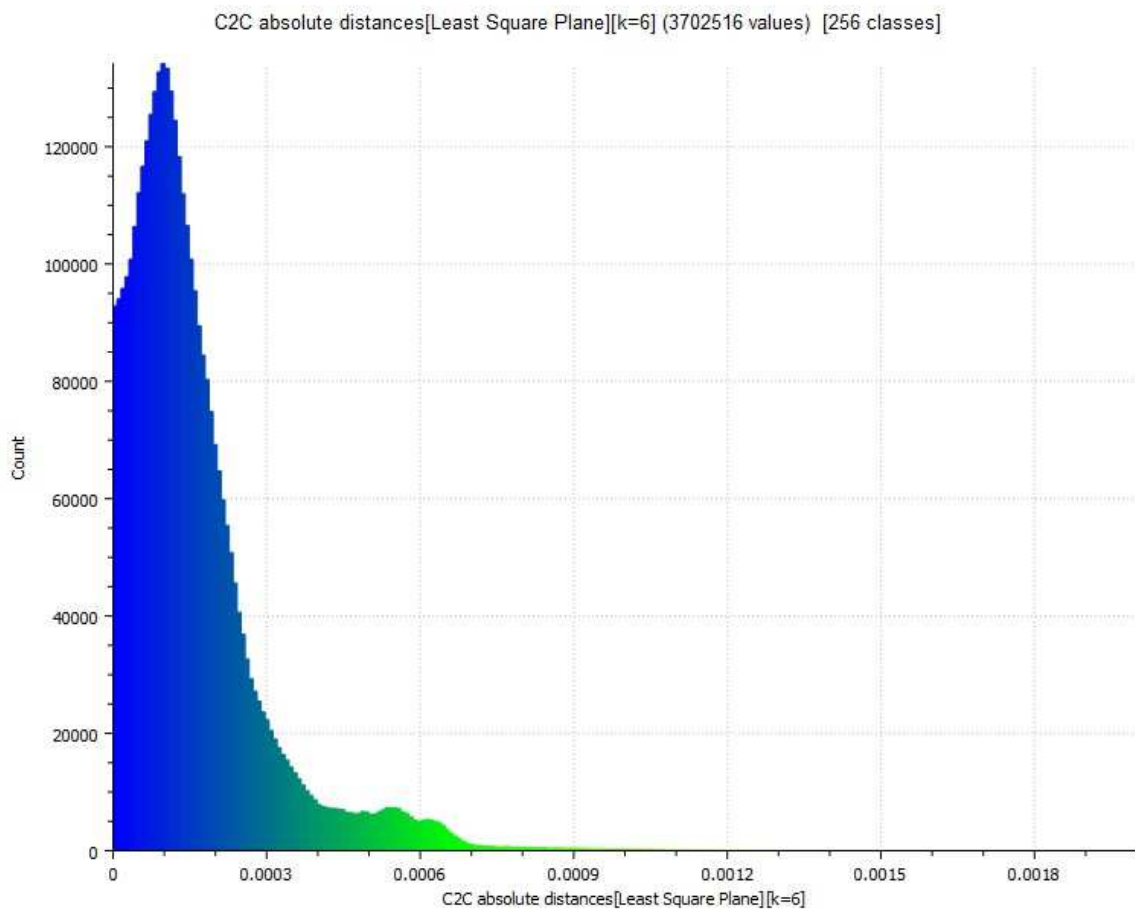


**Fig. 96: Histogram of the points distribution according to the absolute distance**

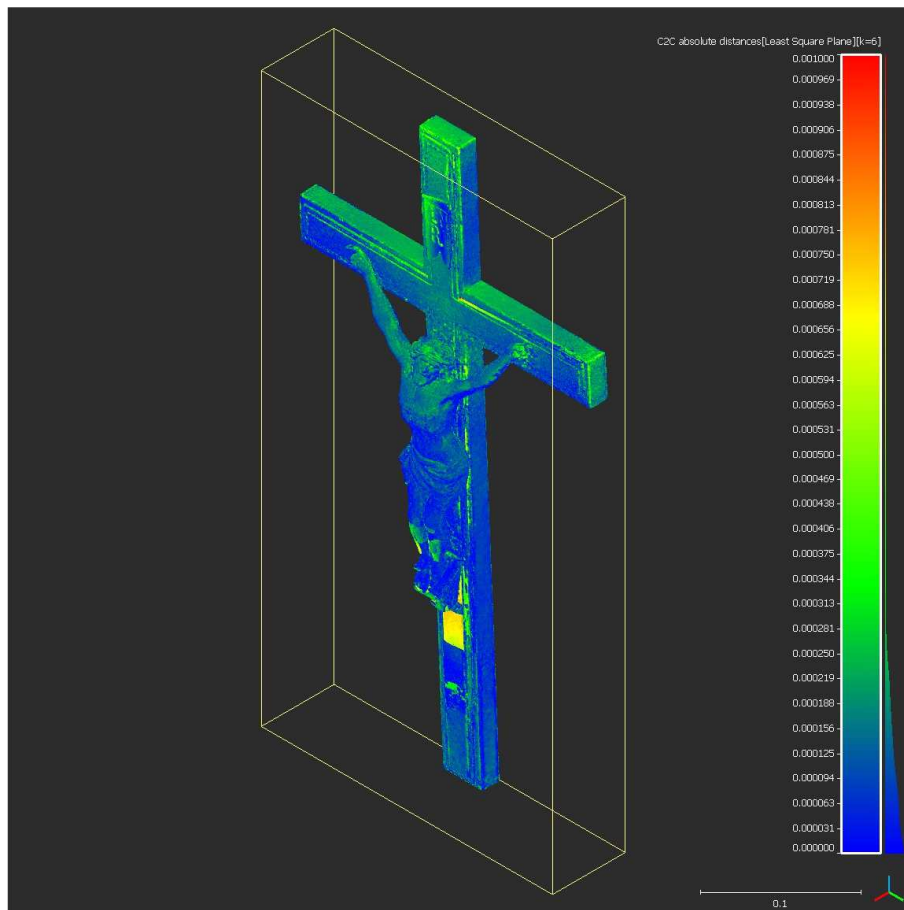


Fig. 97: Visualization of surface deviation

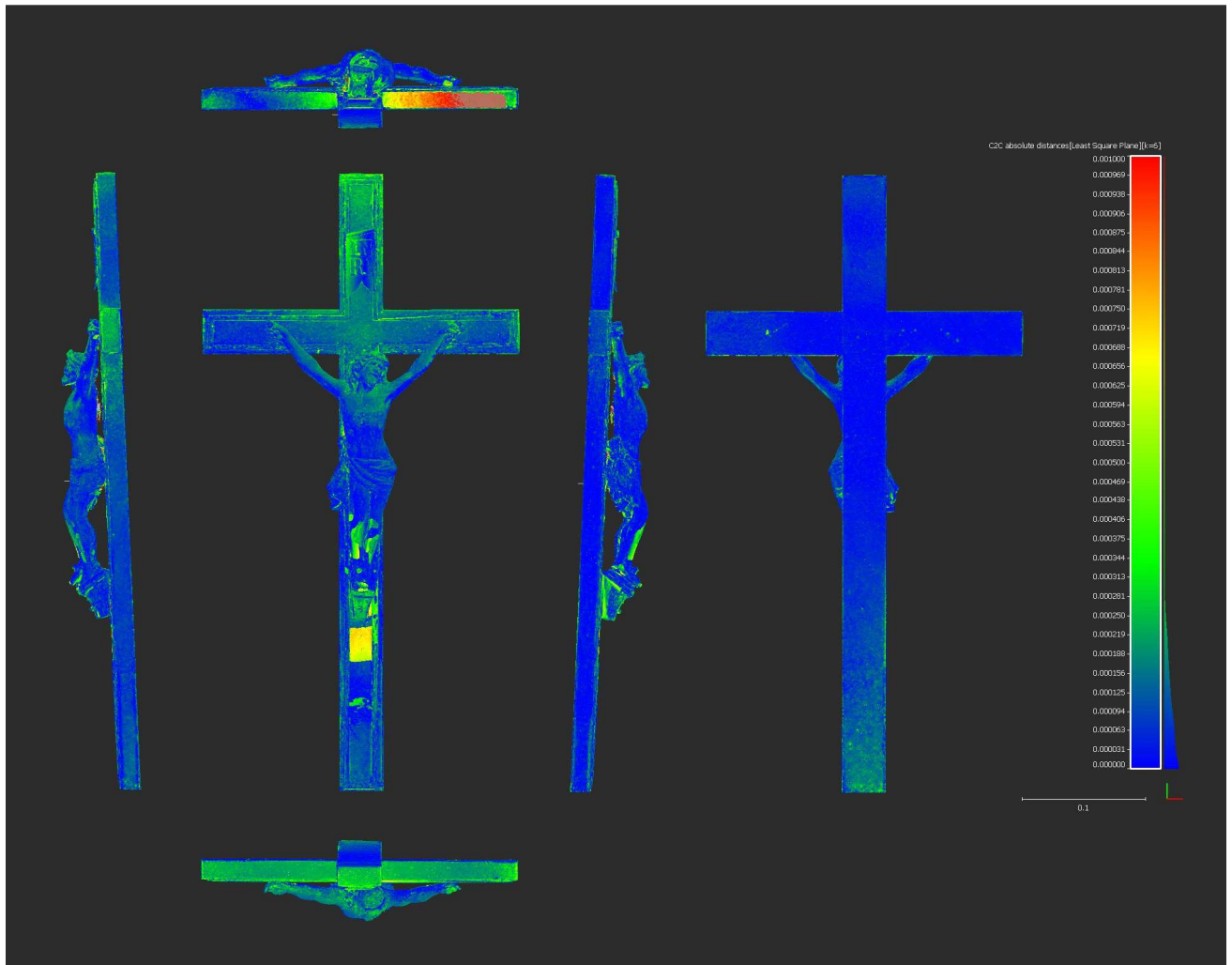


Fig. 98: Visualization of surface deviation

In Tab. 23 are the statistical results from the comparison of both models in CloudCompare:

Tab.23: Analysis results

**CPL vs. scanning spray models comparison**

<b>Mean distance (m)</b>	0,000122
<b>Standard deviation (m)</b>	0,000144
<b>Number of points</b>	6597803

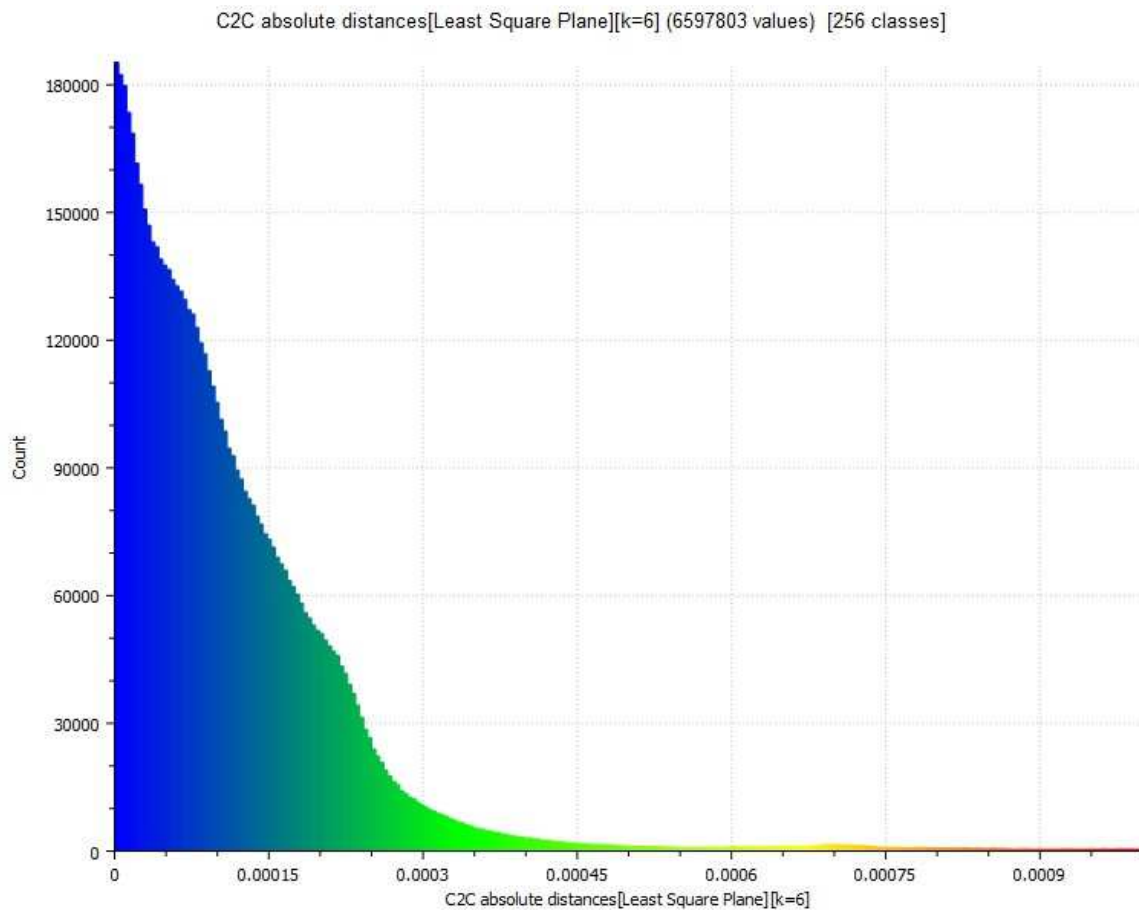


Fig. 99: Histogram of the points distribution according to the absolute distance

### 3.1.3 Quantitative Evaluation

For the quantitative evaluation, accurate measurements on the 3D models and real objects were performed. For this purpose, a digital caliper with accuracy of 0,01 mm was used in order to measure 5 control distances between defined points on each object (Fig. 100 and Fig. 102), (calculated as average based on 3 measurements) and respective distances were measured also on 3D models. The results of these measurements are presented in Tab. 24 and 25.

The absolute distances between the measurements on real models and measurements on 3D models are shown on Fig. 101 and Fig. 103.

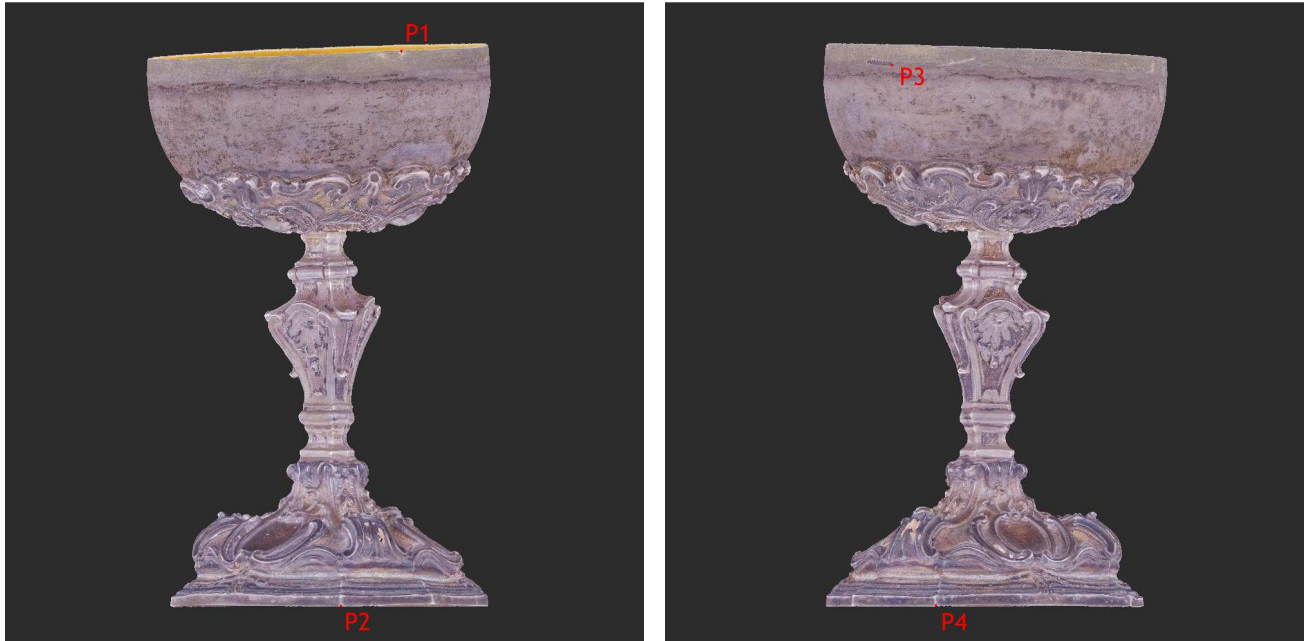


Fig. 100: Definition of measuring points on Object 1

Tab.24: Measured distances between points

Distance	Real object	Diffused light model	CPL model	Scanning spray model
P1-P2	163,86	164,085	163,833	163,562
P1-P3	83,25	83,499	83,350	83,115
P2-P4	93,10	93,081	93,198	93,747
P3-P4	159,38	159,527	159,416	159,595
diameter at P1	98,48	98,736	98,550	98,834

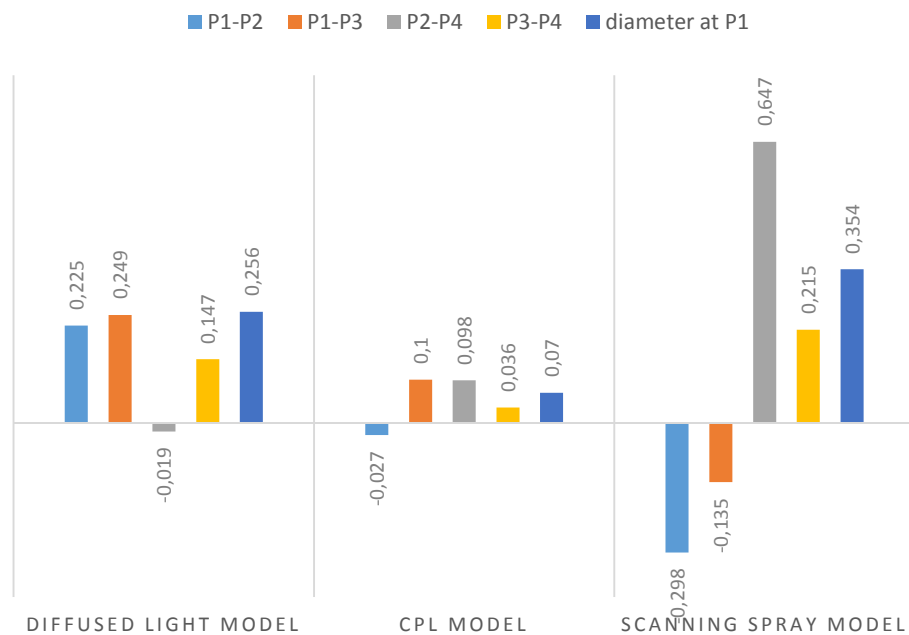


Fig. 101: Absolute distances between the model and real object 1 measurements



Fig. 102: Definition of measuring points on Object 2

Tab.25: Measured distances between points

Distance	Real object	Diffused light model	CPL model	Scanning spray model
P1-P2	254,05	254,638	254,386	254,747
P3-P4	148,36	148,681	148,535	148,350
P5-P6	354,65	355,802	355,533	355,908
P7-P8	99,68	99,815	99,590	100,197
P9-P10	110,15	111,263	110,316	110,644

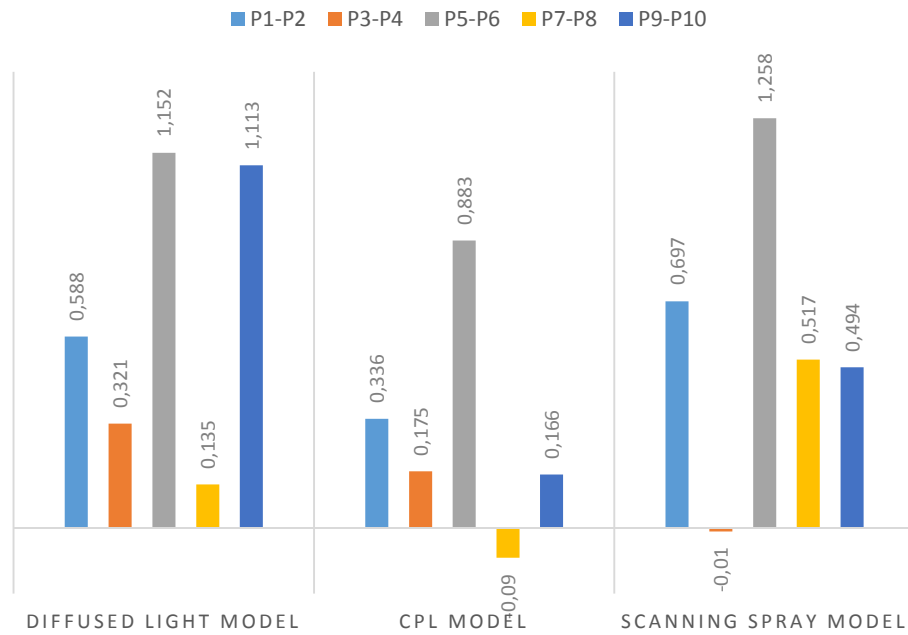


Fig. 103: Absolute distances between the model and real Object 1 measurements

From the distances it's visible, that the CPL model has minimal deviations compared with other models. Of course this comparison is not very precise, however it provides some results, similar as can be seen from difference comparison in the chapter 3.1.2.

### 3.1.4 Qualitative Evaluation

The qualitative evaluation is just a subjective visual comparison of the meshes, their surface quality and the amount of noise. In the following pictures detailed images of the models made of diffused light, CPL and scanning spray photos are compared.

In each picture, left (a) image is the model based on diffused light, in the middle (b) is the CPL model and on the right (c) is the scanning spray model.

#### Object 1:

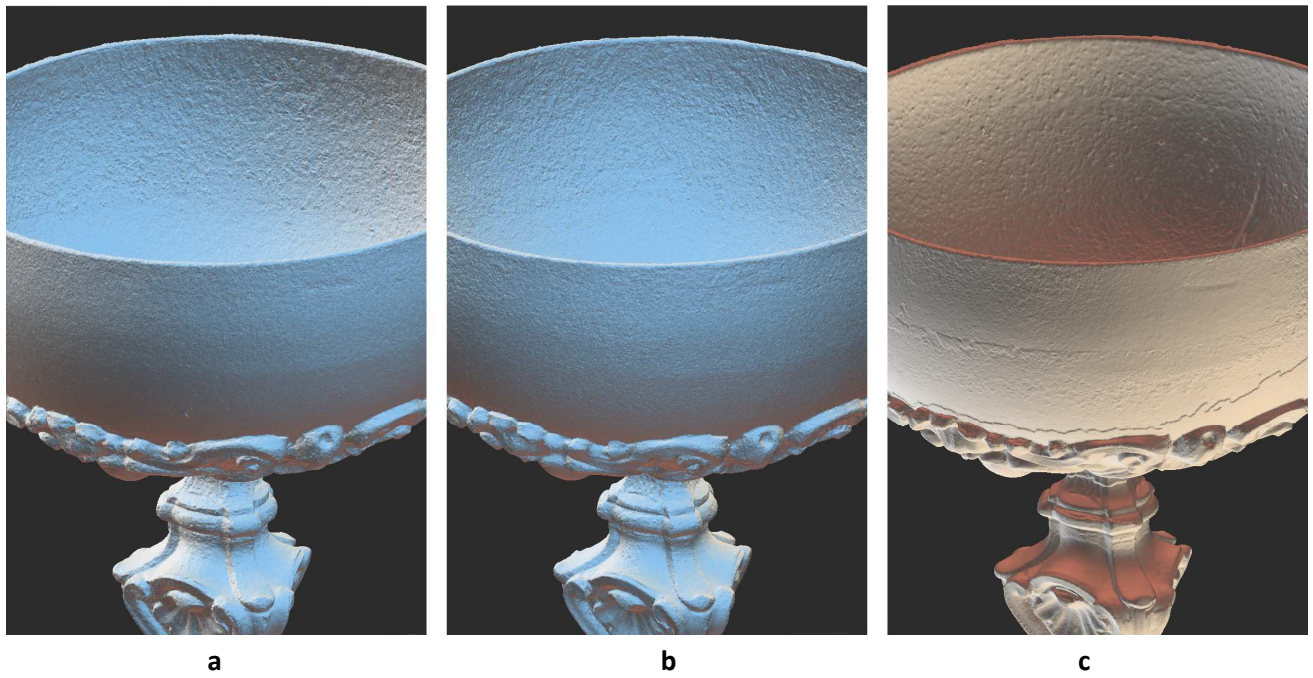


Fig. 104: Comparison of the details of Object 1

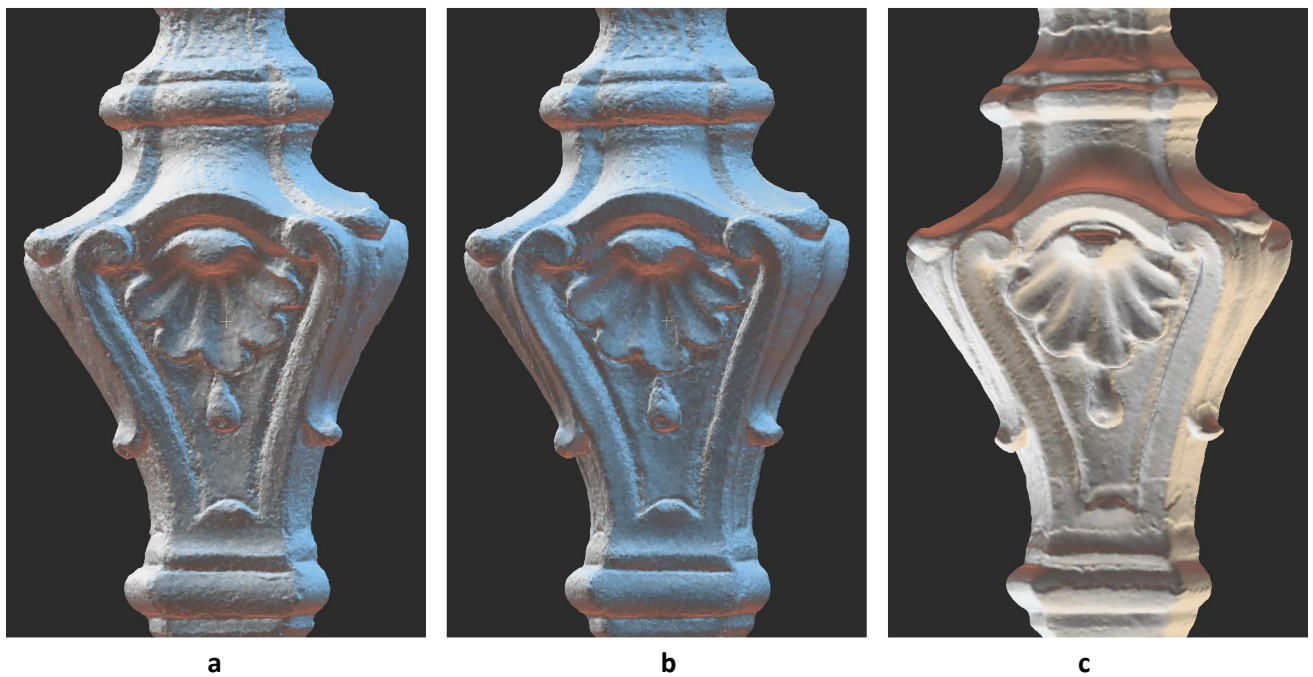
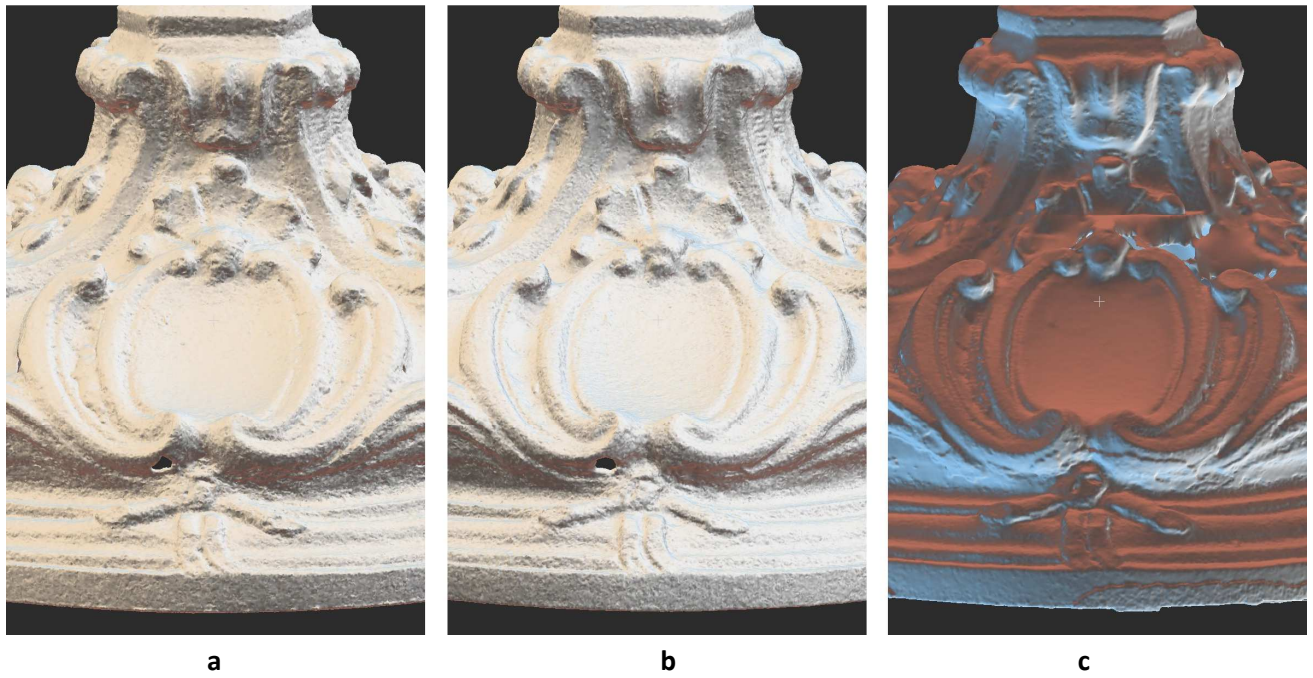


Fig. 105: Comparison of the details of Object 1





**Fig. 106: Comparison of the details of Object 1**

As shown in Fig. 104 – 106 it is clear that the middle image representing the CPL based model shows the minimum amount of noise while the surface is smoother. The scanning spray model has seams due to incorrect alignment of the top and bottom part. The seams are also visible on the diffused light model on Fig. 105 (a)

**Object 2:**

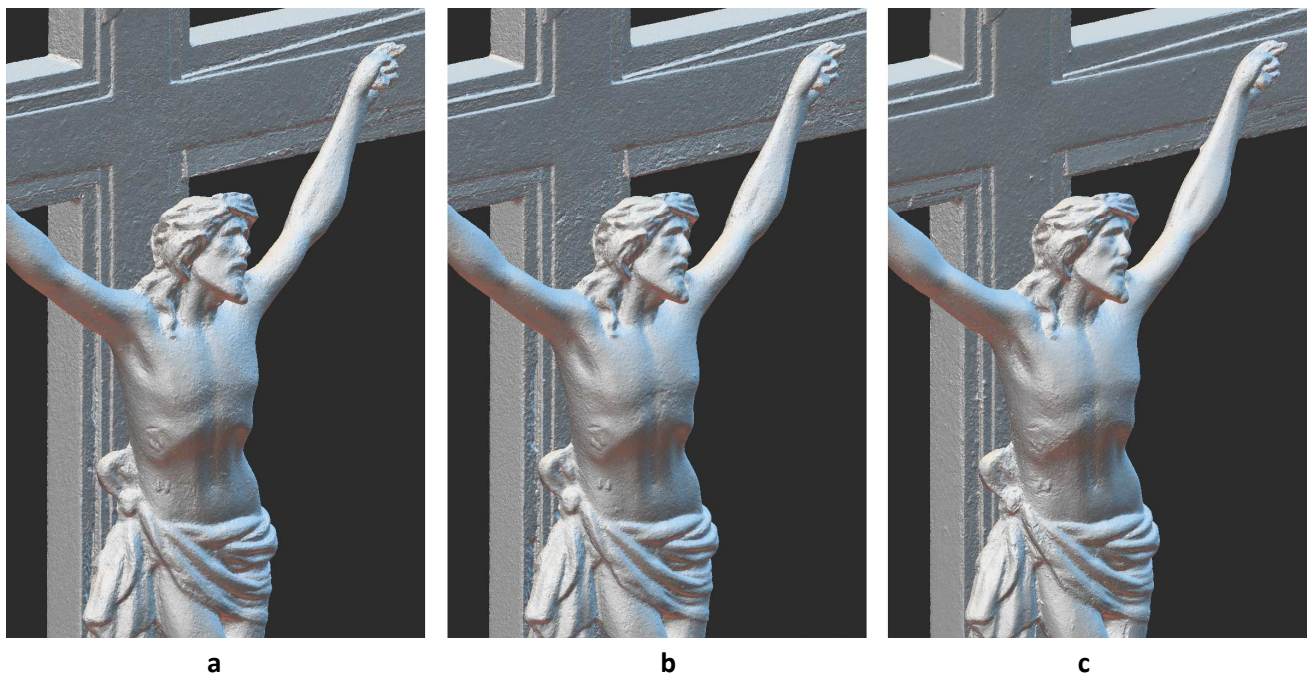


Fig. 107: Comparison of the details of Object 2

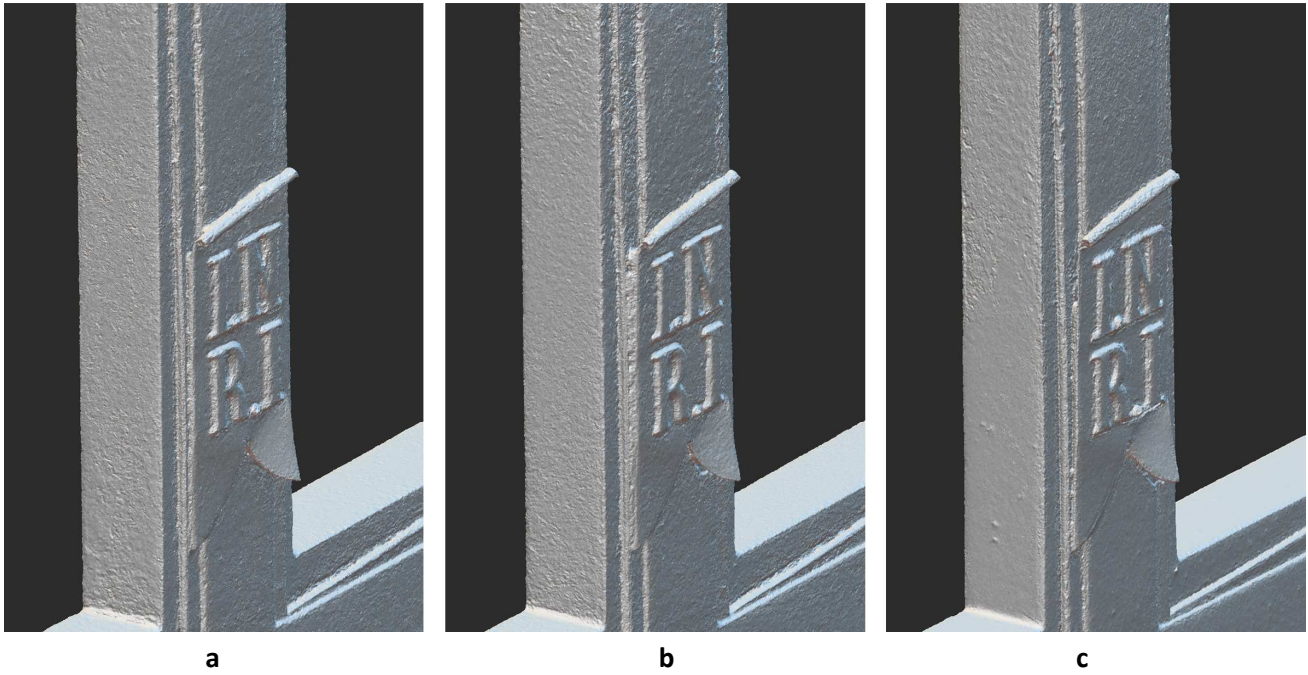


Fig. 108: Comparison of the details of Object 2

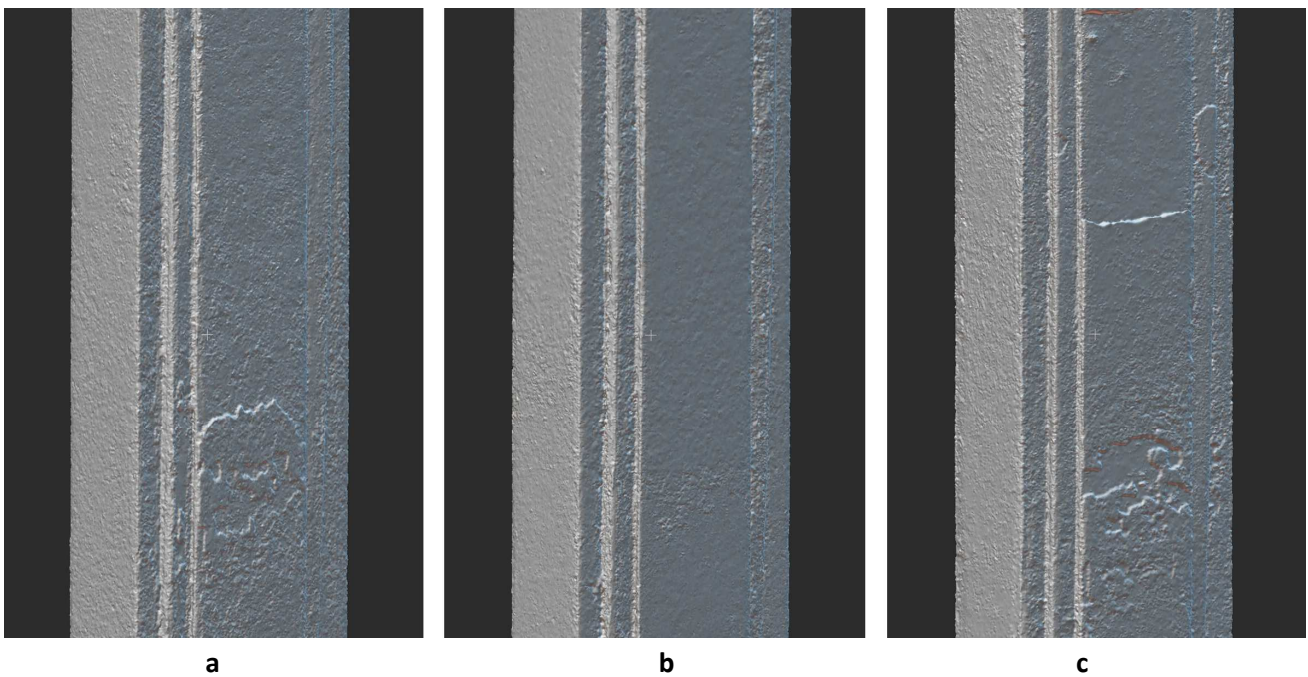


Fig. 109: Comparison of the details of Object 2

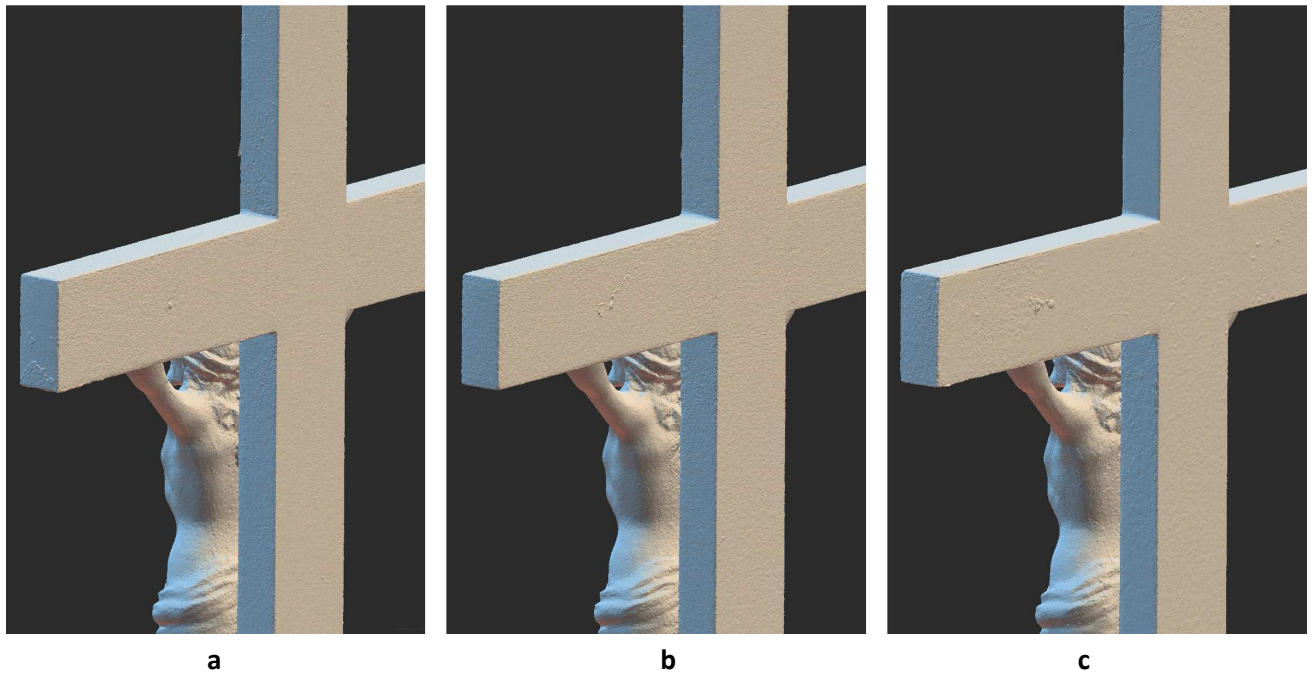


Fig. 110: Comparison of the details of Object 2

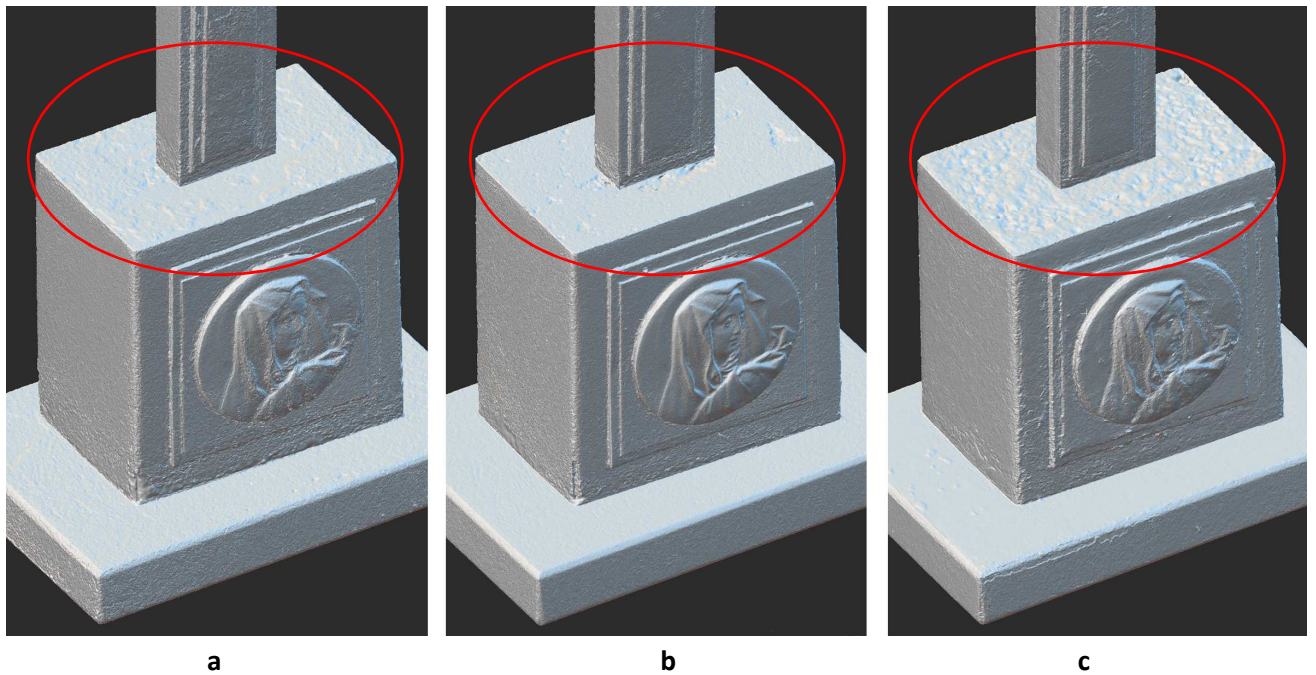


Fig. 111: Comparison of the details of Object 2

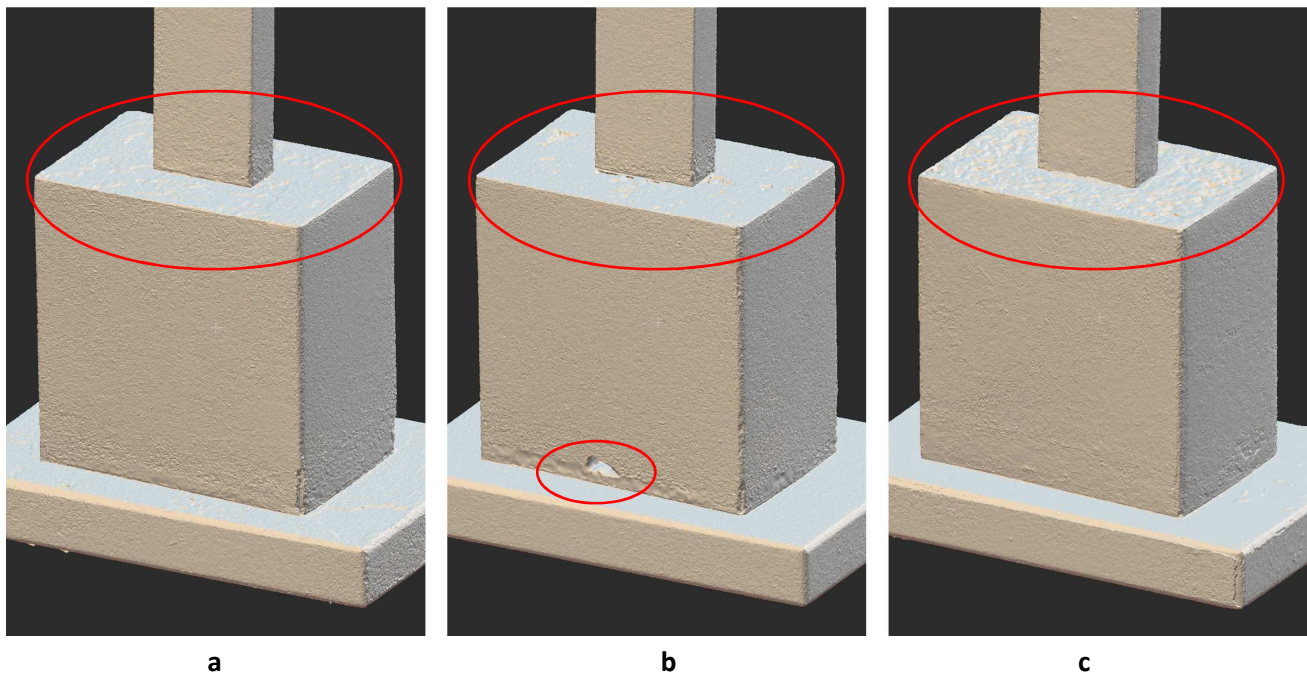


Fig. 112: Comparison of the details of Object 2

Similarly to Object 1, also in this case, Fig. 107 – 112 show clearly that the middle image representing the CPL model produces the minimum amount of noise and the surface is smoother. The CPL model is worse only at the bottom back part of the base (small cavity marked with small ellipse and nearby noisy bottom area), as seen in Fig. 112.

The top of the base, (Fig. 111, 112) marked with the ellipse, has noisy surface, not flat as it should be. This is probably caused by different angles between the cross and the base as mentioned before which caused faulty alignment of both parts together.

### 3.2 Evaluation of the Results

The main advantages of Structure-from-Motion technique with data acquisition by a digital camera are affordability, effectivity, data collection speed, automation and relative simplicity in the processing of photos. Another advantage is also the realistic appearance of the final 3D model, since the resulting texture is calculated from the captured photos. Photogrammetry is accessible to professionals in non-technical fields, for example in museums, both in terms of software and hardware, however the photo acquisition requires high attention and experience, as with bad input even the best software for 3D model calculation fails.

At present, it is difficult to find a reliable, sufficiently accurate and affordable system for a 3D model of objects with a glossy or difficult-to-detect surface. The results of this thesis confirm that it is not possible to apply universal procedures to a whole range of difficult-to-detect surfaces of studied objects. On the other hand, multiple approaches can be applied to different surfaces to obtain image data, which are characterized by different reliability, accuracy and sensitivity to the external environment.

In this work, three data acquisition options were examined – diffused lighting, cross-polarization and scanning spray method which were described in the chapter 2.5.2.

### Observations

The reconstruction from the diffused light photos delivered results of good quality, similar to the CPL method. Despite having used diffused lighting of the studied objects, there were some specular reflexions visible in the photos. The produced mesh however is of a good standard, although there is some noise on the surface. Overall, it confirms that the image acquisition has been performed correctly with high overlapping, which proves that good input can produce a similarly good result.

The scanning spray applied in the third method created additional ‘material’ layer on the surface of the object. This spray was used on both objects twice – for the top and also for the bottom part photo acquisition, thus creating two different surfaces with different thickness, texture and characteristic points, which resulted in problems during the alignment process, when RC tried to find the mutual features between both surfaces while the resulting alignment was not very satisfactory. The seams on the surface are visible, as can be seen on Fig. 43 or on Fig. 45. Even if more control points were added, the seams remained on the mesh.

Another determined issue with the Aesub scanning spray was the applied layer not having vanished completely, despite the official claim of the producer that the coating will self-disappear. This was not the case, as on both objects, some parts were covered with white layer even after a few weeks and it was necessary to carefully clean the surfaces, Fig. 113 and Fig. 114.

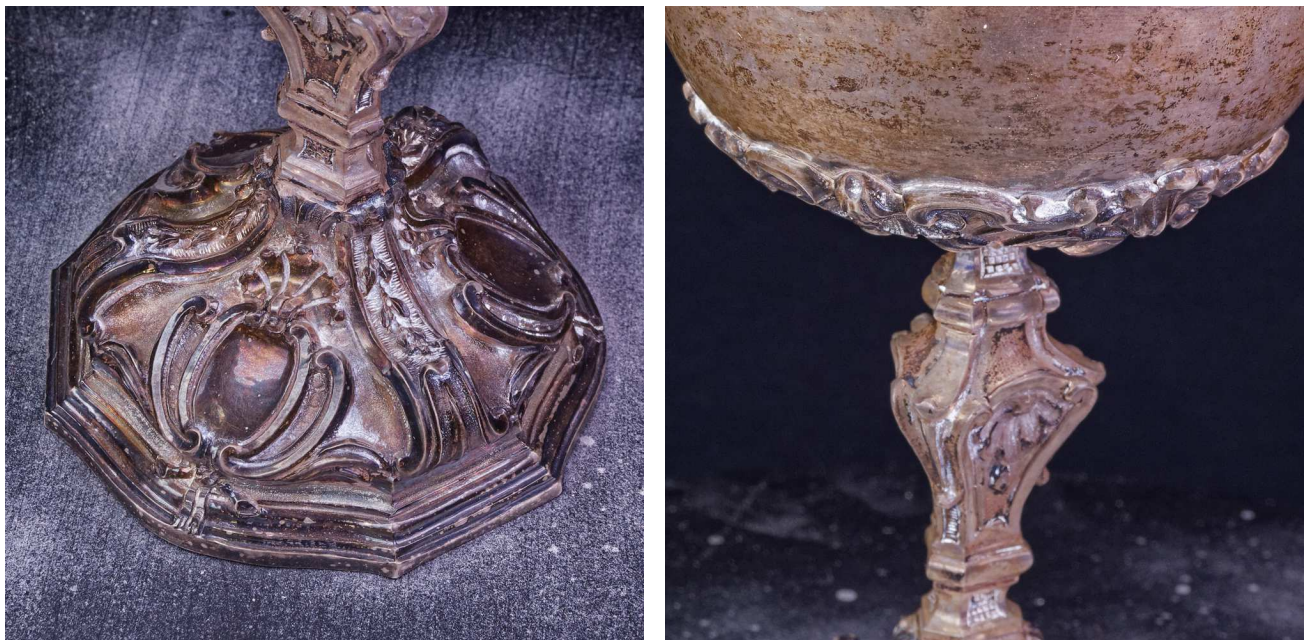


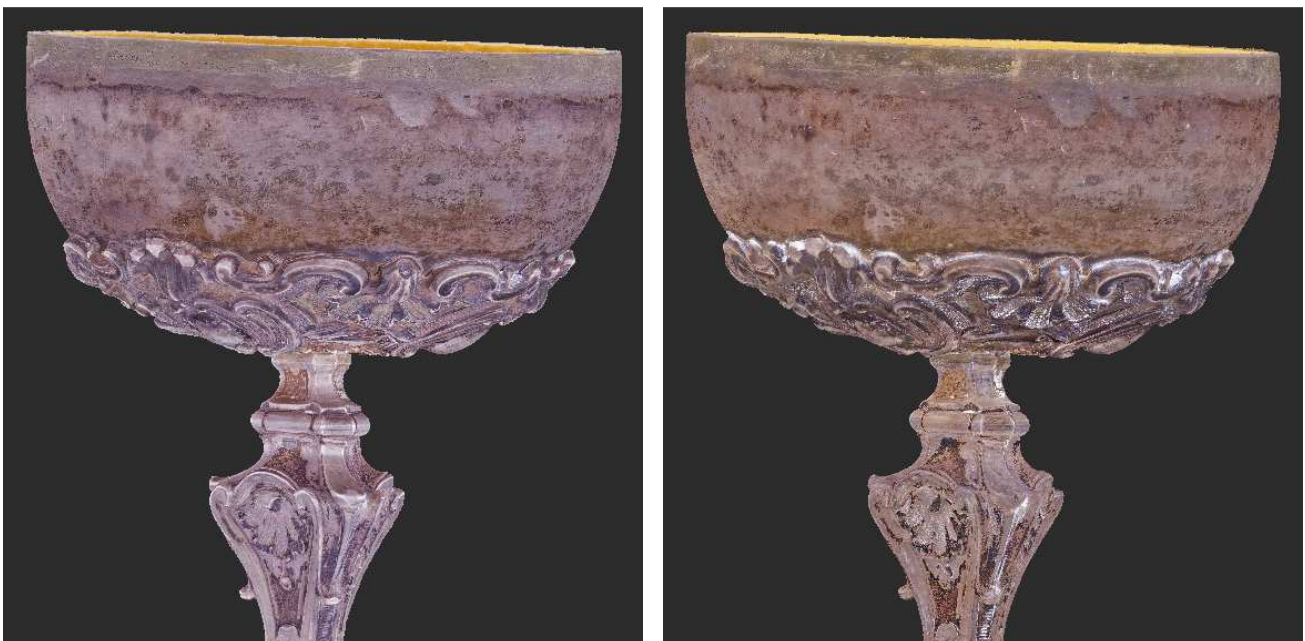
Fig. 113: Remains of Aesub spray on Object 1



Fig. 114: Remains of Aesub spray on Object 2

The mentioned difficulty produced another problem. According to the workflow, as described in the chapter 2.3.2, after the object was covered with scanning spray, the set of photos for scanning spray model was captured, then the object was left a few hours to allow the sprayed layer to evaporate and subsequently the set of cross-polarization photos was taken. These photos were used for texturing of the model while for aligning both CPL photos and sprayed photos were used together, therefore no movement or other manipulation with the object was allowed, even the smallest movement could make it impossible to align both sets.

Since the spray didn't evaporate completely, the texture for cross-polarization model contains white parts on the surface, which can be visible also on the models uploaded to Sketchfab, Fig. 60 and Fig. 61. On Fig. 115 is the comparison of the texture on the diffused light model (left) and CPL model (right) of Object 1.



**Fig. 115: Comparison of the texture on the diffused light model (left) and CPL model (right)**

The difference is clearly visible, affecting the texture of the models. Unfortunately it was not possible to repeat the process.

Regarding the workflow steps, it would be better to take the CPL photos first and then use the scanning spray, however this was not possible as the scanning spray is an extremely flammable aerosol and has to be used only in well-ventilated areas. Therefore the object was removed from the photo studio for spraying and carefully brought back to the studio while continuing with the workflow as planned. As mentioned before, between both photo shootings, it is not allowed to move the object while using the spray in the interior is also not recommended.

The scanning spray could be rather used for objects which are not required to be scanned from all sides (top and bottom), thus no problems with bad alignment of both sides would arise and can be sprayed in well-ventilated space. Then it would be possible to take photos of the object as it is at first and then capture the scanning spray photos.

In all three methods, holes were observed in the bottom of Object 1, which are present due to one of the limitations of photogrammetry, the material of the scanned object being too thin, as was the case here. The bottom part of Object 1 is made from pressed metal sheet and the thickness in these places is about 0,5 mm. When aligning both point clouds of top and bottom parts, there were intersections between them in some places which the software interpreted as holes, as can be seen on Fig. 38. However these holes can be closed (i.e. 'repaired') in an external software. Generally it is suggested to avoid scanning of thin objects.

### Comparison of the Methods in CloudCompare

The final accuracy of these three reconstructed models of both objects made by comparison with an independent technique was unfortunately not possible. Micro-CT scanner didn't provide any reference data. All created models of both objects 1 and 2 were compared between each other in CloudCompare software.

#### Object 1

Comparing CPL model and scanning spray model shows that there is a good match between both models, below 0,2 mm. The maximum difference is on the top of the object, 0,4 mm.

Comparing these models with scanning spray model shows that in some places of the bottom part of the model is a higher deviation, the difference being more than 0,5 mm. Generally, the scanning spray model turned out to be the least accurate. Comparison of the statistical results from Cloudcompare is in Tab. 26 and also in the graph in Fig. 116:

Tab.26: Comparison of the statistical results for Object 1

	Mean distance (m)	Standard deviation (m)
Diffused light/CPL	0,000094	0,000072
Diffused light/scanning spray	0,000159	0,000117
CPL/scanning spray	0,000141	0,000096

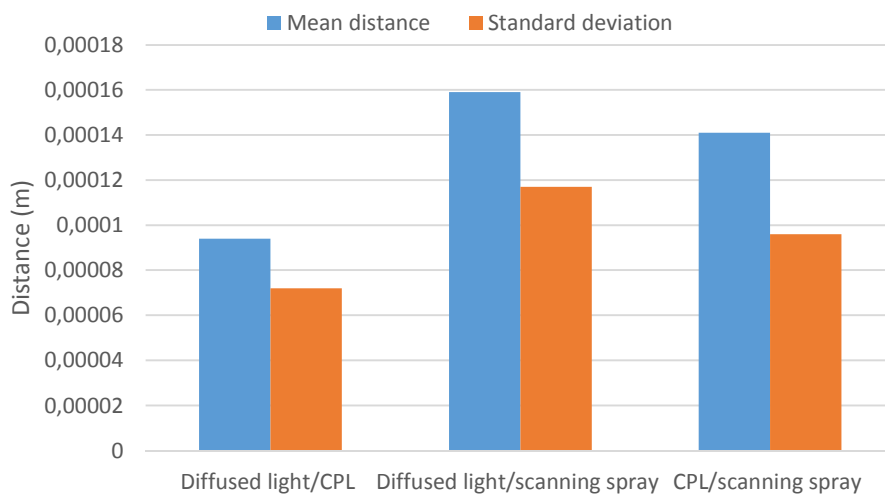


Fig. 116: Comparison of the statistical results for Object 1

The mean distance between Diffused light and CPL model is 0,000094 m (0,094 mm), which is a good match.

## Object 2

Object 2 was a crucifix, consisting of the top cross and bottom base. It was found out that these two parts were not connected firmly and the top part was a little bit loose, therefore the angle was changing. Although this movement was not very substantial, it created two different sets of photos during photo shooting of the top and bottom part separately which caused the noise in the connection of the top and bottom part during the 3D model creation process, as can be seen in Fig. 111. On Fig. 78 is visible the deviation of 3 mm of the top part when comparing the diffused light and CPL models. For this reason, the base and the cross were split and in CloudCompare aligned and compared separately.

The comparison of the base between all 3 models shows minimal deviation between the diffused light and CPL models. As mentioned above, the top part of the base shows noise, which was caused by the alignment of top and bottom sets of photos, as they represented objects with different angle of the top part (cross).

Comparison of the cross shows minimal differences in the central part, the larger deviations are on the top of the cross (>1 mm)



**Tab.27: Comparison of the statistical results for the base of Object 2**

	<b>Mean distance (m)</b>	<b>Standard deviation (m)</b>
<b>Diffused light/CPL</b>	0,000127	0,000146
<b>Diffused light/scanning spray</b>	0,000140	0,000146
<b>CPL/scanning spray</b>	0,000160	0,000159

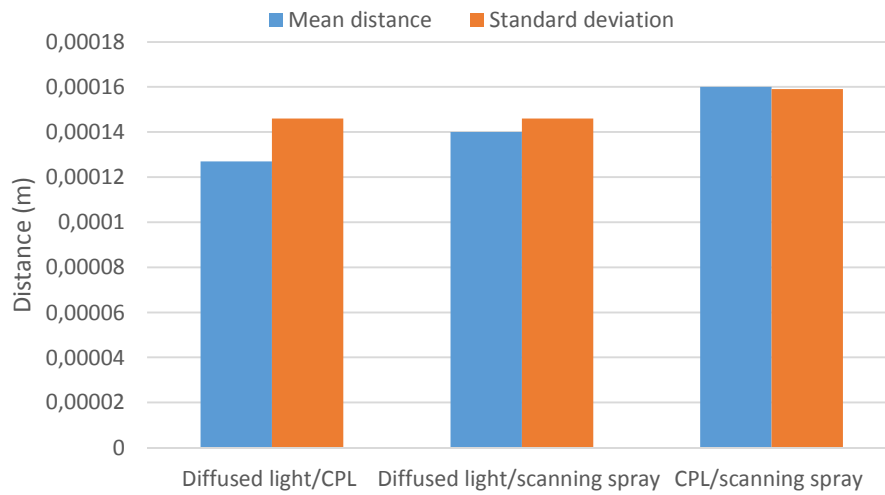


**Fig. 117: Comparison of the statistical results for the base of Object 2**

**Tab.28: Comparison of the statistical results for the cross of Object 2**

	<b>Mean distance (m)</b>	<b>Standard deviation (m)</b>
<b>Diffused light/CPL</b>	0,000149	0,000184
<b>Diffused light/scanning spray</b>	0,000169	0,000189
<b>CPL/scanning spray</b>	0,000122	0,000144

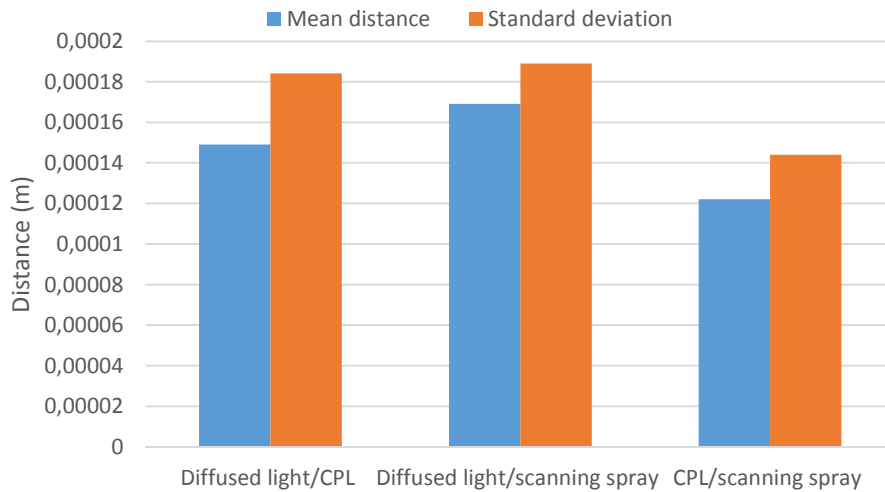


**Fig. 118: Comparison of the statistical results for the cross of Object 2**

Both diffused light and CPL models of the cross show minimal differences between them. The scanning spray model has on the other hand the minimal difference with the CPL model of the base.

Standard deviation (SD) is the average distance from the mean. The lower SD, the less dissimilar are the data from one another, the data are closer to their mean. If SD is zero, it means that there is no variability in the data, they are all identical in value.

An interesting observation has been found in Object 2 - the standard deviation is higher than the mean distance. It is not abnormal as it can mean that there is a wide range of variation amongst the data and there is significant distance between the highest and lowest values. This was mentioned earlier and visible e.g. in histograms on Fig. 82 or Fig. 85, that there is some small numbers of points in bigger distance, probably there were lonesome points outside of the object, which could not be seen and were not deleted, while even during detailed examination of the point clouds they could not be found.

### Quantitative Evaluation

In the chapter 3.1.3 the comparison of measurements on the 3D models and real objects (5 control distances between defined points on each object) was performed. The results were summed up in Tab. 24 and 25 and show that the CPL model has minimal deviations compared with other methods.

### Qualitative Evaluation

Subjective visual comparison of the meshes was performed to analyse their surface quality and amount of noise. Detailed pictures of each model made of diffused light, CPL and scanning spray photos was compared between each other. The CPL model shows also in this case the least amount of noise and the surface is smoother.

The texturing reports show the minimal detail captured with images. In the chapter 2.4.1 was a calculation of the GSD on the final 3D model taken with described camera and lens with given shooting distance. The results are compared in the following table:

**Tab.29: Comparison of the texture details results and calculated GSD**

	<b>Minimal detail in the texture (mm)</b>	<b>Calculated GSD (mm)</b>
<b>Object 1</b>	0,041; 0,043	0,048
<b>Object 2</b>	0,063; 0,069	0,072

When comparing the above mentioned results, the accuracy of the result is clearly achieved.

### 3.3 Conclusions

Based on the observations described above, the cross-polarization technique delivered the best results, producing the most accurate 3D object models, while considerably exceeding the set resolution parameters for the texture. The diffused light method likewise delivered very good results, however with a little more noise in the surface of the model, but again surpassing the optimal criteria for the texture resolution. The scanning spray method supplied acceptable results, albeit with lower accuracy of the 3D model surface, as the spray created a new layer with variable thickness, which was to be expected to a certain extent.

According to the overall results we conclude that the digitization of the inventory of the Order can be realized with the equipment available for this study. Some problematic objects should be excluded however – mostly those having some very thin parts, which as this study confirmed, also represent a serious difficulty for photogrammetric methods.

The results of this study will be presented to the Hospitaller Order while concrete suggestions for possible cooperation on digitizing of their artefact collection will be discussed. For the excluded problematic objects other methods of digitization will be proposed and/or tested. The produced 3D models will be digitally delivered, for the purpose of their internal inventory documentation. Even though it was excluded from the subject of this study, the following step of post-processing of the 3D models, i.e. smoothing, retouching and closing the holes, in an external 3D modelling software (e.g. Blender, Meshlab, etc.) could be suggested. The original models should be kept however for archiving as well as preservation purposes allowing the possibility for the objects to be examined in detail or reproduced in the future according to their accurate representations.

## 4 Bibliography

Act no. 49/2002

Act no. 49/2002 Coll. of the Slovak Republic on the Protection of the Monument Fund, implemented by Decree no. 253/2010 Coll. as amended.

Bartoš and Gregor 1995

BARTOŠ, P., & GREGOR, V. (1995). Aplikácie digitálnej fotogrametrie pri dokumentácii pamiatok. *Geodetický a kartografický obzor*, 12, 261-265.

Conen et al. 2018

Conen, N., Hastedt, H., Kahmen, O., & Luhmann, T. (2018). Improving Image Matching by Reducing Surface Reflections Using Polarising Filter Techniques. *International Archives of the Photogrammetry, Remote Sensing & Spatial Information Sciences*, 42(2).

Crabb 2001

Crabb, P. (2001). The use of polarised light in photography of microfossils. *Palaeontology*, 44(4), 659-664.

Dedík 2016

Dedík, L. (2016). Človek v zdigitalizovanom prostredí. *Vysoká škola múzických umení v Bratislave*.

Edwards 2011

Edwards, N. (2011). Cross-polarisation, making it practical. *Journal of Visual Communication in Medicine*, 34(4), 165-172.

Falkingham 2012

Falkingham, P. L. (2012). Acquisition of high resolution three-dimensional models using free, open-source, photogrammetric software. *Palaeontologia electronica*, 15(1), 15.

Hallot and Gil 2019

Hallot, P., & Gil, M. (2019). METHODOLOGY FOR 3D ACQUISITION OF HIGHLY REFLECTIVE GOLDSMITHING ARTIFACTS.

The Digital Ark 2016

The Digital Ark (2016). How to Use Photogrammetry to Create 3D Models of Cultural Heritage Objects, New England Museum Association, Veteran's Day, November 11, 2016. Available online: [[https://www.nemanet.org/files/2414/7974/4097/NEMA\\_Photogrammetry\\_110616\\_WEB.pdf](https://www.nemanet.org/files/2414/7974/4097/NEMA_Photogrammetry_110616_WEB.pdf)].

Information technology and libraries 2020

Informačné technológie a knižnice, itlib.cvtisr.sk. Available online: [<http://www.pamiatky.sk/en/page/digitalny-pamiatkovy-fond>]

Katuščák 2008

Katuščák, D. (1998). Súčasný stav formovania stratégie digitalizácie na Slovensku. *Colloquium of Library Information Employees of the V4+ Countries*. Brno.

Konrad 2016

Konrad, S. (2016). Reconstruction of specular surfaces from reflectance correspondences, Darmstadt, Technische Universität Darmstadt, [Master Thesis].

Kulíková 2009

Kulíková A. (2009). Metodický manuál pre zabezpečenie konverzie 3D malých objektov. Available online:

[[http://www.opis.culture.gov.sk/uploads/65/e5/65e5a97a01ec0b568721910298511700/07\\_metodicky\\_manual\\_pre-zabezpecenie-konverzie-3d-malych-objektov.pdf](http://www.opis.culture.gov.sk/uploads/65/e5/65e5a97a01ec0b568721910298511700/07_metodicky_manual_pre-zabezpecenie-konverzie-3d-malych-objektov.pdf)]

Koutsoudis et al. 2015

Koutsoudis A., Arnaoutoglou, F., & Pavlidis, G. (2015). Structure from Motion–Multiple View Stereovision (SFM/MVS) An Introduction on how to perform SFM/MVS.

Lachambre et. al. 2017

Lachambre, S., Lagarde, S., & Jover, C. (2017). Unity photogrammetry workflow. Unity Developer—Rendering Research. Available online: [[https://unity3d.com/files/solutions/photogrammetry/Unity-Photogrammetry-Workflow\\_2017-07\\_v2.pdf](https://unity3d.com/files/solutions/photogrammetry/Unity-Photogrammetry-Workflow_2017-07_v2.pdf)].

Logan 2007

Logan, W. S. (2007). Closing Pandora's box: human rights conundrums in cultural heritage protection. In Cultural heritage and human rights (pp. 33-52). Springer, New York, NY.

Luhman et. al. 2006

Luhman, T., Robson, S., Kyle, S., & Harley, J. (2006). Close Range Photogrammetry. Principles, methods and applications.

Mallison and Wings 2014

Mallison, H., & Wings, O. (2014). Photogrammetry in paleontology—a practical guide. *Journal of Paleontological Techniques*, 12(12), 1-31.

McGlone 2004

McGlone, J. C., Mikhail, E., Bethel, J., & Mullen, R. (2004). American Society for Photogrammetry and Remote Sensing. Manual of photogrammetry. American Society for Photogrammetry and Remote Sensing.

Measures for CH SR 2006

Ministerstvo kultúry Slovenskej republiky: Opatrenia na realizáciu ochrany kultúrneho dedičstva Slovenskej republiky, 2006. Available online: [<http://www.culture.gov.sk/kulturne-dedicstvo/ochrana-amiatok/dokumenty/opatrenia-na-zachovanie-kulturneho-dedicstva-sr>]

Michot 2010

Michot Julien (2010). Available online: [at <http://michot.julien.free.fr/drupal/?q=content/research>]

Novaković et al. 2017

Novaković, P., Hornak, M., & Zachar, M. (2017). 3D Digital Recording of Archaeological, Architectural and Artistic Heritage. CONPRA series I.

Pavelka 2009

PAVELKA, K., 2009: Fotogrammetrie 1. Praha.

Protection of Monuments SR 2006

Ministerstvo kultúry Slovenskej republiky: Ochrana pamiatok a pamiatkových území a pôsobnosť orgánov ochrany pamiatkového fondu, 2006. Available online: [<http://www.culture.gov.sk/kulturne-dedicstvo/ochrana-pamiatok>]

Ray 2002

Ray, S.F., (2002). Applied photographic optics: Lenses and optical systems for photography, film, video, electronic and digital imaging.

Schenk 2005

Schenk T. Introduction to Photogrammetry. Department of Civil and Environmental Engineering and Geodetic Science. Athens, USA: The Ohio State University; 2005. pp. 79-95. Available online: [[http://gscphoto.ceegs.ohio-state.edu/courses/GeodSci410/docs/GS410\\_02.pdf](http://gscphoto.ceegs.ohio-state.edu/courses/GeodSci410/docs/GS410_02.pdf)]

Tobler et al. 2006

Tobler, R. F.; Maierhofer, S. (2006): A mesh data structure for rendering and subdivision.

In : Proceedings of WSCG. The 14th international conference in Central Europe on computer graphics, visualisation and computer vision. Plzen, Czech Republic, 31. Jan - 2. Feb: University of West Bohemia, pp. 157-162.

Ullman 1979

Ullman, S. (1979). The interpretation of structure from motion. Proceedings of the Royal Society of London. Series B. Biological Sciences, 203(1153), 405-426.

Wells et al. 2005

Wells, J., Jones, T., & Danehy, P. (2005, April). Polarization and color filtering applied to enhance photogrammetric measurements of reflective surfaces. In 46th AIAA/ASME/ASCE/AHS/ASC Structures, Structural Dynamics and Materials Conference (p. 1887).

Wolf and Dewitt 2000

Wolf, P. R., & Dewitt, B. A. (2000). Elements of photogrammetry: with applications in GIS (Vol. 3). New York: McGraw-Hill.

aesub.com

Available online: [<https://aesub.com>]

cloudcompare.org

Available online: [<https://www.cloudcompare.org>]

capturingreality.com

Available online: [<https://www.capturingreality.com>]

coe.int

Available online: [<https://www.coe.int/en/web/herein-system/glossary>]

Available online: [<https://www.coe.int/en/web/herein-system/thesaurus>]

culturalheritageimaging.org

Available online: [<http://culturalheritageimaging.org/Technologies/Photogrammetry/index.html>]

DoF

Available online: [<https://www.dl-c.com/Products-DoF.html>]

dxo.com

Available online: [<https://www.dxo.com>]

heritageconsulting.sk

Available online: [<https://www.heritageconsulting.sk/kulturne-dedicstvo/>]

opis.gov.sk

Available online: [<https://www.opis.gov.sk>]

pasthorizonstools.com

Available online: [<https://www.pasthorizonstools.com>]

sketchfab.com

Available online: [<https://www.sketchfab.com>]

UV mapping

UV mapping In Wikipedia. June 2020. Available online: [[https://en.wikipedia.org/wiki/UV\\_mapping](https://en.wikipedia.org/wiki/UV_mapping)]

## 5 Appendices

### 5.1 List of Abbreviations

3D	Three-dimensional
CMOS	Complementary Metal Oxide Semi-conductor
CPL	Cross-polarization
CT	Computer Tomography
DOF	Depth of Field
DSLR	Digital Single Lens Reflex
EXIF	Exchangeable Image File
FOV	Field of View
GSD	Ground Sampling Distance
ISO	International Organisation for Standardization
JPEG	Joint Photographic Experts Group
LCD	Liquid Crystal Display
LED	Light Emitting Diode
OBJ	Object File Format
PLY	Polygon File Format
RAM	Random-Access Memory
RC	Reality Capture
RGB	Red, Green, Blue
SfM	Structure from Motion
SSD	Solid State Drive

## 5.2 List of Figures

Fig. 1:	Distribution of light for diffused, glossy and mirror surface	10
Fig. 2:	Object 1 - Ciborium	12
Fig. 3:	Object 2 - Cross	13
Fig. 4:	D500 Camera body	14
Fig. 5:	Sigma 18-50 lens	15
Fig. 6:	Turntable	17
Fig. 7:	Scale bar	18
Fig. 8:	LED light	18
Fig. 9:	Quickset tripod	19
Fig. 10:	Aesub scanning spray	20
Fig. 11:	SfM principle	21
Fig. 12:	Workflow flowchart	23
Fig. 13:	Scheme of the studio	25
Fig. 14:	Scale of the object and the image	26
Fig. 15:	Definition of the steps and angles between the photo shoots	27
Fig. 16:	Capturing the object 1	29
Fig. 17:	Depth of Field Calculator for Windows	31
Fig. 18:	Examples of short depth of field on object 2	32
Fig. 19:	Object 1 and 2 with diffused light	34
Fig. 20:	Orientation of the polarizing filter	35
Fig. 21:	Comparison of parallel and crossed filters	35
Fig. 22:	Comparison of the photos of object 1 with diffused light and cross-polarization	36
Fig. 23:	Comparison of the photos of object 2 with diffused light and cross-polarization	36
Fig. 24:	Comparison of the photos of Object 1 with diffused light (left) and covered with the scanning spray (right)	37
Fig. 25:	Comparison of the photos of Object 2 with diffused light (left) and covered with the scanning spray (right)	38
Fig. 26:	Comparison of the photo before and after adjustments in DxO Photolab	39
Fig. 27:	Alignment settings used for the workflows	41
Fig. 28:	Alignment of top and bottom parts of Object 1	42
Fig. 29:	Alignment of the top and bottom components of Object 1	42
Fig. 30:	Alignment of top and bottom parts of Object 2	43
Fig. 31:	Alignment of the top and bottom components of Object 2	44
Fig. 32:	Alignment of the top and bottom components of Object 1	45
Fig. 33:	Alignment of the top and bottom components of Object 2	46
Fig. 34:	Alignment of the top and bottom components of Object 1	47
Fig. 35:	Alignment of the top and bottom components of Object 2	48
Fig. 36:	Defining the distance constraints on both objects	49
Fig. 37:	Reconstruction of Object 1 from diffused light photos	50
Fig. 38:	Detail of the object	51
Fig. 39:	Reconstruction of Object 2 from diffused light photos	52
Fig. 40:	Reconstruction of Object 1 from cross-polarization photos	53
Fig. 41:	Reconstruction of Object 2 from cross-polarization photos	54



Fig. 42: Reconstruction of Object 1 from scanning spray photos	55
Fig. 43: Seams on the surface	55
Fig. 44: Reconstruction of Object 1 from scanning spray photos	56
Fig. 45: Seams on the surface	57
Fig. 46: Comparison of 10 M mesh and 10 K mesh	57
Fig. 47: UV mapping a globe	58
Fig. 48: Unwrapped model 1	59
Fig. 49: Unwrapped model 1	59
Fig. 50: Exported texture of Object 1 and 2	60
Fig. 51: Textured model 1	61
Fig. 52: Details of the texture of the model 1	61
Fig. 53: Textured model 2	62
Fig. 54: Details of the texture of the model 2	62
Fig. 55: Examples of renderings of Object 1	63
Fig. 56: Examples of renderings of Object 2	63
Fig. 57: Ortho projections of Object 1	64
Fig. 58: Measuring the distance	65
Fig. 59: Measuring the distance	66
Fig. 60: QR code for Object 1 in Sketchfab	67
Fig. 61: QR code for Object 2 in Sketchfab	67
Fig. 62: Scanning of the object 1 in the micro-CT-L240	68
Fig. 63: Scanning of the object 2 in the micro-CT-L240	69
Fig. 64: Examples of bright and dark streaks in Object 1 and 2	69
Fig. 65: Surface determination settings 1 of Object 1	70
Fig. 66: Surface determination settings 2 of Object 1	71
Fig. 67: Surface determination settings 1 of Object 2	71
Fig. 68: Surface determination settings 2 of Object 2	72
Fig. 69: Visualization of surface deviation	73
Fig. 70: Visualization of surface deviation	74
Fig. 71: Histogram of the points distribution according to the absolute distance	75
Fig. 72: Visualization of surface deviation	76
Fig. 73: Visualization of surface deviation	77
Fig. 74: Histogram of the points distribution according to the absolute distance	78
Fig. 75: Visualization of surface deviation	79
Fig. 76: Visualization of surface deviation	80
Fig. 77: Histogram of the points distribution according to the absolute distance	81
Fig. 78: Visualization of surface deviation	82
Fig. 79: Schematic visualisation of the movement and difference in the angle of the cross	83
Fig. 80: Visualization of surface deviation	84
Fig. 81: Visualization of surface deviation	85
Fig. 82: Histogram of the points distribution according to the absolute distance	85
Fig. 83: Visualization of surface deviation	86
Fig. 84: Visualization of surface deviation	87
Fig. 85: Histogram of the points distribution according to the absolute distance	88

Fig. 86: Visualization of surface deviation	89
Fig. 87: Visualization of surface deviation	90
Fig. 88: Visualization of surface deviation	91
Fig. 89: Histogram of the points distribution according to the absolute distance	91
Fig. 90: Visualization of surface deviation	92
Fig. 91: Visualization of surface deviation	93
Fig. 92: Histogram of the points distribution according to the absolute distance	94
Fig. 93: Visualization of surface deviation	95
Fig. 94: Visualization of surface deviation	96
Fig. 95: Visualization of surface deviation	97
Fig. 96: Histogram of the points distribution according to the absolute distance	97
Fig. 97: Visualization of surface deviation	98
Fig. 98: Visualization of surface deviation	99
Fig. 99: Histogram of the points distribution according to the absolute distance	100
Fig. 100: Definition of measuring points on Object 1	101
Fig. 101: Absolute distances between the model and real object 1 measurements	102
Fig. 102: Definition of measuring points on Object 2	102
Fig. 103: Absolute distances between the model and real Object 1 measurements	103
Fig. 104: Comparison of the details of Object 1	104
Fig. 105: Comparison of the details of Object 1	104
Fig. 106: Comparison of the details of Object 1	105
Fig. 107: Comparison of the details of Object 2	106
Fig. 108: Comparison of the details of Object 2	106
Fig. 109: Comparison of the details of Object 2	106
Fig. 110: Comparison of the details of Object 2	107
Fig. 111: Comparison of the details of Object 2	107
Fig. 112: Comparison of the details of Object 2	108
Fig. 113: Remains of Aesub spray on Object 1	109
Fig. 114: Remains of Aesub spray on Object 2	110
Fig. 115: Comparison of the texture on the diffused light model (left) and CPL model (right)	111
Fig. 116: Comparison of the statistical results for Object 1	112
Fig. 117: Comparison of the statistical results for the base of Object 2	113
Fig. 118: Comparison of the statistical results for the cross of Object 2	114

### 5.3 List of Tables

Tab.1:	List of technical equipment	14
Tab.2:	Overview of the most commonly used software:	16
Tab.3:	Used software	17
Tab.4:	Used camera settings during the workflow	30
Tab.5:	Number of photos for each elevation for Object 1:	33
Tab.6:	Number of photos for each elevation for Object 2:	33
Tab.7:	Alignment report for the object 1	43
Tab.8:	Alignment report for Object 2	44
Tab.9:	Alignment report for Object 1	45
Tab.10:	Alignment report for Object 2	46
Tab.11:	Alignment report for Object 1	47
Tab.12:	Alignment report for Object 2	48
Tab.13:	Texturing report for Object 1	60
Tab.14:	Texturing report for Object 2	60
Tab.15:	Analysis results	74
Tab.16:	Analysis results	77
Tab.17:	Analysis results	80
Tab.18:	Analysis results	85
Tab.19:	Analysis results	87
Tab.20:	Analysis results	91
Tab.21:	Analysis results	93
Tab.22:	Analysis results	97
Tab.23:	Analysis results	99
Tab.24:	Measured distances between points	101
Tab.25:	Measured distances between points	102
Tab.26:	Comparison of the statistical results for Object 1	112
Tab.27:	Comparison of the statistical results for the base of Object 2	113
Tab.28:	Comparison of the statistical results for the cross of Object 2	113
Tab.29:	Comparison of the texture details results and calculated GSD	115